Transport Processes of Reactive Trace Gases in the Atmospheric Boundary Layer

A dissertation submitted to the

Faculty of Biology, Chemistry and Geosciences

at the University of Bayreuth

for the degree of

Dr. rer. nat.

presented by

Jens-Christopher Mayer

Dipl. Geoökol.

Born 25 September 1978

In Frankfurt / Main

Bayreuth, November 2008

Transport Processes of Reactive Trace Gases in the Atmospheric Boundary Layer

Supervisor Prof. Dr. Thomas Foken

Vollständiger Abdruck der von der Fakultät für Biologie, Chemie und Geowissenschaften der Universität Bayreuth genehmigten Dissertation zur Erlangung des akademischen Grades eines Doktors der Naturwissenschaften (Dr. rer. nat.).

Diese Arbeit wurde im Zeitraum von April 2005 bis November 2008 in der Abteilung Mikrometeorologie der Universität Bayreuth und am Max-Planck-Institut für Chemie in Mainz unter der Leitung von Prof. Dr. Thomas Foken und Prof. Dr. Franz X. Meixner erstellt.

Dissertation eingereicht am: 21. November 2008

Zulassung durch die Promotionskommission: 03. Dezember 2008

Tag des wissenschaftlichen Kolloquiums: 02. Februar 2009

Amtierender Dekan: Prof. Dr. A. Müller

Erstgutachter: Prof. Dr. Thomas Foken

Zweitgutachter: Prof. Dr. Franz X. Meixner

Contents

List of Manuscripts

The dissertation is presented in cumulative form. It consists of three individual manuscripts. One manuscript has been published in a peer-reviewed journal. The second manuscript is resubmitted as a revised version to the journal. The third manuscript will be submitted for publication soon.

Published manuscripts

Mayer, J.-C., Staudt, K., Gilge, S., Meixner, F.X. and Foken, T.: The impact of free convection on late morning ozone decreases on an Alpine foreland mountain summit, Atmospheric Chemistry and Physics, 8, 5941-5956, 2008.

Previously published as: Mayer, J.-C., Staudt, K., Gilge, S., Meixner, F.X. and Foken, T.: The impact of free convection on late morning ozone decreases on an Alpine foreland mountain summit, Atmospheric Chemistry and Physics Discussions, 8, 5437-5476, 2008.

Submitted manuscript

Mayer, J.-C., Hens, K., Rummel, U. Meixner, F.X. and Foken, T.: Moving measurement platforms – specific challenges and corrections, Meteorologische Zeitschrift, revised version submitted, 2008.

Manuscript to be submitted

Mayer, J.-C., Bargsten, A., Rummel, U., Meixner, F.X. and Foken, T.: Distributed Modified Bowen Ratio Method for Surface Layer Fluxes of reactive and non-reactive Trace Gases, Atmospheric Chemistry and Physics Discussions, to be submitted, 2008.

Other publications, not included in this thesis

Thomas, C., Mayer, J.-C., Meixner, F.X. and Foken, T.: Analysis of Low-Frequency Turbulence Above Tall Vegetation Using a Doppler Sodar, Boundary-Layer Meteorology, 119, 563-587, 2006.

Mayer, J.-C., Gilge, S., Staudt, K., Meixner, F.X. and Foken, T.: Freie Konvektion im Vorland des Hohenpeißenbergs – Einfluss auf Spurengasmessungen, GAW-Brief des DWD, 42, 2008. http://www.dwd.de/gaw.

Acknowledgements

I wish to express my sincere gratitude to all persons who contributed in innumerable ways to the development of this thesis. Particularly, I would like to thank:

Summary

Transport of trace gases within the atmospheric boundary layer plays a key role in feedback processes between the earth's surface and the atmosphere and consequently in ecosystem budgets of carbon and nitrogen (among many more). Therefore, for a correct quantification of the exchange between surface and atmosphere, it is crucial to understand the transport processes involved and to determine limitations of the presently available measurement techniques in order to apply the right technique with respect to the currently active transport processes.

This dissertation focuses on three topics: (a) The analysis of effects of vertical transport mechanisms on surface measurements of trace gases, (b) the appropriate choice of an experimental setup to assess specific measurement errors of moving measurement systems and (c) the application of a series of measurement techniques for surface fluxes of reactive trace gases to determine their degree of agreement and to assess potential source of deviations.

To study the impact of vertical transport mechanisms on surface trace gas measurements, this thesis presents a comprehensive set of measurements at the surface and within the atmospheric boundary layer (by tethered balloon). It enables the attribution of a recurrent negative excursion of O_3 mixing ratios in the morning hours at a mountain summit to a very efficient vertical transport by free convection. It has been shown that, due to the rapid vertical transport, a layer of approximately 20 m thickness developed at the equilibrium height of the free convection, being located within the residual layer. It had a chemical composition similar to the air close to the ground while being surrounded by residual layer air masses. Hence, very strong gradients of the chemical composition were found within the residual layer. Evidence was found, that such a transport occurs rather frequently at this location, affecting at least 18 % of the days between April and September. However, only the combination of ground based measurements and in-situ profiling of the atmosphere by a tethered balloon can exclude all but one explanation for the observations at the mountain summit.

To assess measurement errors introduced by the application of scanning methods as compared to gradient approaches, a higher temporal resolution of the vertical profiles was needed. Because of limitation inherent to a tethered balloon, an elevator based profiling system was installed, providing a temporal resolution of 10 minutes with a maximum ceiling of 100 m. Prior to the investigation of transport processes, the proper

functioning of correction algorithms for the so-called dynamical error was investigated under real atmospheric conditions. This dynamical error is inherent to all moving measurement systems and arises from the non-zero response time of the deployed sensors. It has been shown that existing algorithms as well as one developed by the authors reliably balance the dynamical error. Furthermore it has been demonstrated, that the elevator data correlate with reference data at fixed levels with coefficients of determination being always greater than 0.992 at every level (10, 20, 40, 60, 80, 98 m).

To evaluate the applicability of different flux measurement techniques for the determination of surface fluxes of reactive trace gases, three different approaches were compared. In order to determine surface fluxes of trace gases, a new modification of the modified Bowen ratio method was used. In this modification, the measurements of sensible heat flux and of the gradients were horizontally separated. This allowed the simultaneous measurement of the fluxes of various trace gases without creating errors due to flow distortion by bulky inlet systems. It has been demonstrated that this approach was applicable at a horizontally homogeneous site. Surface emission fluxes of NO were found to be in the range $0.02 - 0.15$ nmol m^{-2} s^{-1} (night/day), NO$_2$ fluxes varied around -0.1 nmol m^{-2} s^{-1} (deposition) with slightly positive values in the early afternoon, indicating emission. O$_3$ deposition fluxes ranged from close to zero to about -6 nmol m^{-2} s^{-1}. A laboratory parameterization of biogenic soil emission fluxes of NO from incubated soil samples yielded values from 0.025 nmol m^{-2} s^{-1} to 0.12 nmol m^{-2} s^{-1} for environmental conditions encountered during the field campaign. This was in excellent agreement with the NO fluxes from field observations. Besides the comparison of field fluxes with laboratory data, a case study (1 night) comparison of CO$_2$ and O$_3$ fluxes between two field methods was done. Results from the modified Bowen ratio method have been compared to fluxes derived from the integral boundary layer budget method. Both methods yielded similar mean CO$_2$ fluxes during the night (3.75 µmol m^{-2} s^{-1} and 3.31 µmol m^{-2} s^{-1}, respectively). In contrast, O$_3$ fluxes deviated between both methods (-0.69 nmol m^{-2} s^{-1} and -2.31 nmol m^{-2} s^{-1}, respectively). This deviation was attributed to chemical in-situ loss of O$_3$ during night time within the profile being integrated by the budget method.

Zusammenfassung

Der Spurengastransport innerhalb der atmosphärischen Grenzschicht spielt eine dominierende Rolle in der Rückkopplung von Erdoberfläche und Atmosphäre. Dadurch kontrolliert er maßgeblich Ökosystembilanzen u.a. von Kohlenstoff und Stickstoff. Um eine quantitative Erfassung der Austauschprozesse zwischen Erdoberfläche und Atmosphäre zu ermöglich, ist ein Verständnis der beteiligten Transportprozesse von großer Bedeutung, ebenso wie Kenntnisse über die Begrenztheit aktueller Messverfahren. Das Ziel sollte die Anwendung eines zu den vorhandenen Transportprozessen passenden Messverfahrens sein.

Diese Dissertation konzentriert sich zunächst auf die Auswirkungen verschiedener Mechanismen des vertikalen Stofftransports auf bodennahe Spurengasmessungen. Des Weiteren wird die Möglichkeit einer experimentellen Bestimmung von Messfehlern, die für bewegte Messsysteme spezifisch sind, untersucht. Im dritten Beitrag werden verschiedene Messtechniken zur Bestimmung von Flüssen reaktiver Spurengase analysiert, um den Grad ihrer Übereinstimmung bzw. mögliche Gründe für Abweichungen zu bestimmen.

Um den Einfluss vertikaler Transportprozesse auf bodennahe Spurengasmessungen zu ermitteln, wurden umfassende Messungen sowohl bodennah als auch in der atmosphärischen Grenzschicht (mittels Fesselballon) durchgeführt. Dadurch konnte man Ozoneinbrüche, die häufig vormittags an einem Gipfelstandort auftraten, zu einem sehr effizienten Vertikaltransport mittels freier Konvektion zuordnen. Es konnte gezeigt werden, dass sich durch den raschen Transport eine ca. 20 m dicke Schicht in der Gleichgewichtshöhe der freien Konvektion, innerhalb der Residualschicht, bildete. Die chemische Signatur dieser Schicht entsprach jener von bodennaher Luft um diese Tageszeit. Somit entstanden starke chemische Gradienten in der Residualschicht. Es wurden zudem Hinweise gefunden, dass solch ein Transport an mindesten 18 % der Tage im Zeitraum von April bis September auftritt. Nur die Kombination bodennaher Messungen mit in-situ Profilmessungen ermöglichte den Ausschluss sämtlicher weiterer Erklärungsansätze für die Ozoneinbrüche im Gipfelbereich.

Um den dynamischen Messfehler eines bewegten (scannenden) Messsystems relativ zu stationären Messungen bestimmten zu können, wurde eine höhere zeitliche Auflösung der Profile benötigt. Wegen technisch bedingter Limitierungen eines Fesselballonsystems wurde hierzu ein aufzuggestütztes Messsystem verwendet. Es

ermöglichte eine zeitliche Auflösung der Profile von 10 Minuten bei 100 m maximaler Höhe und 1 m vertikaler Auflösung. Anhand dieser Profile wurde die adäquate Korrektur des sogenannten dynamischen Fehlers des Aufzugssystems unter realen (atmosphärischen) Bedingungen getestet. Der dynamische Fehler tritt aufgrund der Ansprechzeit der eingesetzten Sensoren bei jedem bewegten Messsystem auf. Sowohl bereits existierende Algorithmen als auch ein von den Autoren selber entwickelter Algorithmus konnten den dynamischen Fehler zuverlässig ausgleichen. Darüber hinaus konnte gezeigt werden, dass die Messungen des Aufzugsystems sehr gut mit den stationären Referenzdaten am Mast korrelierten. Die Korrelationen erreichten ein Bestimmtheitsmaß von ≥ 0.992 in allen Vergleichshöhen (10, 20, 40, 60, 80, 98 m).

Zur Untersuchung der Eignung verschiedener Verfahren zur Messung reaktiver Spurengasflüsse wurden drei Messtechniken verglichen. Um bodennahe Spurengasflüsse zu bestimmen wurde zudem eine neue Variante der modifizierten Bowen Verhältnis Methode eingesetzt, bei der die Messungen von fühlbarem Wärmestrom räumlich von den Gradientmessungen getrennt waren. Diese Variante ermöglichte eine zeitgleiche Messung mehrerer Spurengase, ohne durch umfangreiche Einlasssysteme die Luftströmung zu stören. Es konnte gezeigt werden, dass dieser Ansatz in horizontal homogenem Gelände einsetzbar ist. Auf diese Weise gemessene NO Flüsse lagen im Bereich von $0.02 - 0.15$ nmol m^{-2} s^{-1} (Emission, Nacht/Tag), Flüsse von NO_2 schwankten um -0.1 nmol m^{-2} s^{-1} (Deposition). In den Nachmittagsstunden wurden leicht positive Werte beobachtet. Der Depositionsfluss von O_3 variierte von nahe 0 nmol m^{-2} s^{-1} (nachts) bis -6 nmol m^{-2} s^{-1} am Tage. Eine Parametrisierung der biogenen Bodenemission von NO, basierend auf inkubierten Bodenproben, ergab Flüsse zwischen 0.025 nmol m^{-2} s^{-1} und 0.12 nmol m^{-2} s^{-1} unter Bedingungen, wie sie im Feld angetroffen wurden – eine hervorragende Übereinstimmung mit den Feldmessungen. Neben dem Vergleich für NO wurden in einer Fallstudie (1 Nacht) Flüsse von CO_2 und O_3 aus der modifizierten Bowen Verhältnis Methode mit Ergebnissen der integralen nächtlichen Grenzschichtbilanzmethode verglichen. Beide Verfahren ergaben vergleichbare nächtliche Flüsse für CO_2 (3.75 µmol m^{-2} s^{-1} und 3.31 µmol m^{-2} s^{-1}). Im Gegensatz dazu ergaben sich im O_3 Fluss stärkere Abweichungen (-0.69 nmol m^{-2} s^{-1} und -2.31 nmol m^{-2} s^{-1}). Diese Abweichung wurde als O_3-Verlust innerhalb der Grenzschicht auf Grund chemischer Reaktionen gedeutet.

1   Introduction

All energy and matter that originates from the earth's surface or goes into or onto its surface has at least one important feature in common: transport through the atmosphere. Without transport, exchange processes would run into a state of equilibrium and finally cease. In the first few millimeters above the surface, transport relies on molecular diffusion only. But a second mechanism becomes important as soon as the distance to the surface increases: turbulent transport. The great importance of the turbulent transport arises from the fact, that it is about 5 orders of magnitude more efficient than molecular diffusion. But there is an even more effective vertical transport mechanism: convection. In a convection cell, transport occurs with the mean vertical flow. Under suitable conditions, the vertical velocity can reach up to several m s^{-1} (Stull, 1988). Transfer of trace gases into or out of the atmosphere is therefore critically dependent on the transport processes being active at a certain time.

The layer of the atmosphere directly adjacent to the earth's surface is called the atmospheric boundary layer (ABL) (Stull, 1988; Arya, 2001). It is the layer which is mechanically, thermally and chemically affected by the presence of the surface and which responds to surface forcing on a timescale of about an hour or less. The diurnal variations of transport processes within the ABL are thus key parameters for investigating transport of trace gases from or to the surface.

The mean diurnal cycle of the ABL structure (typically extending above the ground to heights of between 100 m and 1 km (Arya, 2001)) is governed by the change between day and night. During daytime, incoming radiative energy heats the ground, enabling thermally driven turbulence and thus intense mixing processes in the ABL, hence called convective boundary layer (CBL). With sunset, this source of energy vanishes, and energy from the surface is lost to space by longwave radiation, cooling also the air adjacent to the ground. Because cold air has a higher density than warm air, it rests at the ground and accumulates, forming the stable or nocturnal boundary layer (SBL or NBL, respectively). Stability suppresses thermodynamically driven turbulence, and consequently vertical transport processes are usually very small during this period. For more details see textbooks (e.g. Oke, 1987; Stull, 1988; Arya, 2001).

Special attention has to be given to the morning transition from the NBL to the CBL. The early stage of CBL development is characterized by a balance between the shallow layer of intense mixing adjacent to the ground (i.e. the new CBL) and the turbulence

suppressing remainders of the NBL above. The growth of the CBL follows the mean input of energy by radiation. But small scale (some tens of meters) horizontal heterogeneities of the surface can alter the energy budget at these patches. The heterogeneities would then lead to an imbalance of the available energy for the convective transport and consequently to imbalance of the CBL height and with sufficient available energy intense events of vertical transport can occur. These vertical transport events are in the horizontal dimension very limited (Shen and Leclerc, 1997), but exceed the CBL height in the vertical. This type of transport is known as free convection. Free convection is a state of the atmosphere, when air parcels can start to rise just due to their buoyancy. A mechanical trigger, as for "normal" convection, is then no longer needed (Stull, 1988; Arya, 2001). The state of free convection typically needs two preconditions: enough available energy and low horizontal wind speeds.

Evidence for transport by free convection could be found in many datasets, if they were to be analysed in this respect. Evidence of such processes can be found in Hiller et al. (2008), although this phenomenon was not investigated specifically. Yet Eigenmann et al. (2008) observed similar conditions for free convection.

In detail, transport events by free convection in the morning hours were investigated explicitly by Mayer et al. (2008c, Appendix B) during the SALSA campaign (see Section 2.1).

Active transport mechanisms, deviating from vertical transport by turbulent diffusion, can influence measurements of vertical surface fluxes of energy and tracers in different ways. Free convection for example may appear in surface layer measurements as a period of instationarity. Consequently, quality control schemes applied to eddy covariance measurements would filter these periods out (Foken and Wichura, 1996; Foken et al., 2004). Therefore, direct measurements of vertical profiles of trace gases and air temperature are needed to observe temporal variations within the entire ABL, caused by different transport mechanisms.

Vertical profiles of trace gases are often measured with a tethered balloon (e.g. Pisano et al., 1997; Güsten et al., 1998; Greenberg et al., 1999; Eugster and Siegrist, 2000; Piringer et al., 2001; Glaser et al., 2003; Spirig et al., 2004). Two operational setups are common: (a) a "tethered meteorological tower" with several sondes attached to the tether line at fixed intervals while the balloon is held at constant altitude (e.g. Piringer et al., 2001) and (b) a scanning mode, where one sensor package is attached some meters below the balloon at the tether line, and the balloon is raised and lowered (e.g. Glaser et

al., 2003). The scanning mode is preferred in most cases, because of payload limitations and the deployment of only one sensor per quantity. The latter avoids errors of gradient measurements because the absolute accuracy of the sensors is not relevant. The advantage of a tethered balloon, when using it in scanning mode, is a high spatial resolution, depending on the measuring frequency of the sensors (provided the sensor is fast enough). Furthermore, the maximum height is only limited by the length of the tether line or by legal restrictions.

To evaluate the effect of various transport mechanisms on trace gas fluxes during the SALSA campaign, vertical profiles of trace gases were measured with a tethered balloon in scanning mode (Mayer et al., 2008c).

However, under certain conditions, tethered balloon systems are not recommended, due to limited payload with respect to weight and power requirements and limited ascent and descent speed (to maintain safe flight conditions). The worst disadvantage is that flying a tethered balloon is dependent on suitable weather conditions. Wind speeds must remain below a critical value for safe operation (6 - 12 m s^{-1}, depending on balloon size, winch and tether line strength), turbulence intensity must be relatively low, and thunderstorms must be far enough away. Consequently, vertical profile measurements by a tethered balloon are limited to rather calm, fair weather periods. In addition, if profiles with a ceiling of several 100 m are to be measured in scanning mode, the temporal resolution (i.e. the time between two consecutive measurements at the same height) becomes very low.

Alternative approaches to measure vertical in-situ profiles of trace gases in the ABL are: (a) radiosonde soundings, (b) aircraft measurements or (c) elevator based measurements. The first approach has again the disadvantage of limited payload. Additionally, the instrument package is lost after the sounding, making radiosondes unsuitable for continuous profiling. The approach involving aircrafts can not be used for local profiles (i.e. vertical profiles above a point at the surface) starting at the ground. Legal and safety restrictions limit the lowest flight level to approximately 30 m above ground. Thus, the necessary connection to surface measurements is naturally missing in this approach. Furthermore, because of the high horizontal speed of the aircraft, ultrafast sensors would be needed. Therefore, special attention was given to elevator based measurements. Besides tethered balloon based approaches, elevator based systems, mounted for example on towers or masts, were successfully used for measuring profiles of trace gases (Kottmeier et al., 1980; Wittich and Roth, 1984; Imhof et al., 2005;

Brown et al., 2007). They allowed continuous measurements, independent of weather conditions.

With higher temporal resolution (i.e. the time between two consecutive profiles), also the demands concerning the accuracy of the measurements rise. All moving measurement systems have one possible error source in common: the dynamical error. The dynamical error is caused by the non-zero response time of the sensors deployed. This means that the sensors need some time to equilibrate with the true level of the measured quantity. On a moving system, the sensor is moved further during this equilibration time, encountering a different level of the measured quantity. Thus there will never be a full equilibration during a profile scan (unless the measured quantity is constant with height). This is consequently most important for fast moving systems. Accordingly, algorithms to correct measured data for the dynamical error were developed for aircraft based measurements (Rodi and Spyers-Duran, 1972; McCarthy, 1973; Friehe and Khelif, 1993; Inverarity, 2000). However, they can be also applied to elevator based measurements. The quality of the final data depends on the magnitude of the corrections applied. To exclude artifacts due to the correction, the proper functioning of the algorithms has to be assured. So far, this has been done mostly either theoretically or in laboratory environment, because in-situ reference data are naturally missing for aircraft measurements. These approaches had the disadvantage of not testing the algorithms under the same conditions as the measurements were done.

Mayer et al. (2008b, Appendix C) investigated the accuracy of the correction scheme relative to high quality in-situ reference data during the LIBRETTO campaign (see Section 2.2), and the impact of the correction to the measured profiles. In parallel, a mathematically more simple correction scheme was developed, allowing the correction of sensors with non-exponential response characteristics.

Currently available instruments for measuring trace gases cover a wide range of response times (i.e. how quickly a measurement is completed), ranging from 0.1 s to 30 minutes and more, depending on the trace gas to be measured. Because the different techniques to measure vertical surface fluxes have different intrinsic requirements regarding the temporal resolution of the sensors, various techniques must be used in order to simultaneously measure a comprehensive set of trace gas fluxes. For those trace gases being measurable by more than one method, a comparison of the different techniques can be done in order to (a) prove the similarity of the results from these methods or (b) to explain reasons for deviations. Besides small scale horizontal

heterogeneities of the surface, orographic effects can additionally induce local transport phenomena, which may obscure measurements of turbulent trace gas fluxes at the surface. This would hamper a sound comparison of different techniques for measuring these fluxes. In order to avoid such complications, comparisons of different techniques for measuring vertical turbulent fluxes of trace gases at the surface were done at a flat and thus more ideal site during the LIBRETTO campaign (see Section 2.2). The vertical surface fluxes of trace gases were investigated by applying different measuring techniques: (a) modified Bowen ratio (MBR) (Businger, 1986; Müller et al., 1993; Liu and Foken, 2001), (b) nocturnal boundary layer budget method (BLB) (Denmead et al., 1996; Eugster and Siegrist, 2000) and (c) incubation of soil samples in the laboratory, resulting in the determination of biogenic soil emission fluxes of NO (applying a method similar to van Dijk and Meixner (2001)). If the fluxes of several trace gases have to be measured and analyzer or inlet constructions are somewhat bulky, measurement errors due to flow distortion could become substantial (Dyer, 1981). This problem was addressed by Mayer et al. (2008a, Appendix D) by altering the MBR method in a way, that flux and gradient measurements were spatially separated. This so called distributed modified Bowen ratio method (DMBR) has the advantage of minimizing flow distortion by the instrumentation, because a potentially bulky setup is split (distributed) into different and thus smaller subsets. The application of the DMBR method involves the absolute precondition of horizontal homogeneity with respect to thermal (e.g. soil, vegetation) and turbulent properties (e.g. surface roughness).

To comprehensively explain turbulent surface fluxes of trace gases, the characterization of the ABL with respect to the corresponding trace gases is necessary. This is achieved by the BLB method. It is an integral method to derive vertical surface fluxes of trace gases by relating the temporal difference between the integrals of consecutive profiles (in the absence of advection) to the surface flux. Because this method explicitly uses the vertical profiles, it is dependent on the quality of the profile measurements. Therefore, the proper correction of the dynamical error is a necessary precondition for a sound comparison of the BLB method to others.

All three methods have been compared by Mayer et al. (2008a), with a special emphasis on the reactive trace gases.

1.1 Objectives of this thesis

The overall aim of this thesis is the investigation and description of transport phenomena of reactive and non-reactive trace gases within the ABL with an emphasis on local transport processes. Therefore, simultaneous observations of surface layer fluxes of energy and trace gases are combined with in-situ vertical profiles of the respective quantity. Where possible, different techniques of flux measurements are used and compared with each other in order (a) to determine their degree of agreement and (b) to understand reasons for deviations. The different flux measurement techniques include the (a) eddy covariance method, (b) modified Bowen ratio method (c) nocturnal boundary layer budget method and (d) incubation of soil samples in the laboratory to determine biogenic soil emission fluxes of NO.

The first objective of this thesis is the explanation of a strong and recurrent deviation of the time series of ozone measured at a mountain site from the expected diurnal course. The analyses of the origin of these recurrent deviations involve simultaneous measurements at the mountain summit, at locations at the flank and the foot of the mountain and of in-situ profiles of energy and trace gases within the ABL (by tethered balloon), obtained during the SALSA experiment (see Section 2.1). It is shown by Mayer et al. (2008c, Appendix B), that only the combination of near-surface measurements and ABL profiles enables an unambiguous clarification of the processes behind this phenomenon. Furthermore, the result of this study warrants a modification of the typical assumption of transport patterns in the newly developing CBL.

The second objective is the assessment of measurement errors of (fast) moving sensors and the quality control of specific corrections for this source of errors (Mayer et al., 2008b, Appendix C). Almost every in-situ profiling of the ABL involves moving sensors. The accuracy of applied corrections is thus crucial for flawless observations of the spatial and temporal structure of the ABL. While correction algorithms exist already, their performance under real outdoor conditions has not been examined prior to this thesis. Data for this investigation is from the LIBRETTO campaign (see Section 2.2). The magnitude of the dynamical error is presented relative to quality assured in-situ reference data (Mayer et al., 2008b, Appendix C). Also the effect of applied corrections and the residing error after the application of the corrections is shown in this study.

The third objective is the determination of fluxes of reactive and non-reactive trace gases in the surface layer and the comparison of different measurement methods (Mayer

et al., 2008a, Appendix D). As soon as reactive trace gases are measured, a critical balance between transport time and the speed of chemical reactions comes into play. Chemical reactions affect different flux measuring methods in different ways. This leads to deviations of the measured fluxes between the methods investigated. Therefore, a comparison of different techniques for the determination of fluxes of reactive trace gases can reveal the reasons for the deviations and consequently provide additional information about the magnitude of the chemical alteration.

2   Experiments and data sets

The results presented in this thesis are based on datasets obtained during two field campaigns in which the author participated.

2.1   SALSA

The field experiment SALSA (Beitrag von **SAL**petriger **S**äure zur **A**tmosphärischen OH-Konzentration) was a cooperation project between the Max Planck Institute for Chemistry, Mainz, Department of Biogeochemistry, the German Meteorological Service (DWD), namely its observatory Hohenpeissenberg (MOHp) and the Technical University of Cottbus. Additional contributions to this experiment came from the University of Bayreuth, Department of Micrometeorology, from the University Wuppertal and from the Ludwig Maximilians University Munich, Radiation and Remote Sensing Section.

The SALSA experiment took place from 22 August 2005 until 23 September 2005 at and around the Hohenpeissenberg (German spelling: Hohenpeißenberg), an isolated mountain (47°48'N, 11°02'E, 998 m a.s.l.) in Bavaria, southern Germany. The mountain Hohenpeissenberg is located approximately 70 km southwest of the city of Munich and 40 km north of the northern ridge of the Alps. It is covered by coniferous and mixed forest with some clearings and agriculturally used areas (managed pastures).

The main focus of the SALSA experiment was to investigate the role of nitrous acid (HNO_2) in the atmospheric chemistry, especially its contribution to the concentration of OH radicals. For that, HNO_2 was simultaneously measured at the foot of the mountain (field stations) and on its top (meteorological observatory, MOHp), together with ozone (O_3), nitric oxide (NO), nitrogen dioxide (NO_2), carbon dioxide (CO_2) and water vapour (H_2O). To address the vertical transport between the foot of the mountain and MOHp, a boundary layer profiling station was installed, comprising a SODAR-RASS system (METEK, DSDPA90.64 with 1.29 GHz RASS extension) and a tethered balloon (Vaisala TMT, Boulder, USA). The latter was equipped with meteorological sensors for air temperature, relative humidity, wind speed, wind direction and barometric pressure as well as with trace gas sensors for CO_2 (Vaisala GMP343, Finland) and O_3 (Talbot et al., 2006). Data from this boundary layer profiling station in conjunction with time series of chemical and meteorological quantities at MOHp are the basis of the investigations by Mayer et al. (2008c).

2.2 LIBRETTO

The LIBRETTO (**LI**nden**B**erg **RE**ac**T**ive **T**race gas pr**O**files) experiment took place in late summer 2006, from 01 August 2006 until 31 August 2006 at the Falkenberg Boundary Layer Field Site of the Meteorological Observatory Lindenberg (Richard-Aßmann Observatory) (Beyrich and Adam, 2007). The field site is located at 52°10'01"N, 14°07'27"E, 73 m a.s.l.. LIBRETTO was a small experiment from the Max Planck Institute for Chemistry, Mainz, in cooperation with the Meteorological Observatory Lindenberg (MOL) of the German Meteorological Service (DWD).

The primary scope of the LIBRETTO experiment was the determination of fluxes of reactive trace gases in the surface layer with different methods. For that, two independent measuring setups were installed.

(1) An elevator on a 100 m mast at the site, usually used for service and maintenance, was equipped with sensors for O_3, CO_2, H_2O and air temperature. With a customized control unit, this elevator was continuously run up and down, providing one vertical profile every 10 minutes, with a vertical resolution of 1 m. Comparisons of the deployed sensors with stationary reference sensors at the mast top and at the ground position accompanied every measured profile. More details about the setup of the LIBRETTO experiment are given by Mayer et al. (2008a).

(2) A distributed version of the modified Bowen ratio setup (DMBR) for the determination of the fluxes of CO_2, H_2O, O_3, NO and NO_2 was set up approximately 50 m apart from the elevator profile. It comprised sampling inlets for the trace gas measurements at 0.15 m, 1.0 m and 2.0 m and temperature sensors at 0.25 m, 0.5 m, 1.0 m and 2.0 m. The corresponding determination of the sensible heat flux by eddy covariance technique was done approximately 50 m apart from these measurements on a continuous basis by the DWD.

To yield high quality profile data, a second focus of the LIBRETTO campaign was the correction of the (scanned) elevator profiles. The collocation of the moving elevator system and stationary (i.e. fixed height levels) measurement on the 100 m mast allowed the evaluation of the effectiveness of correction algorithms (McCarthy, 1973; Inverarity, 2000). These algorithms, and a new one (Mayer et al., 2008b) were used to reconstruct the original signal from the recorded elevator system data.

The weather situation during the experiment was moderate. Clouds were present most of the time, heavy rain occurred on 5 days of the experiment. A thunderstorm caused some damage to the trace gas reference system at the mast top in the middle of the

experiment. Wind direction was variable, but westerly winds dominated. Daytime temperature maxima ranged from 20 °C to 25 °C, night time minima sometimes reached down to 10 °C, but in the second half of the experiment they dropped only to about 14 °C. This already indicates that the desired strong atmospheric stability during night times was very rare during LIBRETTO.

3   Results

3.1   Free convection in the morning hours

After sunrise, the development of a convective boundary layer (CBL) with the associated burning off of a surface inversion (Stull, 1988; Arya, 2001) is commonly assumed to be the dominating process for increasing vertical mixing and thus the transition from night time composition of trace gas species near the ground to their typical daytime values. Mayer et al. (2008c) observed during the SALSA experiment (see Section 2.1) another process in the late morning hours, when a pulse of free convection injected air masses from close to the ground into layers well above the top of the developing CBL. Recently, more evidence for such a process was found by Eigenmann et al. (2008). Additional hints for a similar process being active at a third location can be found in the work of Hiller et al. (2008), although they did not address this specific phenomenon.

The consequences of this free convection event were firstly visible in time series of O_3 at the mountain top (Figure 1). A total number of six significant negative excursions of O_3 mixing ratio in the morning hours were observed during the SALSA campaign. The durations of these excursions ranged from 10 to 118 minutes (defined as the span of time during which O_3 levels remained below the half drop value). The observed O_3 reductions ranged from 23 % to 80 % of the initially present O_3. All of the observed events occurred at low wind speeds, in five cases there was a distinct wind speed minimum, lasting 2 to 3 hours.
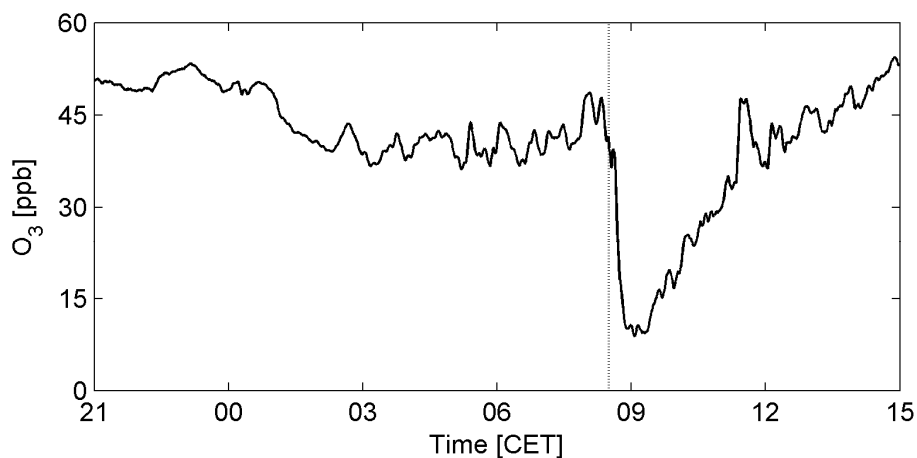
Figure 1: Example of a negative O_3 excursion event at the mountain summit, observed during the SALSA campaign on 5th September 2005. The grey line indicates the onset of the event. Figure taken from Mayer et al. (2008c, Appendix B).

As a case study, the most intensive event was analyzed in detail by Mayer et al. (2008c). The advantage of this study was to have simultaneous observations of trace gas concentration and meteorological parameters at a mountain summit, at the flank and at the foot of the mountain. In parallel, profiles of meteorological quantities and the trace gases CO_2, H_2O and O_3 were measured from the foot of the mountain up to well above
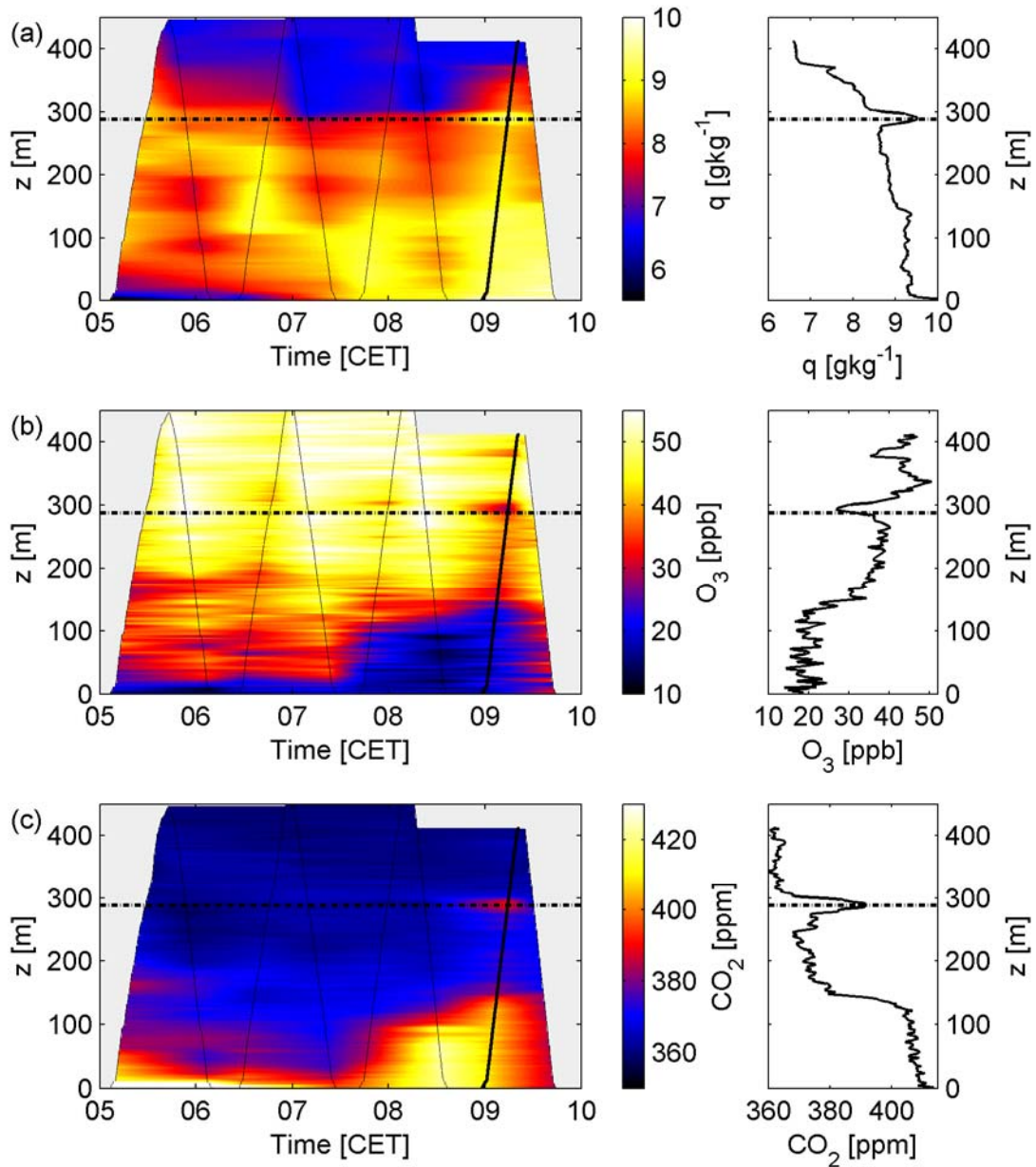
Figure 2: Time-height cross sections and profiles of (a) specific humidity q, (b) O_3 mixing ratio and (c) CO_2 mixing ratio for the morning of 5th September 2005 ca. 09:00 h. The actual flight path of the tethered balloon is indicated by the thin black line. Profiles on the right side show the upward scan of the tethered balloon at the time when the O_3 drop was observed at the mountain summit (corresponding to the actual flight path marked with a thick black line). Figure taken from Mayer et al. (2008c, Appendix B).

its summit by a tethered balloon. Only this setup allowed the linking of the following simultaneous observations: (a) O_3 decrease events at the mountain top, (b) temperature decreases at the foot of the mountain although there was clear sky, (c) the possibility of free convection, indicated by a dynamic stability measure and (d) a layer with low O_3 but high CO_2 and H_2O values at the altitude of the mountain summit, but in a horizontal distance of about 1.6 km over its foot. This was a location well within the residual layer. The corresponding profiles, obtained with a tethered balloon system, are shown in Figure 2.

An analysis of a 5 year long O_3 time series at the mountain summit for similar O_3 decrease events confirmed, that the O_3 drop events were not only observed during the field experiment but were present throughout the entire time series from October 2000 to December 2005. It was found, that on 18 % of the days between April and September, the O_3 decreases were most likely the result of a free convective pulse in the early morning.

Considering the observed event durations in comparison with the profiling frequency (as it is indicated by the lines in Figure 2, left panels), the need for a higher temporal resolution is obvious. This was realized in a following experiment by using an elevator based measuring system. As soon as higher scanning speeds play a role, special attention has to be paid to specific errors of moving sensors. This topic will be addressed in the following section.

3.2 Correction for moving measurement systems

The unprecedented advantage of the LIBRETTO setup was the coexistence of (a) high quality reference data, provided by the stationary measurements at the tower, and (b) the high-resolution experimental data, provided by the elevator. This allowed us to directly quantify the effect of the applied corrections relative to parallel measured reference data. The correction of the dynamical error had to adjust for two aspects: firstly, the low sensor response dampened the amplitude of the small scale temporal fluctuations (durations of some seconds), which were to be intensified by the correction. Secondly, the mean shape of the (uncorrected) profiles was altered due to the delay induced by the response time. In contrast to a continuous lag time, this delay depended on the magnitude of the gradients encountered by the sensor. The algorithm thus had to correct this gradient dependent delay. A demonstration of both effects as well as of the applied correction is given in Figure 3, where corresponding profiles of air temperature (19
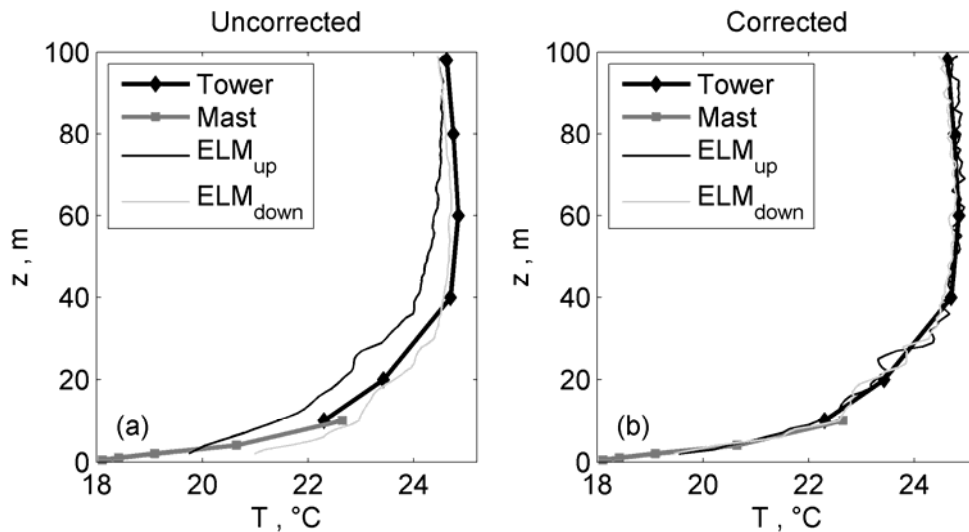
Figure 3: Vertical profiles of air temperature around 21:30 h (19 August 2006). Between 2 m and 40 m, there is a very strong surface inversion (>6 K). The deviation of the profiles measured by the elevator system (ELM, thin lines) from the reference tower and profile (thick lines) vanishes after application of the corrections, while the intensity of small scale fluctuations increases visually. Figure taken from Mayer et al. (2008b, Appendix C).

August, 2006; 21:30 h local), for upward and downward movement of the elevator are shown.

In order to demonstrate the power of the correction schemes, we selected from the entire experimental period the sub-set of data where the largest dynamical errors of the moving sensor are to be expected ("worst case scenario"). A very strong surface inversion was identifiable in the lowest 40 m, with a temperature increase of more than 6 K. Above the inversion, the temperature profile showed neutral conditions with respect to static stability. Besides this mean profile shape, the elevator profiles showed small scale fluctuations in the order of few meters, embedded in the mean profile. The strongest one could be seen in the upward scanned profile at 25 m. It showed a neutral layer of approximately 3 m thickness within the stably stratified surrounding. Especially noteworthy is the discrepancy between the upward and the downward scanned profile of the ELM (Figure 3a). At 99 m, both profiles yielded the same value, but at lower levels they differed significantly. This was the result of a hysteresis, introduced by the slowing part of the sensor, i.e. the sensors housing. In the presence of a gradient, such as the temperature inversion shown here, the low sensor response lead to a memory of the sensor about temperatures encountered in the seconds before. If it was colder, the actual measured value was too cold compared to the true value (upward scan under inversion conditions), and vice versa. After the application of the corrections, the hysteresis was no longer observable (Figure 3b).

3.3   Surface layer fluxes of trace gases

3.3.1   Trace gas fluxes with DMBR method

During the LIBRETTO campaign the surface layer fluxes of non-reactive (CO_2, H_2O) and also of reactive trace gases (NO, NO_2, O_3) were computed by using a distributed modified Bowen ratio method (DMBR) (Mayer et al., 2008a, Appendix, D). Because of the spatial separation between the measurements included in this method, the horizontal homogeneity of the experimental site with respect to the sensible heat flux H was an absolute precondition for the application of the DMBR method. The fulfilment of this precondition was tested by comparing vertical temperature difference at the place of the measurements of H and at the place of the measurements of trace gas concentration differences. Figure 4 shows the comparison, confirming the homogeneity by a good agreement between the temperature differences at both locations.
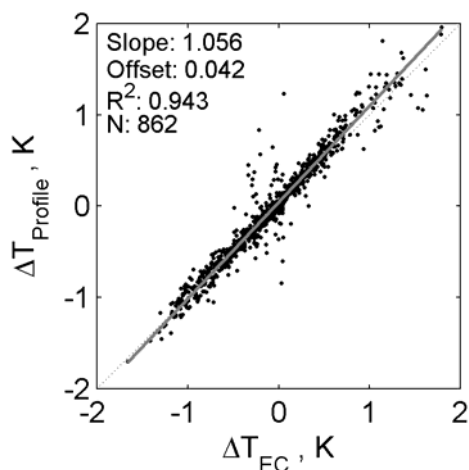
Figure 4: Comparison of measured temperature differences at the profile station with the temperature differences at the EC station. The dashed line gives the 1:1 ratio, the solid grey line indicates the linear regression. Figure taken from Mayer et al. (2008a, Appendix D).

For passive trace gases, the corresponding fluxes, as computed from the measured vertical difference of mixing ratios, can be regarded as valid without further considerations. During 20 days of the LIBRETTO campaign, the median fluxes of CO_2 (Figure 5a) were of comparable magnitude as reported from other sites (Frank and Dugas, 2001; Frank, 2002). The flux of H_2O showed a very clear diurnal cycle with low or almost slightly negative values during night times (Figure 5b).
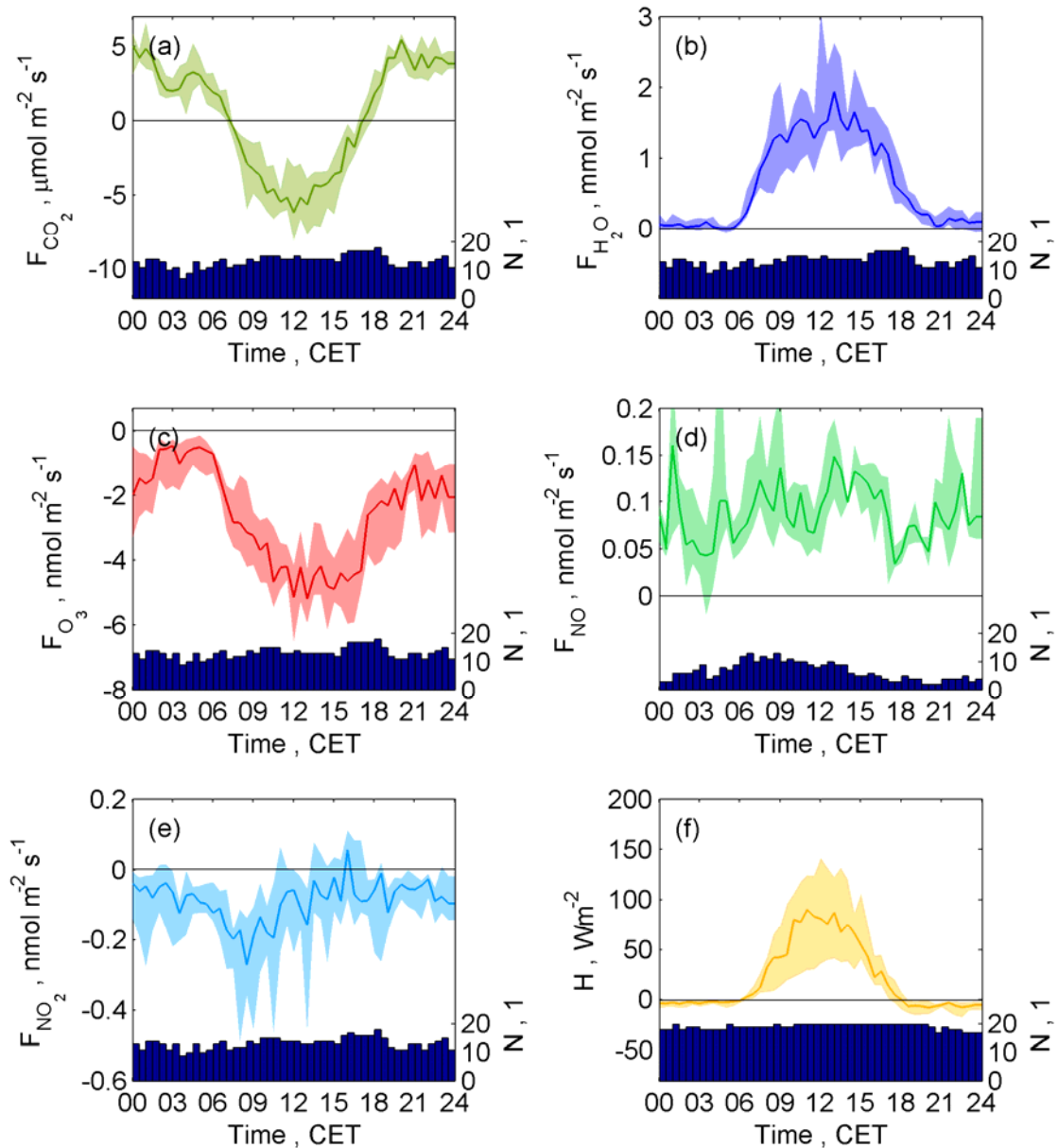
Figure 5: Median (lines) diurnal course of the fluxes of (a) CO_2, (b) H_2O, (c) O_3, (d) NO, (e) NO_2 and (f) sensible heat from 11 August 2006 to 30 August 2006. Colored areas comprise the respective inter quartile ranges. The bars at the bottom of each graph show the number of values available for the corresponding median and quartiles. Figure taken from Mayer et al. (2008a, Appendix D).

The flux of O_3 was found to be always directed towards the surface (Figure 5c). This was expected, as no source of O_3 is known at the surface, while O_3 is destroyed by dry deposition onto surfaces (soil, plants) and during daytime additionally by stomatal uptake. An additional O_3 sink at the surface results from NO emission from the soil. The effect of the additional sink of O_3 during daytime is clearly visible in the median diurnal flux of O_3, showing strongest downward fluxes in the early afternoon. The higher fluxes started with sunrise around 06:00 h and ended with sunset around 18:00 h.

In contrast to O_3, NO has a source at the ground. It is produced by microorganisms in the soil, leading to a net production and thus a positive flux (Figure 5d). Considering only meteorological parameters, microbial NO production is, besides soil moisture, primarily dependent on soil temperature (Q_{10} law). Thus, highest production rates and therefore fluxes were expected around noon or early afternoon, when highest soil temperatures were observed. While positive fluxes were observed throughout the day, a diurnal cycle of the flux was barely visible with values around $0.1\ \mathrm{nmol\ m^{-2}\ s^{-1}}$. Nevertheless, a small decrease in the NO flux was observed shortly before sunset. During the night, the NO flux slowly increased back to its previous level.

The median NO_2 flux remained most of the time negative (Figure 5e), indicating a net deposition. A maximum deposition flux was observed at 08:30 h. This could be attributed to advection events. If days with advection affecting the site were excluded in the analysis, the NO_2 flux did not show the negative excursion. In the early afternoon, small positive NO_2 fluxes were observed. During the night, the NO_2 flux remained slightly negative. Besides the trace gases, H is also shown (Figure 5f). It exhibited very small, negative values during night time (not more than $-5\ \mathrm{W\ m^{-2}}$). With sunrise, H increased rapidly, reaching maximum values around noon. In the afternoon, H decreased again and dropped below zero around 18:00 h, indicating the onset of surface cooling.

In contrast to passive trace gases, the calculation of fluxes of reactive trace gases must take into account possible influences due to chemical reactions. The intensity of chemical alteration of the mixing ratios during the vertical transport between the DMBR
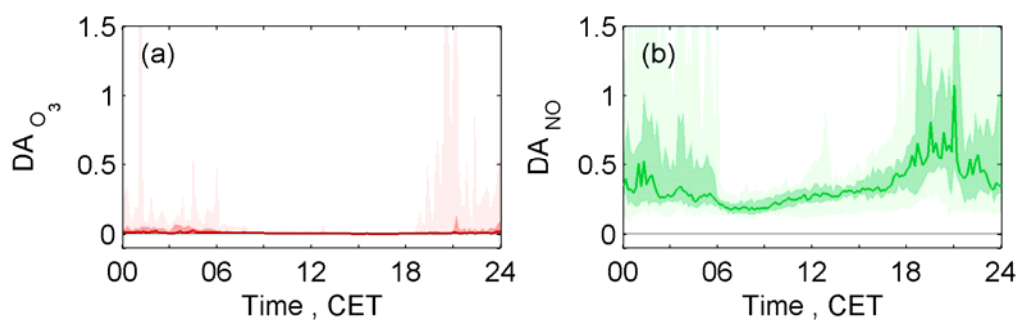
Figure 6: Median diurnal cycle of the dimensionless Damköhler numbers (DA) for the period of 11 August 2006 – 30 August 2006. The individual Damköhler numbers for (a) O_3 and (b) NO are shown. The solid line indicates the median, the dark shaded areas cover the interquartile range, and the light shaded areas comprise the range from the 5th percentile to the 95th percentile. Figure taken from Mayer et al. (2008a, Appendix D).

measuring heights is reflected by the Damköhler number (Figure 6). The Damköhler number represents the ratio of turbulent transport time scale to the timescales of relevant chemical reactions during the transport. It is shown by Mayer et al. (2008a), that O_3 at a site with low NO mixing ratio (typically less than 1 ppb during the LIBRETTO campaign) can be assumed as quasi passive (Figure 6a). However, some measurements during night are nevertheless affected by chemical reactions. This happens, if turbulence ceases, and the transport time increases dramatically. Such situations are often observed in the first part of the night, when turbulence is suppressed due to very strong stabilization. Also NO_2 was found to act quasi passively. For NO, the situation is different. NO is destroyed by reaction with O_3. Low NO values together with relative high O_3 mixing ratios (typically more than 20 ppb during the LIBRETTO campaign) lead to fast destruction of NO. This is clearly visible in the Damköhler number for NO (Figure 6b). The median Damköhler number was about 0.25, indicating that more than 50 % of the NO concentration difference data were severely affected by chemical reaction. To derive correct flux data from the concentration differences, only NO data with corresponding Damköhler number < 0.25 were used. This assured derived fluxes to be only negligibly affected by chemical reactions, because turbulent transport is assured to be at least four times faster than the chemistry

3.3.2 Comparison DMBR and laboratory: NO fluxes

Because chemical reaction will affect different methods for flux measurements differently, additional information and certainty about the derived fluxes can be gained
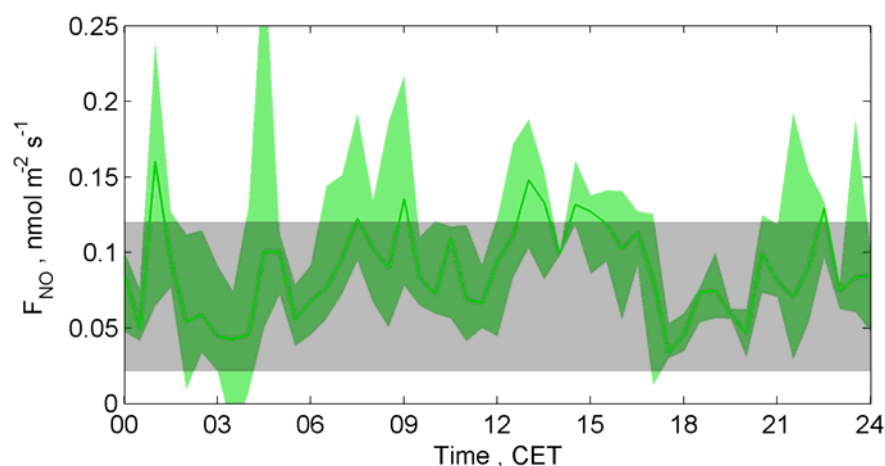
Figure 7: Median diurnal course of NO flux from field measurements using the DMBR method (green) and range of flux data from laboratory measurements (grey) for the period of 11 August 2006 – 30 August 2006. The laboratory data were parameterized with the field data of soil moisture and soil surface temperature. Figure taken from Mayer et al. (2008a, Appendix D).

by comparing different approaches. Two such comparisons are presented by Mayer et al. (2008a). For the flux of NO, the micrometeorological DMBR method is compared with laboratory parameterizations based on the analysis of soil samples. The resulting range of the NO flux is shown together with the field data in Figure 7. The large scatter in the DMBR results originates from the limitation of data validity to Damköhler numbers less than 0.25. Nevertheless, an excellent agreement within a factor of two can be found between laboratory data and field data.

3.3.3 Comparison of DMBR and boundary layer budget method

As a case study for O_3, the nocturnal boundary layer budget method was compared with the fluxes derived with the DMBR method. In this second comparison, the passive tracer CO_2 was included to distinguish whether differences between the methods originated from the different methods themselves or from the reactivity of O_3. The combination of reactive and passive tracers revealed principle differences between the two methods. While for passive tracers both methods yielded similar results, at least
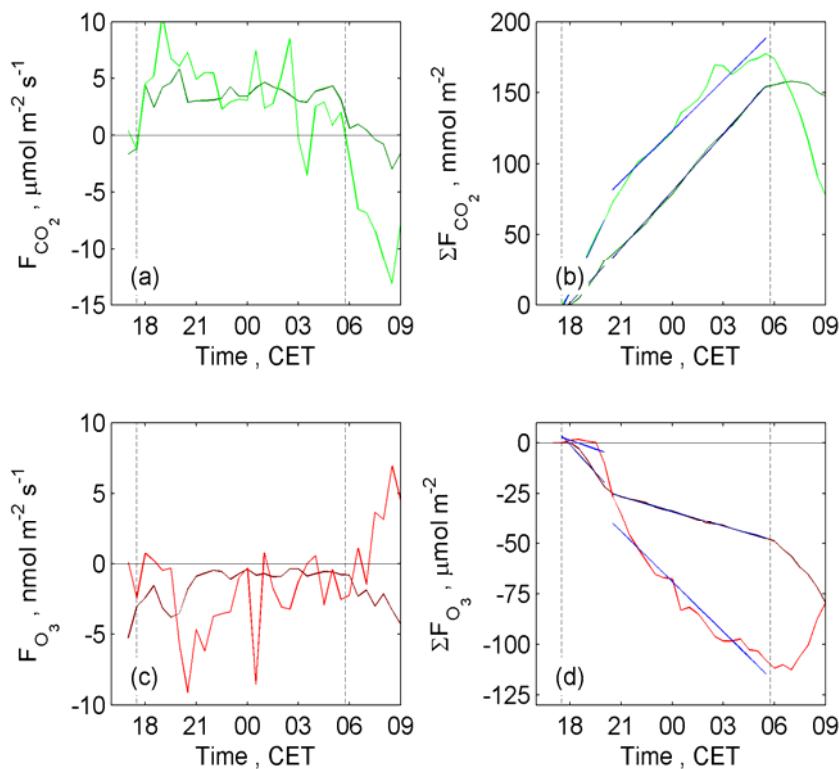
Figure 8: Comparison of fluxes of CO_2 (F_{CO2}) and O_3 (F_{O3}) measured with the DMBR method (dark colors) and derived with the NBL budget method (light colors). Panels (a) and (c) show the 30 minute values of the respective fluxes, while panels (b) and (d) show the cumulative flux since onset of surface cooling (indicated by the left dashed line) The right dashed line marks the onset of heating after sunrise. Figure taken from Mayer et al. (2008a, Appendix D), modified.

after an initial equilibration time of the ABL (i.e. after 21:00 h), deviations were observed for O_3 (Figure 8). Fluxes from the NBL budget method exceeded the fluxes measured with the DMBR method. This difference resulted from the large spatial scale of the NBL budget measurements, comprising the first 100 m above ground level (Mayer et al., 2008a). Within this spatial dimension, also O_3 suffered from chemical destruction. This in-situ loss added to the loss onto the surface. The combined loss per unit time was then recalculated into a flux, resulting in the greater magnitude of the NBL budget derived O_3 flux. With simultaneous determination of the O_3 flux with the DMBR and the NBL budget method, the magnitude of chemical loss of O_3 within the layer covered by the profile measurements can be determined.

4 Conclusions

The main findings of the present work (this PhD thesis) can be concluded as follows:

(1) Free convection can occur rather frequently at certain locations in the morning hours. It then provides a powerful (even spatially very limited) vertical transport mechanism for trace gases, far exceeding the intensity of mean turbulent vertical transport at this time. Although hints pointing toward such a transport process can be found in other works (e.g. Hiller et al., 2008) it was the study by Mayer et al. (2008c) which clearly linked cause and effect of early morning free convection transport. Furthermore, the successful combination of simultaneous profile and ground based measurements proved to be important for identifying transport phenomena in the ABL (Mayer et al., 2008c).

(2) It has been shown that the mean diurnal cycle of the state of the ABL (Stull, 1988) is not sufficient to even estimate the magnitude of vertical transport on a more local scale. A revision of the picture about the evolution of the CBL under certain conditions is thus needed, especially if exchange processes between the surface and higher altitudes within the ABL are investigated. Injection of air masses into levels above the top of the CBL by means of free convection pulses are rather frequent, and may be a typical feature in the morning hours at many sites which are prone to these events. Nevertheless, the consequences of this fast transport mechanism on the chemistry of the ABL are yet unsettled and should be subject to intensive future research.

(3) It has to be admitted that Mayer et al. (2008c) had some luck when observing the free convection event with the tethered balloon system. In fact, the temporal distance of two subsequent profiles with a tethered balloon system in scanning mode is too long for a monitoring of such transport events. The higher the profiles become, the worse the temporal resolution. The risk of just missing an event between two scans increases. Only a partial improvement is thus the limitation to shorter profiles, preferably measured with an elevator based system to be independent of weather conditions. For a 100 m profile, a temporal resolution of 10 minutes can be realized (Mayer et al., 2008b).

(4) Concerning the dynamical error, it was demonstrated with field and laboratory data by Mayer et al. (2008b), that presently used correction algorithms (McCarthy, 1973; Inverarity, 2000) provide an accurate reproduction of the original signal. The

advantage of the present work is to evaluate the performance of the correction algorithms under realistic conditions with a variety of air flow and radiation conditions. Also a simpler correction algorithm, developed by Mayer et al. (2008b), yields reliable results.

(5) Elevator based scanning profiling systems can provide data of sufficient quality to replace measurements at fixed levels under stationary conditions (Mayer et al., 2008b). For instationary conditions, the comparison of scanning profiling system and fixed-level measurements is more complex. While fixed-level measurements provide simultaneous measurements at all levels with limited spatial resolution, this simultaneity is sacrificed in scanning systems to yield a higher spatial resolution. Under instationary conditions, the non-simultaneity will lead to some errors in the determination of vertical gradients from single profiles. However, if processes with longer typical time scales are to be investigated (e.g. turbulent surface fluxes are typically measured with 30 minutes resolution), the disadvantage of non-simultaneity becomes less important. But the high spatial resolution remains relevant. Thus, the scanning measuring system is the preferred setup to investigate vertical profiles of trace gases with in-situ measurements on time scales larger than the time needed to perform a full scan.

However, for the investigation of small scale processes, the time of a scanning profiling system needed for consecutive profiles provides a lower limit for the temporal dimensions of observable structures. In contrast, the fixed-level measurements are limited in the spatial dimension. Because both scales are linked for atmospheric processes (Orlanski, 1975), the limitation is basically not solved, unless the temporal resolution of scanning profiling systems can be increased.

(6) For non-moving systems, a correction of the dynamical error may be also relevant in case of instationary periods. Such situations may occur close to thunderstorms, when cold air downdrafts change local air temperature very rapidly. Also the advection of trace gas plumes (in vertically very limited layers) can create very high instationarities, resulting in an underestimation of the peak magnitude of the plume, unless a correction is applied.

(7) For the determination of surface fluxes it is possible to horizontally separate the measurements of the sensible heat flux from the gradient measurements when applying the modified Bowen ratio method (Mayer et al., 2008a). However, this is

only permitted in horizontally homogeneous terrain – a precondition which has to be tested under field conditions. This distributed approach enables various trace gas fluxes to be measured without creating flow distortion due to bulky instrumentation.

(8) The combination of different methods for the determination of trace gas fluxes, as demonstrated by Mayer et al. (2008a), can reveal additional information about the magnitude of chemical alterations within the ABL. However, such an approach is limited to uniform and flat terrain. Complex terrain would increase the complexity of the boundary layer structure. A three dimensional sensor array would be needed to discriminate between chemically induced and terrain induced variations.

5   References

Arya, S. P. S.: Introduction to Micrometeorology, Intern. Geophys. Ser., Academic Press, San Diego, CA., 420 pp., 2001.

Beyrich, F., and Adam, W. K.: Site and Data Report for the Lindenberg Reference Site in CEOP – Phase I, Deutscher Wetterdienst, Offenbach, 230, 55 pp., 2007.

Brown, S. S., Dubé, W. P., Osthoff, H. D., Wolfe, D. E., Angevine, W. M., and Ravishankara, A. R.: High resolution vertical distributions of NO3 and N2O5 through the nocturnal boundary layer, Atmos. Chem. Phys., 7, 139-149, 2007.

Businger, J. A.: Evaluation of the Accuracy with Which Dry Deposition Can Be Measured with Current Micrometeorological Techniques, J. Clim. Appl. Meteorol., 25, 1100-1124, 1986.

Denmead, O. T., Raupach, M. R., Dunin, F. X., Cleugh, H. A., and Leuning, R.: Boundary layer budgets for regional estimates of scalar fluxes, Global Change Biology, 2, 255-264, 1996.

Dyer, A. J.: Flow distortion by supporting structures, Boundary-Layer Meteorol., 20, 243-251, 1981.

Eigenmann, R., Metzger, S., Siebicke, L., Staudt, K., Serafimovich, A., and Foken, T.: Generation of free convection in a valley due to changes of the local circulation system, 18th Symposium on Boundary Layers and Turbulence, Am. Meteorol. Soc., Stockholm, June 09-13, 2008.

Eugster, W., and Siegrist, F.: The influence of nocturnal CO_2 advection on CO_2 flux measurements, Bas. Appl. Ecol., 1, 177-188, 2000.

Foken, T., and Wichura, B.: Tools for quality assessment of surface-based flux measurements, Agric. For. Meteorol., 78, 83-105, 1996.

Foken, T., Göckede, M., Mauder, M., Mahrt, L., Amiro, B. D., and Munger, J. W.: Post-field data quality control, in: Handbook of Micrometeorology: A Guide for Surface Flux Measurements, edited by: Lee, X., Kluwer, Dordrecht, 81-108, 2004.

Frank, A. B., and Dugas, W. A.: Carbon dioxide fluxes over a northern, semiarid, mixed-grass prairie, Agric. For. Meteorol., 108, 317-326, 2001.

Frank, A. B.: Carbon dioxide fluxes over a grazed prairie and seeded pasture in the Northern Great Plains, Env. Pollut., 116, 397-403, 2002.

Friehe, C. A., and Khelif, D.: Fast-Response Aircraft Temperature Sensors, J. Atmos. Ocean. Technol., 9, 784-795, 1993.

Glaser, K., Vogt, U., Baumbach, G., Volz-Thomas, A., and Geiss, H.: Vertical profiles of O_3, NO_2, NO_x, VOC, and meteorological parameters during the Berlin Ozone Experiment (BERLIOZ) campaign, J. Geophys. Res., 108, 8253-8253, 2003.

Greenberg, J. P., Guenther, A., Zimmerman, P., Baugh, W., Geron, C., Davis, K., Helmig, D., and Klinger, L. F.: Tethered balloon measurements of biogenic VOCs in the atmospheric boundary layer, Atmos. Environ., 33, 855-867, 1999.

Güsten, H., Heinrich, G., and Sprung, D.: Nocturnal depletion of ozone in the Upper Rhine Valley, Atmos. Environ., 32, 1195-1202, 1998.

Hiller, R., Zeeman, M. J., and Eugster, W.: Eddy-covariance flux measurements in the complex terrain of an Alpine valley in Switzerland, Boundary-Layer Meteorol., 127, 449-467, 2008.

Imhof, D., Weingartner, E., Vogt, U., Dreiseidler, A., Rosenbohm, E., Scheer, V., Vogt, R., Nielsen, O. J., Kurtenbach, R., Corsmeier, U., Kohler, M., and Baltensperger, U.: Vertical distribution of aerosol particles and NOx close to a motorway, Atmos. Environ., 39, 5710-5721, 2005.

Inverarity, G. W.: Correcting Airborne Temperature Data for Lags Introduced by Instruments with Two-Time-Constant Responses, J. Atmos. Ocean. Technol., 17, 176-184, 2000.

Kottmeier, C., Lege, D., and Roth, R.: Ein Meßsystem zur Sondierung der planetaren Grenzschicht, Meteorol. Rdsch., 33, 9-13, 1980.

Liu, H., and Foken, T.: A modified Bowen ratio method to determine sensible and latent heat fluxes, Meteorol. Z., 10, 71-80, 2001.

Mayer, J.-C., Bargsten, A., Rummel, U., Meixner, F. X., and Foken, T.: Distributed Modified Bowen Ratio Method for Surface Layer Fluxes of reactive and non-reactive Trace Gases, Atmos. Chem. Phys., in preparation, 2008a.

Mayer, J.-C., Hens, K., Rummel, U., Meixner, F. X., and Foken, T.: Moving measurement platforms - specific challenges and corrections, Meteorol. Z., resubmitted, 2008b.

Mayer, J.-C., Staudt, K., Gilge, S., Meixner, F. X., and Foken, T.: The impact of free convection on late morning ozone decreases on an Alpine foreland mountain summit, Atmos. Chem. Phys., 8, 5941–5956, 2008c.

McCarthy, J.: A Method for Correcting Airborne Temperature Data for Sensor Response Time, J. Appl. Meteorol., 12, 211-214, 1973.

Müller, H., Kramm, G., Meixner, F., Dollard, G. J., Fowler, D., and Possanzini, M.: Determination of HNO_3 Dry Deposition by Modified Bowen-Ratio and Aerodynamic Profile Techniques, Tellus Series B, 45, 346-367, 1993.

Oke, T. R.: Boundary layer climate, Routledge, London and New York, 435 pp., 1987.

Orlanski, I.: A rational subdivision of scales for atmospheric processes, Bull. Amer. Meteorol. Soc., 56, 527-530, 1975.

Piringer, M., Baumann, K., Pechinger, U., and Vogt, S.: Meteorological and ozone sounding experience during a strong foehn event - a MAP case study, Meteorol. Z., 10, 445-455, 2001.

Pisano, J. T., McKendry, I., Steyn, D. G., and Hastie, D. R.: Vertical nitrogen dioxide and ozone concentrations measured from a tethered balloon in the Lower Fraser Valley, Atmos. Environ., 31, 2071-2078, 1997.

Rodi, A. R., and Spyers-Duran, P. A.: Analysis of Time Response of Airborne Temperature Sensors, J. Appl. Meteorol., 11, 554-556, 1972.

Shen, S., and Leclerc, M. Y.: Modelling the turbulence structure in the canopy layer, Physical and Biophysical Processes in the Vegetation Environment, 87, 3-25, 1997.

Spirig, C., Guenther, A., Greenberg, J. P., Calanca, P., and Tarvainen, V.: Tethered balloon measurements of biogenic volatile organic compounds at a Boreal forest site, Atmos. Chem. Phys., 4, 215-229, 2004.

Stull, R. B.: An introduction to boundary layer meteorology, Kluwer Academic Puplisher, Dordrecht, 666 pp., 1988.

Talbot, R., Mao, H., Troop, D., Moore, B., Johnson, R., and Businger, S.: Smart balloon observations over the North Atlantic: Part I - Mini-O_3 sampling of urban plumes, J. Geophys. Res., in press, 2006.

van Dijk, S. M., and Meixner, F. X.: Production and Consumption of NO in Forest and Pasture Soils from the Amazon Basin, Water, Air, & Soil Pollution: Focus, 1, 119-130, 2001.

Wittich, K.-P., and Roth, R.: A Case Study of Nocturnal Wind and Temperature Profiles over the Inhomogeneous Terrain of Northern Germany with some Considerations of Turbulent Fluxes, Boundary-Layer Meteorol., 28, 169-186, 1984.

List of Appendices

List of Appendices

APPENDIX A: Individual contributions to the joint publications

APPENDIX B: <u>Mayer, J.-C.</u>, Staudt, K., Gilge, S., Meixner, F.X. and Foken, T.: The impact of free convection on late morning ozone decreases on an Alpine foreland mountain summit, Atmospheric Chemistry and Physics, 8, 5941-5956, 2008.

APPENDIX C: <u>Mayer, J.-C.</u>, Hens, K., Rummel, U. Meixner, F.X. and Foken, T.: Moving measurement platforms – specific challenges and corrections, Meteorologische Zeitschrift, revised version submitted, 2008.

APPENDIX D: <u>Mayer, J.-C.</u>, Bargsten, A., Rummel, U., Meixner, F.X. and Foken, T.: Distributed Modified Bowen Ratio Method for Surface Layer Fluxes of reactive and non-reactive Trace Gases, Atmospheric Chemistry and Physics Discussions, to be submitted, 2008.

APPENDIX A: INDIVIDUAL CONTRIBUTIONS TO THE JOINT PUBLICATIONS

The publications of which this cumulative thesis consists were composed in close cooperation with other researchers. Hence, other authors also contributed to the publications listed in appendices B to D in different ways. This section is to specify my own contributions to the individual manuscripts.

APPENDIX B

Mayer, J.-C., Staudt, K., Gilge, S., Meixner, F.X. and Foken, T.: The impact of free convection on late morning ozone decreases on an Alpine foreland mountain summit, Atmospheric Chemistry and Physics, 8, 5941–5956, 2008.

I was fully responsible for the planning, set-up, test, and performance of station "BASE#2", where boundary layer observations were done by a SODAR-RASS system and a collocated tethered balloon system. Responsibilities comprised (among others) decisions about the timing of tethered balloon flights, operation mode of SODAR-RASS and tethered balloon systems and the design and construction of the trace gas sensor package for the tethered balloon. The post processing of the tethered balloon data (calculation of height a.g.l., temperature and pressure corrections of data) was done by me as well as processing of the SODAR data with a strong quality control scheme. I developed the presented scheme for the automated detection used for the analysis of a more than 5 year long dataset from the Hohenpeissenberg observatory, and it was primarily me who analyzed the data from all stations involved in the field campaign for the periods of O_3 decrease events. The entire publication was written by me, except for Section 4.5.

I advised partly the Diploma thesis of K. Staudt, who assisted me in the analysis of data obtained simultaneously with the O_3 drop events and did the computation of mixed layer height (Section 4.5). She also wrote the paragraphs dealing with the mixed layer development.

S. Gilge provided all the data from the observatory and helped in several discussions to exclude local effects from the very surrounding of the observatory.

F.X. Meixner provided additional ground based data (forest station) and contributed to this work in helpful discussion and critical manuscript reviews.

T. Foken, as my supervisor, encouraged the structure of this publication and contributed to it through many discussions and initially pointed to the possibility of free convection as one process to be considered.

APPENDIX C

Mayer, J.-C., Hens, K., Rummel, U. Meixner, F.X. and Foken, T.: Moving measurement platforms - specific challenges and corrections, Meteorologische Zeitschrift, revised version submitted, 2008.

Data used in this manuscript were obtained during the LIBRETTO campaign. In this campaign, I had the full responsibility for the entire logistics, the experimental design, the development of special instrumentation, the performance of the measurements and the entire data processing. I did all necessary corrections and data conversions and applied a quality control scheme developed by me to the measured data. The structure of this manuscript was developed by me, and I wrote most of the manuscript.

K. Hens programmed the pre-existing correction algorithms and contributed with the mathematical descriptions (Section 2.2.2). He also contributed in several discussions during the preparation of the manuscript.

U. Rummel was the responsible contact person at the site of the LIBRETTO campaign. He coordinated the interaction between the German Meteorological Service and us, and he provided additional data from the site, being measured there on a routine basis.

F.X. Meixner contributed to the field campaign and to this manuscript in several scientific discussions.

T. Foken helped to design the field campaign, especially in separating important and not so important measurements. As my doctoral advisor, he contributed to this manuscript in many fruitful scientific discussions.

APPENDIX D

Mayer, J.-C., Bargsten, A., Rummel, U., Meixner, F.X. and Foken, T.: Distributed Modified Bowen Ratio Method for Surface Layer Fluxes of reactive and non-reactive Trace Gases, Atmospheric Chemistry and Physics Discussions, to be submitted, 2008.

I was fully responsible for the entire logistics, the experimental design, the development of special instrumentation, the performance of the measurements and the entire data processing. I did all necessary corrections and data conversions and applied a quality control scheme developed by me to the measured data. The structure of this manuscript was developed by me, and I wrote all parts of the manuscript, except the description of the laboratory setup and measurements.

A. Bargsten did the laboratory analyses of the soil samples and provided the description of the dependency of soil NO emissions on soil moisture and soil temperature. She contributed the description of the laboratory setup and the corresponding measurements.

U. Rummel provided additional meteorological data from the field site and contributed with suggestions to the preparation of the manuscript.

F.X. Meixner contributed to the field campaign and to this manuscript in several scientific discussions and was an invaluable help during the revisions of the manuscript.

T. Foken helped to design the field campaign, especially in separating important and not so important measurements. As my doctoral advisor, he contributed to this manuscript in many fruitful scientific discussions.

Appendix B:

The impact of free convection on late morning ozone decreases on an Alpine foreland mountain summit

J.-C. Mayer[1], K. Staudt[2], S. Gilge[3], F.X. Meixner[1,4] and T. Foken[2]

[1] Biogeochemistry Department, Max Planck Institute for Chemistry, Mainz, Germany
[2] Department of Micrometeorology, University of Bayreuth, Bayreuth, Germany
[3] German Meteorological Service, Observatory Hohenpeißenberg, Hohenpeißenberg, Germany
[4] Department of Physics, University of Zimbabwe, Harare, Zimbabwe

Abstract

Exceptional patterns in the diurnal course of ozone mixing ratio at a mountain top site (998 m a.s.l.) were observed during a field experiment (September 2005). They manifested themselves as strong and sudden decreases of ozone mixing ratio with a subsequent return to previous levels. The evaluation of corresponding long-term time series (2000-2005) revealed that such events occur mainly during summer, and affect the mountain top site on about 18 % of the summer days. Combining (a) surface layer measurements at mountain summit and at the foot of the mountain, (b) in-situ (tethered balloon) and remote sensing (SODAR-RASS) measurements within the atmospheric boundary layer, the origin of these events of sudden ozone decrease could be attributed to free convection. The free convection was triggered by a rather frequently occurring wind speed minimum around the location of the mountain.

1 Introduction

A sudden drop of the mean mixing ratio of any trace gas species down to around 20 % of its initial value is, without doubt, noticeable. If this happens at a place and time of the day, where it is not expected from present knowledge, it is worth to be studied more thoroughly. Furthermore, if such events occur frequently, it warrants further study,

Correspondence to: J.-C. Mayer
(jcmayer@mpch-mainz.mpg.de)

particularly for measurements being made at comparable sites. Because a high frequency of occurrence may affect the statistical description of the mean temporal behaviour, these events should be well understood.

The mean diurnal cycle (i.e. the expected course) of ozone (O_3) mixing ratio in the surface layer and at higher altitudes of the atmospheric boundary layer (ABL) is primarily dependent on the photostationary state. Within the surface layer, O_3 is depleted during night time due to deposition processes and reaction with nitric oxide (NO). During daytime, this process is overcompensated by photolysis of nitrogen dioxide (NO_2) followed by O_3 production and transport of O_3 (Aneja et al., 2000). These changes are less and less pronounced towards higher altitudes and finally become unimportant when reaching altitudes above nocturnal inversions, where O_3 mixing ratio is expected to maintain its level from the preceding day during the night (residual layer) (Aneja et al., 2000; Fast et al., 2000). However, the diurnal cycle of O_3 mixing ratio is subject to a variety of influences, from which some may still be unknown. They manifest themselves in sudden changes of mixing ratio on different time scales, ranging from minutes to days.

In general, changing O_3 levels are frequently observed and reported. Some reports address the expected diurnal cycle of O_3, either from ground based data (Wanner et al., 1993; Lin et al., 2004; Rummel, 2005) or from profile data (Güsten et al., 1998; Cheng, 2000). On the other hand, several studies report deviations from the "typical" behaviour. Possible reasons were found to be (a) large scale processes like frontal passages (Müller and Sladkovic, 1990), (b) changes of air masses (Strong et al., 2002), (c) mesoscale circulations like sea breezes (Hastie et al., 1999), and (d) mountain-valley circulations (Prévôt et al., 2000). Nocturnal low-level jets (LLJ) frequently cause secondary O_3 maxima during night time (Corsmeier et al., 1997; Reitebuch et al., 2000; Lee et al., 2003; Salmond and McKendry, 2002), while advection of polluted air masses has been observed as a pronounced layering in O_3 profiles in the ABL (McKendry et al., 1997; Güsten et al., 1998; Beyrich et al., 1996; McKendry et al., 1998). There are only a few reports on exceptional patterns in diurnal O_3 courses at mountain tops, and the observed deviations were always towards higher than the expected O_3 mixing ratios (Attmannspacher and Hartmannsgruber, 1973; Yelansky and Senik, 1995). However, an explanation for short time decreases of O_3 (0.5 to 2 hours) at a mountain top was not given in any of the mentioned reports. Therefore, a comprehensive set of noticeable
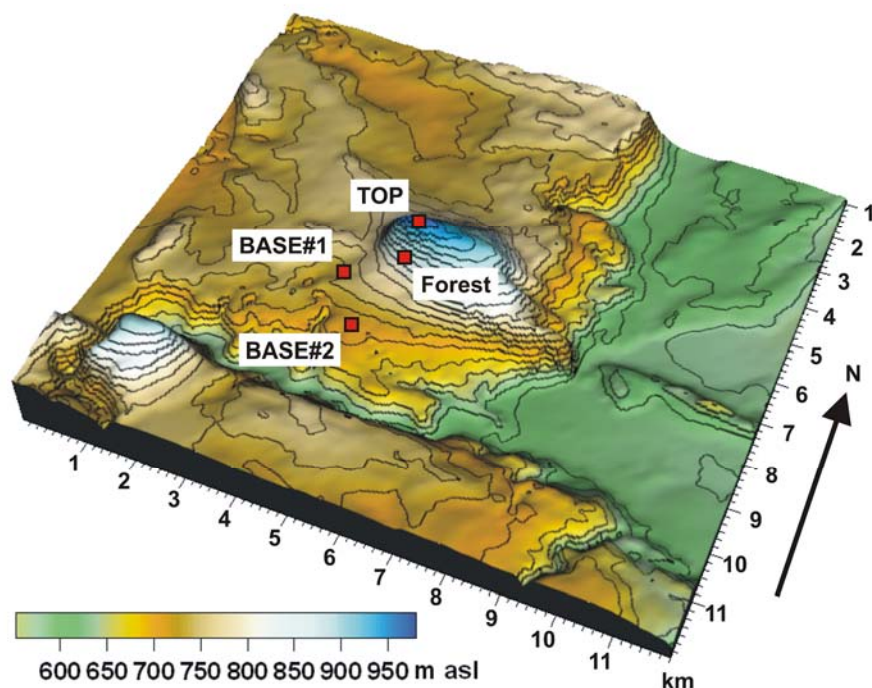
Fig. 1. Contour map of the SALSA site. Red dots indicate locations of the meteorological observatory at top of the mountain (TOP station, 998 m a.s.l.), of the forest station (850 m a.s.l.) and of the two field stations at the foot of the mountain, stations BASE#1 (flux station, 735 m a.s.l.) and BASE#2 (sounding station, 710 m a.s.l.).

observations at a mountain top, at the foot of the mountain and from profiles within the ABL will be used in this study to explain the origin of such short time events.

2   Material and methods

2.1   The SALSA site

Our measurements were conducted during the SALSA2005 campaign (22 August 2005 – 23 September 2005) which took place at and around the Hohenpeissenberg (German spelling: Hohenpeißenberg), an isolated mountain (47°48'N, 11°02'E, 998 m a.s.l.) in Bavaria, southern Germany. The mountain Hohenpeissenberg is located approximately 70 km southwest of the city of Munich and 40 km north of the northern ridge of the Alps. It is covered by coniferous and mixed forest with some clearings and agriculturally used areas (managed pastures). The mountain summit is approx. 300 m higher than the surrounding area (Fig. 1). In the east of the mountain, the terrain slopes abruptly to a considerably lower level (approx. 600 m a.s.l.), while in the south the Ammer river cuts into the terrain, forming a deep canyon. SALSA is a German

acronym, which stands for "Contribution of nitrous acid to atmospheric OH concentration".

2.2   The SALSA set-up

The set-up of the field experiment was designed to account for (a) the complex terrain, (b) the expected main regime of wind flow and (c) the existing infrastructure, i.e. the Hohenpeissenberg observatory of the German Meteorological Service (DWD), situated on top of the mountain, later referred to as the "TOP" station. All parameters measured at TOP station, being relevant for this paper, are listed in Table 1.

In addition to the TOP station, two field stations were set up. At the south-western foot of the mountain, on a managed pasture site (approx 1.1 km from TOP, see Fig. 1), eddy covariance systems for the measurement of sensible and latent heat fluxes were set up (BASE#1; see Table 1). The second field station was installed to monitor the state of the ABL with respect to wind velocity, turbulence intensity and thermal stratification. This site (BASE#2, s. Table 1) was located directly south of the mountain (approx. 1.6 km from TOP, and approx. 1 km southeast of BASE#1), on a plateau between the mountain and the Ammer river (see Fig. 1). Two sounding systems were deployed here: (1) a SODAR-RASS system (DSDPA90.64, METEK, with 1.29 GHz RASS extension), providing vertical profiles (20 m resolution) of wind velocity, fluctuation of the vertical wind speed and acoustic temperature, and (2) a tethered balloon system (Vaisala TMT, Boulder; CO; USA), which was used for discontinuous profiling of the ABL for air temperature, relative humidity, as well as mixing ratios of CO_2 and O_3. The meteorological sensor package of the tethered balloon system consisted of a thermistor for air temperature, a polymer based sensor for relative humidity, and a semiconductor technique based transducer for barometric pressure measurements. Wind speed (v_h) was measured by a 3-cup anemometer, and wind direction (φ) was determined by a vane referring to an electronic compass. The CO_2 sonde was constructed around the GMP343 sensor (Carbocap[®], Vaisala), which uses a single-beam dual-wavelength NDIR technology. Data were stored in a small data logger every 2 s. The lightweight O_3 sonde, a development of the University New Hampshire, is based on single beam UV absorption (Talbot et al., 2006). Its data were internally stored to a memory and downloaded after the flight. Flights with the tethered balloon were performed only in the evening and morning hours. Around noon, turbulence became too strong for safe and undisturbed measurements. Furthermore, for security reasons, the flights were generally limited to conditions of wind speeds less than 9 m s^{-1}. The trace gas sondes

Table 1. Measured parameters at the TOP station, forest station and the two sites of the BASE.

Parameter	Symbol	Unit	Temporal resolution (min)	Sampling height (m) a.g.l.	Instrument (Model)
TOP station, 998 m above sea level					
Air temperature	T	°C	1	2	PT100
Relative Humidity	rH	%	1	2	LiCl-Sensor, Rotronic
Air pressure	P	hPa	1	2	
Horizontal wind speed	v_h	ms^{-1}	1	40.5	Cup anemometer, heated
Wind direction	φ	°	1	40.5	Vane, heated
Global radiation	R_g	Wm^{-2}	1	18	CM11, Kipp & Zonen
Ozone	O_3	ppb	1	18	UV absorption; ThermoElectron, 49C
Nitric oxide	NO	ppb	1	18	Chemiluminescence; ECO Physics CLD 770 AL ppt
Nitrogen dioxide	NO_2	ppb	1	18	ECO Physics CLD 770 AL ppt with PLC 760
Carbon monoxide	CO	ppb	1	18	Resonance fluorescence; Aero Laser AL 5001
BASE#1 station, 735 m above sea level, flux site					
Sensible heat flux	H	Wm^{-2}	30	2	Campbell CSAT3
Friction velocity	u∗	ms^{-1}	30	2	Campbell CSAT3
BASE#2 station, 710 m above sea level, sounding site					
Air temperature	T	°C	5	2	Rotronic
Relative humidity	rH	%	5	2	Rotronic
Air pressure	P	hPa	5	1	Vaisala, PTB101B
Horizontal wind speed	v_h	ms^{-1}	5	2	Vector instruments
Wind direction	φ	°	5	2	Vector instruments
Ozone	O_3	ppb	5	3.5	ThermoElectron, 49C
Nitric oxide	NO	ppb	5	3.5	TECAN 700 AL
Nitrogen dioxide	NO_2	ppb	5	3.5	TECAN 700 AL
Carbon dioxide	CO_2	ppm	5	3.5	LiCor 840
Water vapour	H_2O	ppth	5	3.5	LiCor 840
Acoustic temperature	T_a	°C	5	40 - 450	RASS, METEK
Horizontal wind speed	v_h	ms^{-1}	5	40 - 450	SODAR, METEK
Wind direction	φ	°	5	40 - 450	SODAR, METEK
Reflectivity	R	dB	5	40 - 450	SODAR, METEK
Air temperature	T	°C	Approx. 30	1 - 450	Tethered balloon, TMT, Vaisala
Relative humidity	rH	%	Approx. 30	1 - 450	Tethered balloon, TMT, Vaisala
Air pressure	P	hPa	Approx. 30	1 - 450	Tethered balloon, TMT, Vaisala
Forest station, 850 m above sea level					
Horizontal wind speed	v_h	ms^{-1}	5	2	Vector instruments
Wind direction	φ	°	5	2	Vector instruments

were attached directly below the belly of the blimp-shaped balloon to avoid swinging payload. Three meteorological probes, each measuring wind speed and wind direction, air temperature, relative humidity and barometric pressure, were attached to the tether line with 5 m vertical spacing between each other. The uppermost probe was located approximately 5 m below the balloon.

An additional forest station was located directly down slope (south flank) of the TOP station, halfway to the village of Hohenpeissenberg. Its data of wind speed and wind direction were used to check if air masses could have been transported very close to the ground toward the TOP station.

All measured parameters are listed in Table 1. For practical reasons, both field sites at the foot of the mountain (BASE#1 and BASE#2) will be considered as the "BASE" (in contrast to TOP station).

2.3   Quality control

Data from all ground based measurements were checked for periods with erroneous data due to power failures and subsequent restarting procedures as well as for artificial trace gas peaks originating from farming and other agricultural management activities close by. Flux data were prepared for analysis by applying an established quality control scheme (Foken et al., 2004).

Profile data obtained by the SODAR-RASS system were quality controlled by using an internal quality code, provided by the SODAR-RASS system (METEK User handbook of SODAR/RASS, 2000). Subsequently, a despiking procedure was applied, based on the procedure published elsewhere (Vickers and Mahrt, 1997).

All deployed meteorological sondes were compared against the current data of the ground based system before flight (i.e. typically in the early morning and late afternoon). These parameters were: air temperature, relative humidity and barometric pressure. Tethersonde flight data were quality controlled by cross checking all parameters, measured independently by the three meteorological sondes, for consistency. The altitude of the sonde was recalculated after each flight (ascent and descent) by comparing the barometric pressure readings from the sondes against the pressure of the ground based weather station. Drifts of the pressure derived altitude were distributed linearly over the preceding flight. As a last step, the corresponding altitude for each data point was calculated by stepwise solving the barometric formula. After each pair of ascent and descent, the final height deviation from 0 (i.e. ground level), which is a result of the discrete computation, was distributed linearly over the preceding flight. CO_2 data were corrected for changing barometric pressure, a temperature correction was not applied, as the CO_2 and the O_3 sensor perform an online temperature correction (O_3 also pressure correction).

2.4   Computed parameters

Additional supporting parameters were derived from the measured quantities, such as for atmospheric stability. To assess the state of atmospheric stability, the dimensionless stability parameter $\zeta = z/L$ was used, where z is the height of measurement and L is the Obukhov length, calculated according to Eq. (1).

$$L = -\frac{u_*^3}{\kappa \dfrac{g}{T_V} \dfrac{Q_{HB}}{\rho \cdot c_p}}$$

(1)

Here, u_* is the friction velocity, κ is the von-Kármán constant, g is the acceleration due to gravity, T_V is the virtual air temperature, Q_{HB} is the buoyancy flux, ρ is the air density, and c_p is the specific heat of air at constant pressure. Usually, L is computed by using the sensible heat flux and air temperature. However, we explicitly used the buoyancy flux and the virtual temperature instead, as the high humidity is expected to play a major role in atmospheric stability in the morning hours, the period of focus. From the equation of turbulent kinetic energy (see e.g. (Stull, 1988)) it follows that for $\zeta < -1$ the buoyancy term is dominant compared to the shear term, which is a precondition for free convection.

The height of the convective boundary layer (CBL) was determined from SODAR-RASS data by applying (1) the parcel method to profiles of air temperature (Holzworth, 1967; , 1964) and (2) a method described by Beyrich (1997) to profiles of backscatter intensity.

2.5   Investigation of long-term (monitoring) measurements

A dataset extending over 5 years (October 2000 – December 2005), obtained at the TOP station, was investigated for the occurrence of O_3 drop events. This was done to determine if the SALSA field observations were the result of an exceptional situation, or if similar events occur frequently at the Hohenpeissenberg observatory. An automated detection scheme was developed and applied to the time series of the O_3 mixing ratio (1 min. resolution). This detection was conducted as follows: (1) a moving minimum was computed, comprising $\pm$ 180 minutes around the current value of the O_3 time series. The time of the actual occurrence of the minimum was taken as input data for subsequent filtering procedures (Fig. 2, black square). (2) To ensure a clear separation of O_3 minima, only detected minima with a temporal spacing of at least 60 minutes were investigated. (3) Half drop values were computed by considering the detected minimum values and the median O_3 mixing ratios within 90 to 30 minutes before the minimum (Fig. 2, black and grey dots). (4) The detection of the onset of O_3 drop event was done with a geometrical approach. For that, virtual lines were constructed from the point, where the rising flank of the O_3 drop reached its half drop value after the minimum to data points prior to the event. The data point in the time
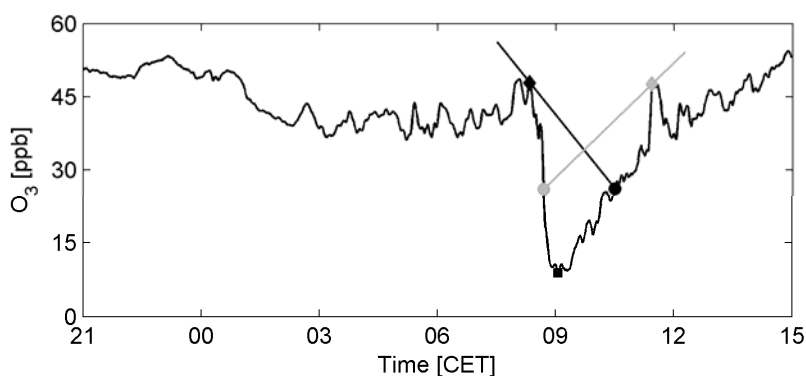
Fig. 2. Course of O_3 mixing ratio at 05 September 2005 at the TOP station. The principal operation of the detection algorithm described in Sect. 2.5 is also shown. The black square indicates the detected minimum, the black and grey dots at the peak flank give the half peak values. The intercept of the grey straight line with the time series after the minimum indicates the end of the event (grey diamond), the intercept of the black straight line with the time series before the minimum marks the begin of the event (black diamond).

series, corresponding to the virtual line with most negative slope, was taken as preliminary point of onset. The first local maximum of O_3 before this point was taken as final point of the onset of the O_3 drop event. A similar approach was used for determination of the end of the O_3 drop event, using the half event value at the falling flank of the O_3 drop, and a maximum positive slope criterion (see Fig. 2 for clarification). These geometrical approaches were chosen, because the O_3 drops can also occur during changing background levels of O_3, making a detection based on fixed thresholds impossible. Furthermore, all events detected by this scheme were subsequently filtered: (1) the minimum had to be more than 5 ppb below the value at begin and end of the event; (2) the O_3 level at the end of the event had to be within ±25 % and ± standard deviation of the O_3 level before the event; (3) the relative O_3 drop had to exceed 10 % of the previous O_3 level; (4) the corresponding value of NO mixing ratio at the O_3 minimum had to exceed its pre-event level plus standard deviation, and had to reach at least 0.5 ppb. The last criterion was introduced to limit the detection to O_3 drop events with characteristics similar to those observed during the SALSA campaign.

An index, whether or not a mesoscale circulation system called Alpine Pumping (see Lugauer and Winkler, (2005); also described below) was active at a certain day, was computed by checking the South-North wind component (V). If it changed from positive values before 06:00 h to negative values after 12:00 h, while the total global radiation exceeded 20 MJ m^{-2} at this day, Alpine Pumping was assumed to be active.

3   Results

This chapter is subdivided into five parts. First, a typical "event" course of O_3 mixing ratio at the TOP station in the morning hours is presented. Then we describe the general characteristics of all observed events during the SALSA campaign. Third, mean diurnal cycles of the flow characteristics for a subgroup of three events are presented. Fourth, we focus on the strongest event within this subgroup (as a case study) and describe its characteristics as observed at TOP station, within the ABL and at the BASE. Fifth, the frequency of O_3 mixing ratio drop at the TOP station is determined by inspecting a more than 5 years dataset. All times and dates are given in the following are Central European Time (CET = UTC+1h).

3.1   The O_3 drop events

On several days during the SALSA campaign, a significant negative excursion of O_3 mixing ratio at the TOP station has been observed. An example is shown in Fig. 2. Although not every observed event was as strong as that on 05 September 2005, they were always a significant deviation from the expected (quasi constant) mixing ratio of O_3 at the TOP station. Further analyses revealed that the O_3 events were associated with a couple of other distinctive features, which will be presented in the following.

3.2   General characteristics

A total number of six O_3 drop events were observed during the SALSA campaign (22 August 2005 – 23 September 2005). The event durations ranged from 10 to 118 minutes (defined as the span of time during which O_3 levels remained below the half drop value). The observed O_3 reductions ranged from 23 to 80 % of the initially present O_3. Characteristics of the O_3 drop events are summarized in Tab. 2.

No correlation was found between the event duration and its intensity. All event days had almost clear skies during the morning, except for 03 September 2005, when a considerable number of cumulus clouds were present. The irradiated shortwave energy from 00:00 h until the onset of the event, ranged between 1.8 MJ m^{-2} and 2.4 MJ m^{-2}, depending on the onset time and the presence of scattered clouds. Neither the event duration nor the O_3 decrease intensity correlated with the irradiated energy.

All of the observed events occurred at low wind speeds, in five cases there was a distinct wind speed minimum, lasting 2 to 3 hours. In three cases, a sudden change of wind direction during the event was observed. Wind direction before the event was around south, after the event wind came from north-eastern directions. Two other events

Table 2. Characteristics of O_3 drop events. Event durations are defined as the span of time during which the O_3 level remains below 50 % of maximum drop intensity (full width of half event maximum). Minimum O_3 shows the O_3 mixing ratio at event maximum, the relative O_3 decrease gives the percentage of initially present O_3 being missed during the event.

	30 Aug	31 Aug	03 Sep	05 Sep	07 Sep	08 Sep
Onset time (CET)	08:00	09:00	08:15	08:30	09:15	09:30
Peak time (CET)	08:30	10:30	08:54	09:05	09:48	09:50
Duration [minutes]	13	71	27	118	15	10
Initial O_3 level [ppb]	45	45	48	41	46	48
Minimum O_3 level [ppb]	27	20	22	7	19	37
Relative O_3 decrease [%]	40	56	54	81	59	23
Initial NO level [ppb]	0.2	0.4	0.1	0.1	0.1	0.2
Maximum NO level [ppb]	0.7	6.1	1.4	12.7	4.1	0.7
Initial specific humidity [g kg^{-1}]	11.1	12.2	11.3	8.8	7.1	8.6
Maximum specific humidity [g kg^{-1}]	11.7	14.0	12.2	11.1	11.4	10.1
φ before event [°]	90	180	90	180	180	180
φ after event [°]	50	360	30	45	45	50
v_h minimum observed?	Yes	No	Yes	Yes	Yes	Yes

were characterised by more or less stable wind directions around east, while the last event was accompanied by a continuously turning wind from east at midnight over south in the early morning to west at the time of the event and then continuing over north to east again in the evening.

3.3   Mean characteristics

From the wind characteristics of the six observed O_3 events (Table 2), a group of three O_3 depletion events with more or less similar flow patterns can be discerned. These are the last three events observed during the experiment (05, 07 and 08 September 2005). For this group, the mean diurnal course of the wind velocity and the absolute range of values were computed. The latter demonstrates the quasi identical flow regime on all three days. Figure 3 shows the mean diurnal course of horizontal wind speed (v_h), its west-east and south-north components (U and V, respectively), and the degree of persistence (P) of the wind direction at any time of the day. Additionally, the mean diurnal cycle of air temperature and specific humidity are displayed. The calculation of P is done according to Lugauer and Winkler (2005), following Eq. (2), where P is defined as the temporal vector mean of the horizontal wind speed divided by the temporal arithmetic mean of the horizontal wind speed at any time of the day.
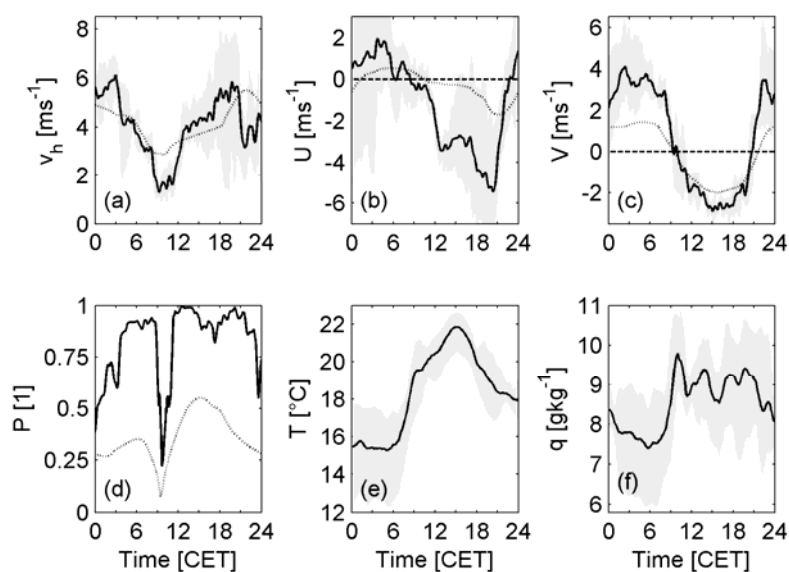
Fig. 3. Mean diurnal course of (a) scalar horizontal wind speed v_h, (b) west-east wind component U, (c) south-north wind component V, (d) persistence of wind direction P, (e) air temperature T and (f) specific humidity q at TOP station for the last three event days (05, 07, & 08 September, 2005). The grey shaded area gives the absolute range of values, the dotted line shows the corresponding result reported by (Lugauer and Winkler, 2005).

$$P(t) = \frac{\sqrt{\overline{U(t)}^2 + \overline{V(t)}^2}}{\overline{v_h(t)}} \qquad (2)$$

A value for P of 1 indicates that every day at that time the wind blew from the same direction, a value of 0 indicates that at that time all wind directions occurred at the same frequency.

A distinct, absolute minimum of v_h (Fig. 3a) can be observed around 09:00 h to 11:00 h in the morning. Additionally, P (Fig. 3d) approaches its minimum at the same time, indicating highly variable wind directions during that period. The quasi reversal of the mean flow becomes especially visible in the vector component V (Fig. 3c), where a fast change from southern directions (positive values) to northern directions (negative values) is obvious around that time. Coincidentally with the flow reversal, a period of stagnant or even falling air temperature is visible (Fig. 3e), while the specific humidity (Fig. 3f) reaches its maximum values.

To get better insight into the potential processes being active in the ABL on these days, we now focus on the day with the strongest occurrence of the O_3 drop at TOP station, namely the 05 September 2005. This event was selected, as all accompanying processes are expected to be best observable during the most intensive event.
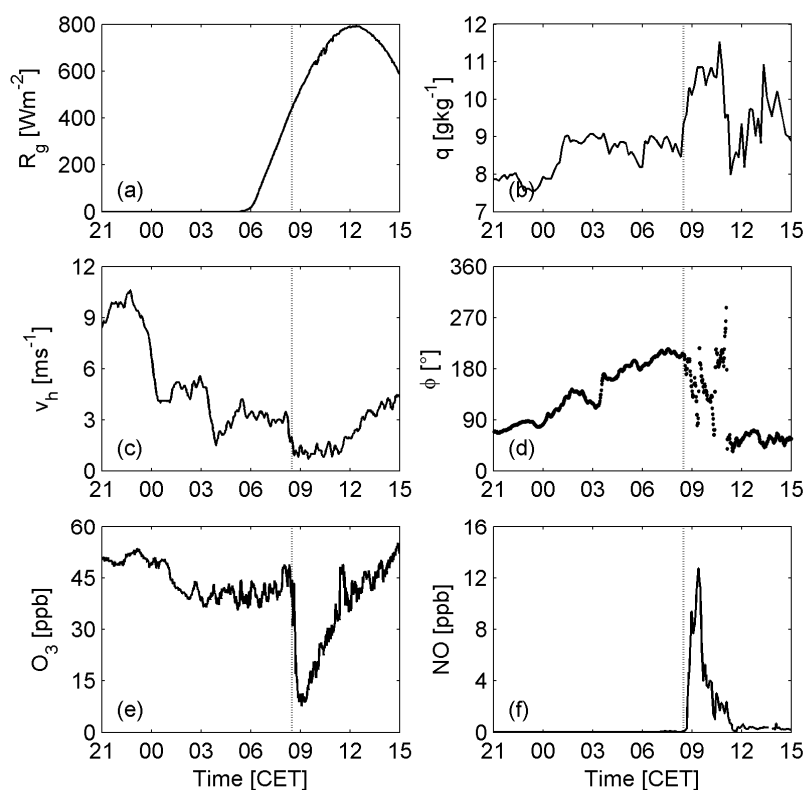
Fig. 4. Hohenpeissenberg observatory (TOP station), 04 September 2005, 21:00 h to 05 September 2005, 15:00 h, diurnal variations of: course of (a) global radiation R_g, (b) specific humidity q, (c) horizontal wind speed v_h, (d) wind direction φ, (e) ozone mixing ratio O_3 and (f) nitric oxide mixing ratio NO. Note the coinciding change of wind direction and the drop of O_3 mixing ratio together with the peak of NO mixing ratio. The dashed line indicates the onset of the O_3 event.

3.4   05 September 2005: Case study

The 05 September 2005 was a clear, sunny and warm day. The global radiation R_g at TOP station (Fig. 4a), showed a nearly perfect bell-shaped curve in the absence of clouds. The specific humidity q at the TOP station (Fig. 4b) varied only slightly during the night and early morning. Shortly before 09:00 h, it increased rapidly from about 9 g kg^{-1} to 11 g kg^{-1}. Around 11:00 h, the specific humidity dropped, but remained very variable during the afternoon. The horizontal wind speed v_h at the mountain summit (Fig. 4c) decreased from higher night time values to a minimum around 09:00 h, while slightly increasing again from afternoon to evening. The wind direction (Fig. 4d) changed slowly from east to south during the night and early morning, until around 09:00 h when an abrupt change to easterly directions occurred. After 11:00 h, the wind direction remained around north-east. O_3 mixing ratios (Fig. 4e) were quasi constant during night within a range of 40 to 50 ppb. Together with the change of wind direction
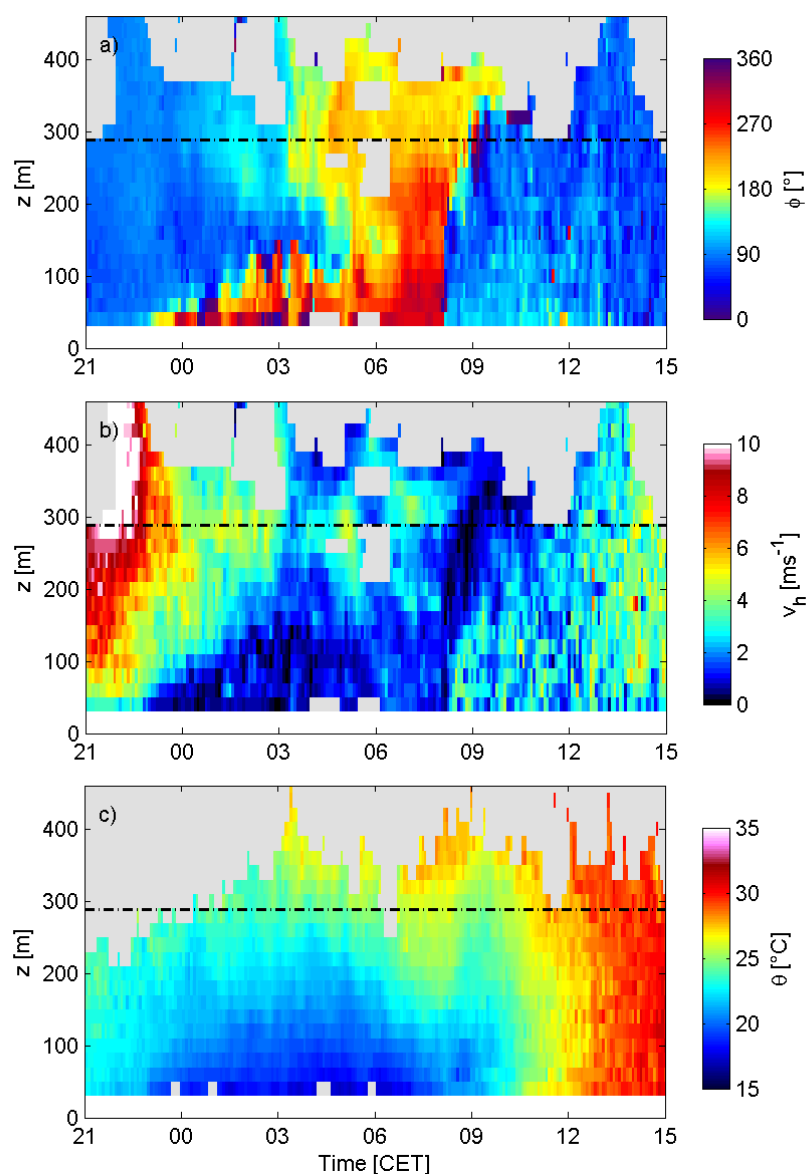
Fig. 5. Time-height cross sections of (a) wind direction φ, (b) horizontal wind speed v_h, and (c) potential air temperature θ, measured by SODAR-RASS, from 04 September 21:00 h to 05 September 15:00 h. The dash-dotted line marks the altitude of the TOP station. Note around 09:00 h the sudden change of wind direction in (a), the pronounced minimum of horizontal wind speed around the altitude of TOP in (b), and the temperature drop within the entire ABL in (c).

around 09:00 h mixing ratios collapsed to 7 ppb and recovered during the following three hours. Coincidentally, NO mixing ratios increased from below the detection limit to 12 ppb and decreased during the following hours (Fig. 4f).

The presence of SODAR-RASS and tethered balloon systems provided the unique chance of observing the state of the ABL up to well above the mountain summit with respect to wind, turbulence, air temperature and the mixing ratios of the trace gases CO_2, O_3 and H_2O. Figure 5 presents time-height cross sections of wind direction φ (Fig.

5a), horizontal wind speed v_h (Fig. 5b) and potential air temperature θ (Fig. 5c), all for the interval from 04 September, 21:00 h to 05 September 2005, 15:00 h.

In the lowest 130 m, a layer with westerly winds developed during the night (Fig. 5a), beginning around 23:00 h in the evening. The different wind direction within this layer (compared to the layer above) indicated that it was completely decoupled from the air above. The lower layer was the nocturnal boundary layer, while the upper one was the residual layer. The nocturnal boundary layer reached its maximum vertical extent shortly after 03:00 h in the morning. At this time, wind direction changed also in higher altitudes from easterly to southerly directions. A distinct spatial boundary with respect to directional wind shear, was no longer observable from this time on. After sunrise around 06:00 h, the entire observable ABL was characterized by a smooth transition from westerly winds close to the ground to southerly wind directions above 300 m a.g.l. Shortly after 08:00 h, the wind changed abruptly to easterly directions. This change affected all levels in the lowest 200 m at the same time, while the change was gradually delayed at higher altitudes.

Coinciding with the change of wind direction, the horizontal wind speed (Fig. 5b) dropped to very low values (< 1 m s^{-1}). These low wind speeds prevailed only shortly in the lowest 200 m of the atmosphere, being followed by stronger fluctuations with peak values of approx. 4 m s^{-1}. Above 200 m a.g.l., the calm period lasted considerably longer and the onset of the fluctuations was delayed by approximately two hours. The last parameter of the SODAR-RASS system considered here is the potential air temperature θ (Fig. 5c). Starting in the late evening, a very stable thermal stratification of the ABL developed by radiative cooling of the surface. A gradual increase of θ in the entire profile was interrupted around 09:00 h by a temperature drop. It became first visible close to the ground, but affected the entire observable atmosphere within half an hour. After that, the ongoing solar heating of the ground led to the development of a thermally unstable ABL.

The height of the boundary layer BL (z_{BL}) was determined from 15 minutes average profiles of θ using the parcel method (Holzworth, 1967; , 1964) and from half-hourly average profiles of the reflectivity of the vertical acoustical antenna by visual inspection. A secondary maximum of reflectivity indicates the BL height (Beyrich, 1997). Both methods yielded similar BL heights (Fig. 6) with a maximum of 380 m a.g.l. at 13:30 h. The onset of the evolution of the convective boundary layer CBL detected by the parcel method (09:00 h) was one hour later than inferred from the
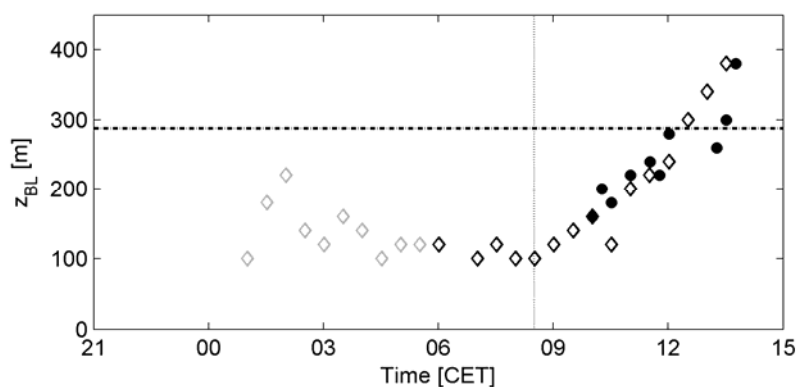
Fig. 6. Development of the BL height (z_{BL}), from 4 September 21:00 h to 5 September 15:00 h, derived from the parcel method (dots) and from secondary maximum of reflectivity (open diamonds). Grey diamonds indicate nocturnal inversion height, black diamonds indicate CBL height. The dash-dotted line marks the altitude of the TOP station, the dotted line indicates the onset of the O_3 decrease at the TOP station.

reflectivity data (08:00 h). Growth rates of the CBL were around 50 m h^{-1} with both methods. The height of the CBL reached the TOP station around 12:00 h, that means, the TOP station was clearly outside the CBL around 09:00 h.

Besides the profiles with high temporal resolution obtained by the SODAR-RASS system, profile data from the tethered balloon system were available for the morning hours of 05 September 2005. The system was operated in scanning mode, i.e. the profiles were obtained by raising and lowering the balloon continuously. The scanning mode provided a good spatial resolution but with some temporal ambiguity in the profiles, resulting from the time needed for a complete scan. The main advantage of the tethered balloon system was its ability to measure profiles of the trace gases CO_2, O_3 and the specific humidity q besides the meteorological data. However, trace gas data added invaluable information to the profiles obtained by the SODAR-RASS system. By chance, one of these scanned profiles at 05 September 2005 captured the event and gave insight into its vertical structure. A set of time-height cross sections and profiles for q, O_3, CO_2 and θ is shown in Fig. 7. The time-height cross sections of q, O_3, CO_2 and θ (Fig. 7a-d) show a growing but clearly confined layer of higher q and CO_2 and lower O_3 and θ compared to the air above from about 07:30 h. After 09:30 h, in the last descent of the tethered balloon, this confinement was no longer visible. In Fig. 7d (θ), a pool of cold, nocturnal air close to the ground could be identified. Between 07:00 h and 08:00 h, this surface air rapidly warmed up, but still remained colder than the air above. The profiles on the right side of Fig. 7 depict the upward scan of the tethered balloon at the time of the O_3 drop at TOP station. All profiles could be divided into the following
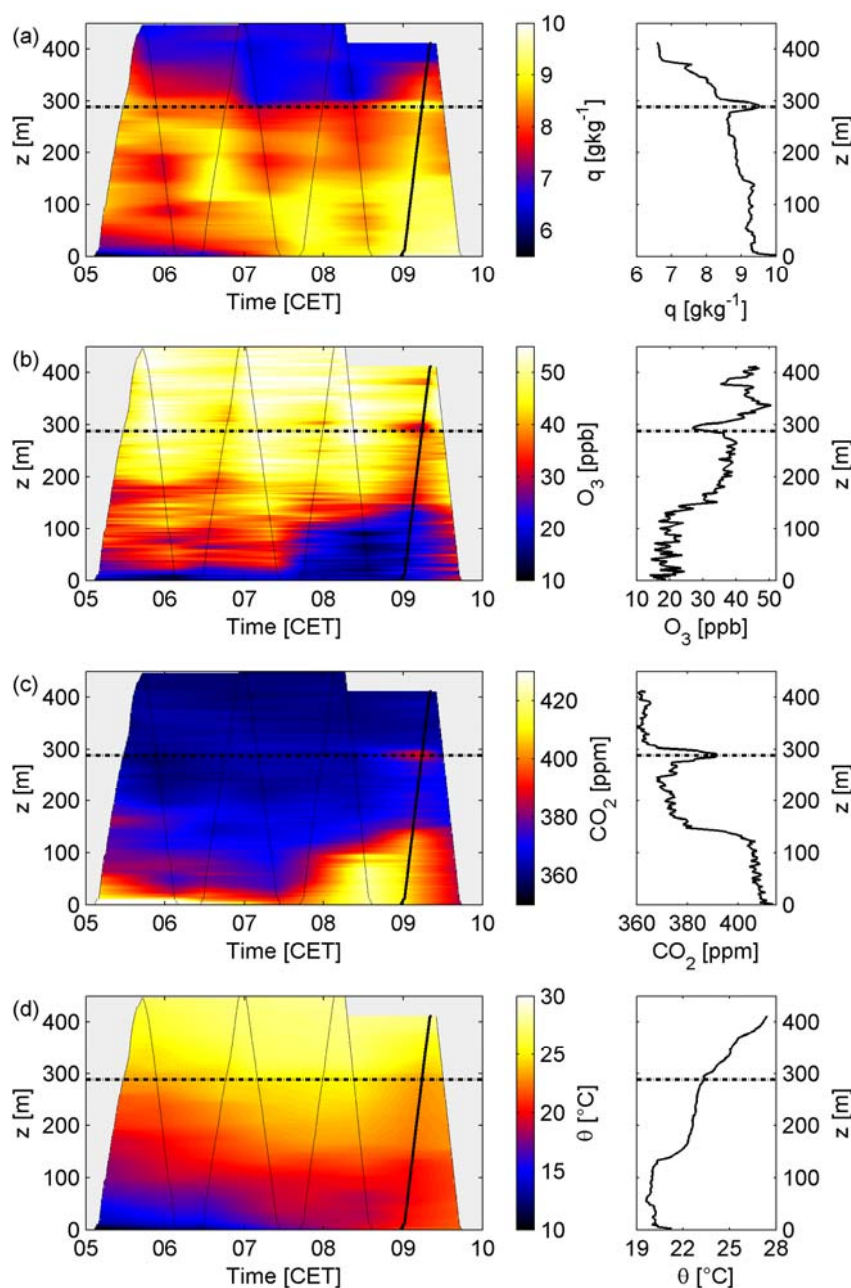
Fig. 7. Time-height cross sections and profiles of (a) specific humidity q, (b) O_3 mixing ratio, (c) CO_2 mixing ratio, and (d) potential temperature θ for the morning of 05 September 2005. The actual flight path of the tethered balloon is indicated by the thin black line. Profiles on the right side show the upward scan of the tethered balloon at the time when the O_3 drop reached the TOP station (corresponding to the actual flight path marked with a thick black line).

segments: (1) a lower part up to 130 m a.g.l. with almost constant values for all parameters, capped by a temperature inversion (Fig. 7d), which resulted in a drop of q and also of CO_2, whereas O_3 started to increase from this altitude on (this layer coincided very well with the CBL determined from the SODAR-RASS data); (2) at 290 m a.g.l., a distinct layer of approx. 30 m thickness became obvious, being
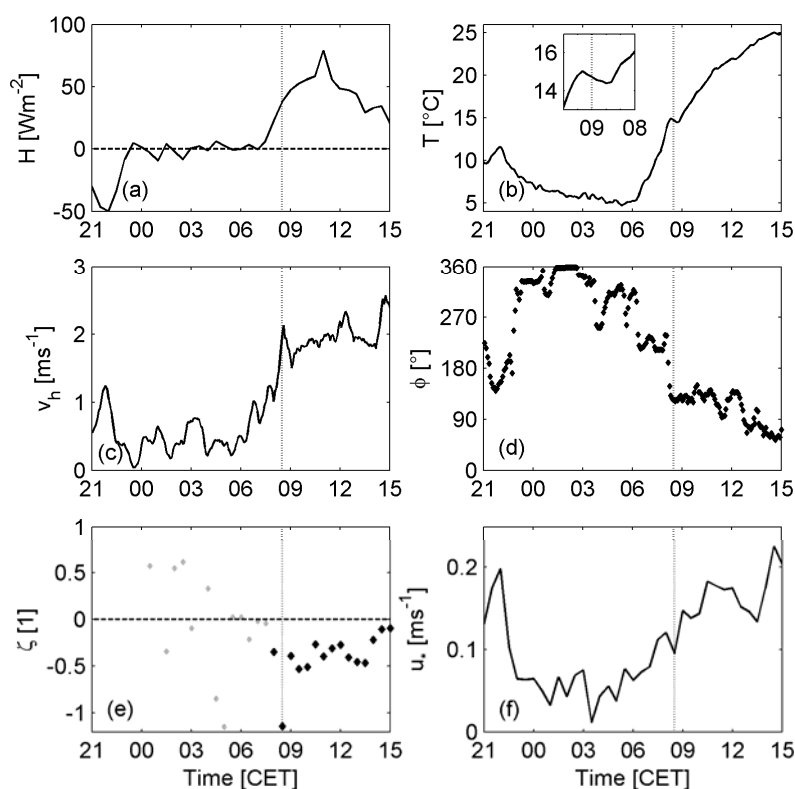
Fig. 8. Course of (a) sensible heat flux H, (b) air temperature T (exceptional drop of T enlarged), (c) horizontal wind speed v_h, (d) wind direction φ, (e) stability parameter ζ and (f) friction velocity u_* from 04 September 21:00 h to 05 September 15:00 h at BASE. Grey dots for ζ denote low quality of ζ due to low sensible heat flux ($-10 < H < 10$), black dots for ζ indicate high quality of derived ζ values. The dashed line indicates the onset of the O_3 event at the TOP station.

characterized by enhanced water content, higher CO_2 values and by a reduced O_3 level; (3) at the top of the profiles at 420 m a.g.l., the trace gases CO_2 and O_3 reached typical lower tropospherical background levels of 360 ppm and 50 ppb, respectively, while q reached approx. 6.5 g kg^{-1}.

After the temporal and spatial changes within the ABL have been described in detail, the observations at the BASE will be examined.

The characteristics of the wind at the BASE with respect to speed and direction were comparable to that within the ABL, especially the sudden change of the flow direction around 09:00 h (see Fig. 8c,d). Following the cold night, the sensible heat flux started to increase shortly after sunrise (Fig. 8a) together with increasing air temperature (Fig. 8b). The relative humidity at the BASE (not shown) dropped down from saturation almost 1 h before the onset of the event. With the onset of the event, a clear drop of air temperature was observed, lasting for almost one hour. The time of the temperature decrease coincided well with the temperature decrease of the entire ABL, observed by
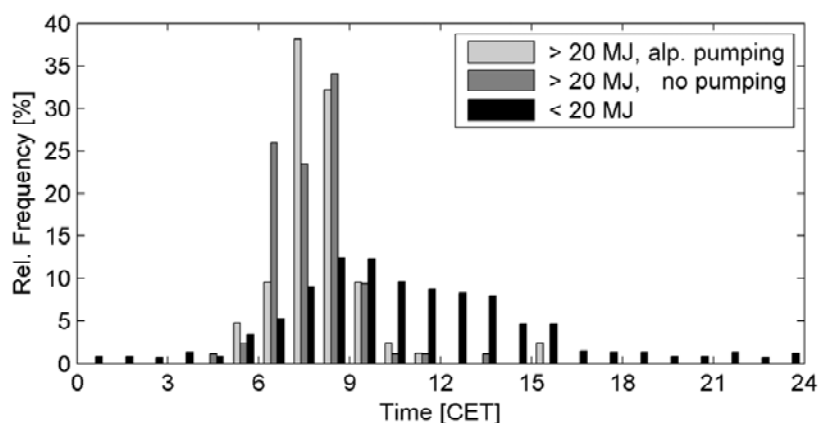
Fig. 9. Diurnal variation of relative frequency of O_3 events for days with high irradiation and Alpine Pumping (light grey, N = 84), with high irradiation but without Alpine Pumping (dark grey, N = 85) and for days with total irradiated energy of less than 20 MJ m^{-2} (black, N = 587).

the SODAR-RASS system (Fig. 5c). The stability parameter ζ (Fig. 8e), being valid for the surface layer, showed mostly positive values during night, indicating stable conditions. But with H around zero, values of ζ were of low quality and had to be considered with care. The most unstable situation within the surface layer was found around 08:30 h, when ζ reached values of -1.2. Later towards noon, unstable conditions prevailed ($\zeta \approx -0.3$). Friction velocity u_* (Fig. 8f) was slightly increased from its night time values (≈ 0 m s^{-1}), and reached only small secondary minimum values (≈ 0.1 m s^{-1}) at 09:00 h. The conditions needed for free convection were met (Stull, 1988) with the increasing buoyancy due to increasing sensible heat flux, and the decreasing shear, indicated by low u_* values. O_3 mixing ratio decreased during night at the BASE to zero (not shown here). With increasing insolation and developing turbulence, it started to increase until shortly before 09:00 h, when a decline to the low nocturnal values occurred. The later increase of O_3 mixing ratio was again interrupted around 10:30 h, when O_3 mixing ratio remained for approximately two hours at a more or less constant level.

3.5   Long dataset

After the detailed investigation of the observations coinciding with the O_3 drop at TOP station, within the ABL, and at the BASE, we also evaluated a 5 year dataset (October 2000 to December 2005) of the TOP station for the occurrence of sudden O_3 decreases. As the events observed during the SALSA experiment were restricted to days with high irradiation, we split the analysis into days with total irradiated energy exceeding

20 MJ m^{-2} and days with less energy input. The radiation days were further subdivided into days with and without Alpine Pumping. The resulting diurnal histogram is shown in Fig. 9. The class with low radiation shows a smooth distribution curve, with highest values between 08:00 h and 10:00 h. During night, only few events were detected. Both classes with high irradiated energy were characterized by a sharp peak in the early morning, with maximum frequencies between 08:00 h and 09:00 h. Almost no events were found in the afternoon and during night time.

4   Discussion

At a first glance, several explanations for the O_3 drop events seem to be possible from our observations. "Transport" is common to all of them, however varying in important aspects. It is known from earlier studies (Lugauer and Winkler, 2005) that the region of the SALSA experiment is occasionally affected by a mesoscale circulation system between the Alps and their northern foreland (Alpine Pumping). Whether or not this circulation was present during the experiment and whether it impacts the observations will be discussed in the first section.

The variability of the O_3 drop intensity, its peak time and its event duration (see Tab. 2) suggest highly dynamical processes behind this phenomenon. A number of processes leading to the observed O_3 drop events are conceivable: (1) a local, temporally limited O_3 sink close to the mountain summit, (2) a local valley-to-mountain circulation, including the influence from a national road passing the foot of the mountain in east-west direction, (3) change of air masses (passage of fronts), (4) immersion of the mountain summit into the developing convective boundary layer, and (5) direct injection of air masses by free convection from the foot of the mountain into higher ABL altitudes. From the observations presented in the results chapter, we will demonstrate that it is possible to narrow the number of these processes down to one final explanation: free convection. For that, after a brief description of the mesoscale circulation system "Alpine Pumping", we will start with the most local process and will increase the spatial dimension step by step.

4.1   Mesoscale circulation system – Alpine Pumping

On days of high solar irradiance, barometric pressure in the valleys of the Alps becomes low relative to the Alpine foreland due to enhanced heating up of the valley air. This horizontal pressure difference forces air during day time to flow from the foreland

plains towards the mountains of the Alps, where it rises convectively. The diurnal counter flow from mountain to foreland occurs at higher altitudes. For dynamical reasons, it causes a subsidence over the foreland with typically cloud free skies. During night time, stronger cooling in the valleys leads to higher barometric pressure in the valleys, resulting in an outflow of air towards the foreland plains (Whiteman and Bian, 1998; Whiteman, 2000).

The influence of thermally driven wind systems in the area of the SALSA experiment was intensively investigated by Lugauer and Winkler (2005). The diurnal oscillation of the wind direction, caused by the heating and cooling of the Alps, was found to affect the Alpine foreland up to 100 km to the north with a vertical extent of 1 km at the Alpine margin. From 340 days with strong irradiation (out of 5 years), Lugauer and Winkler (2005) calculated mean diurnal cycles of horizontal wind speed, west-east and south-north wind components and the persistence of wind direction at the Hohenpeissenberg summit.

The comparison of the mean diurnal cycles from Lugauer and Winkler (2005) with mean diurnal cycles from the SALSA experiment (Fig. 3) reveals a striking similarity, although our results are only based on 3 days. Nevertheless, for these 3 days, we can assume that a similar flow regime, the Alpine Pumping, was dominating the experimental site. Additionally, in accordance with Lugauer and Winkler (2005), a slight delay of the wind direction change in higher altitudes occurred compared to the surface layer (Figure 5a). This was in agreement with the typical speed at which this circulation system develops.

A fast change of wind direction, especially when it comes close to a flow reversal, always implies a period of low to zero wind speed. With the Alpine Pumping starting to affect the TOP station (indicated by the South-North wind component (V) changing from positive to negative values), such calm conditions were found. They lasted from a few minutes up to more than half an hour. This is noteworthy, as low horizontal wind speeds can trigger some of the processes discussed in the following (i.e. free convection).

4.2   Local sink for O_3 at mountain summit

Strong local sinks for O_3 within 300 m to the TOP station, which could facilitate a substantial drop of O_3 mixing ratio at the TOP station, can be excluded. Adverse (chemical) effects of the station itself (exhaust from lab vents etc.) are not likely, since the setup of the observatory as a background trace gas measurement station of the

Global Atmosphere Watch (GAW) program has to follow strict operational guidelines. In the unlikely case that some exhaust gas from cars in the parking lot at Hohenpeissenberg summit would have reached the gas sampling inlet, it would have resulted in a sharp but short O_3 drop rather than in an O_3 reduction lasting half an hour and more. Furthermore, this would happen only in the case of (local) wind directions around 90° – 100°. However, the mean annual frequency of these wind directions is less than 5 %. On 05 September 2005, the mean wind direction at the time of the onset of the O_3 drop event was from south, so the parking lot was not upwind of the TOP station. Having demonstrated that there was no current chemical destruction of O_3 at the mountain summit, we will now focus on the area south of the mountain summit because, as concluded from the wind direction, the reason for the O_3 drop must be located there.

4.3   Valley-to-mountain circulation

The high frequency of O_3 drop events in the morning hours may point to a local, thermally driven, valley-to-mountain circulation at the Hohenpeissenberg mountain. The high solar irradiance and the partly deforested slope of the mountain would support this idea. Furthermore, the village of Hohenpeissenberg is located at the lower end of the deforested south flank of the mountain, and a national road passes by. Together, village and road would provide enough O_3 destructors (mainly NO from heating and exhaust gases). But although this mechanism might seem to be the most probable one, several results of our measurements point into a different direction.

First, at the SALSA forest station at the southern slope of the mountain, half way between the deforested area and the summit, the wind direction remained around North, which is a downhill flow, at mean wind speeds around 0.5 m s^{-1}. From that, an upslope wind, at least in the trunk space of the forest, can be excluded.

Second, one of the vertical scans of the tethered balloon (Fig. 7, right panels) encountered an O_3 poor layer at approx. 300 m a.g.l. on 05 September 2005, 09:16 h, which was shortly after the maximum intensity of the O_3 drop at the TOP station. The tethered balloon profiles were measured in a horizontal distance of approx. 1.6 km from the TOP station (as referenced to the launching site of the balloon). Even with some northward drift of the balloon due to the southerly winds, the O_3 poor air mass was detected still more than 1 km south of the summit. The wind direction from south (at the height of TOP) makes it impossible for an air mass being upslope transported by a valley-to-mountain circulation to be found 1 km south of the mountain summit. Under

the assumption that the O_3 poor air mass observed by the balloon is in coherence with the O_3 event at the TOP station, which will be proven below, a local valley to mountain circulation has to be definitely excluded as the dominating process.

4.4   Airmass change, passage of fronts

The sudden drop of O_3 mixing ratio at the TOP station, together with the change of wind direction, could suggest a change of air masses. But in this case, O_3 values would have to stay low after the event and would not recover to values comparable to those before. Additionally, a peak in NO would not be expected, as NO must have been transported very fast towards the TOP site to not be converted into NO_2 due to reaction with the present O_3 during the transport. Instead, comparable levels of O_3 mixing ratio were observed, and NO (Fig. 4f) as well as NO_2 (not shown) dropped back to its pre event values close to 0. This indicates that only a temporary excursion from the state prior to the event had occurred and not a general change. Furthermore, the sharp boundaries of the O_3 depleted layer observed by the tethered balloon (Fig. 7b) suggest only a short transport time. Longer lasting transport would have smeared out the boundaries due to turbulent diffusion. Based on that, advection from greater distance, embedded in a different air mass, becomes highly unlikely. Around the O_3 drop event, a slight cooling of the entire ABL was observable (Fig. 5c), although the irradiation remained undisturbed (Fig. 4a). Since coincidences are always eye-catching, and an air mass change can be excluded, an independent explanation for the cooling has to be found, preferably a process, comprising the cooling and the simultaneous presence of the O_3 depleted layer. This could provide a proper explanation of the dynamics behind the O_3 drop events. But before such an attempt will be made, other processes being relevant in the morning hours have to be examined (and finally excluded).

4.5   Immersion of TOP station into CBL

The altitude of the wind direction change (Fig. 5a) did not coincide with the height of the CBL at this time. Although the CBL growth started at the same time as the wind direction started to change at the BASE, its height was still about 150 m less than the altitude of the layer affected by wind direction change (i.e. the altitude, where the transition of wind direction before to the wind direction after the onset of Alpine Pumping actually occurred). In Fig. 5b, the CBL can be identified as the region of enhanced wind speed fluctuations, reaching values of around 5 m s^{-1} in the afternoon. An independent confirmation is given by Fig. 6, where the CBL height is derived from

the profile of θ, which gives the height up to which an air parcel may rise by buoyancy if released at the ground, as well as the CBL height derived by visual inspection of the reflectivity data. Compared to other fair weather days during the experiment (not shown here) the evolution of the CBL started late, the growth rate was much lower and the CBL height reached a very low maximum height. Growth rates of $100...1000$ m h^{-1} (Seibert et al., 1998) were reported and maximum heights of the CBL on the order of 1 to 2 km (Stull, 1988) can be expected on clear, sunny days over terrestrial surfaces in mid latitudes. The lateral heterogeneity of the land, with patches contributing more (grassland, villages) or less (forest, rivers, lakes) to the development of the CBL reduced the expected growth rates and maximum CBL height around the SALSA site. Furthermore, subsidence over the Alpine foreland, as a result of Alpine Pumping (Lugauer and Winkler, 2005), suppressed the CBL growth even more. The combination of both processes led to a height of the CBL well below the summit of the Hohenpeissenberg mountain at the time of the O_3 drop event. Immersion of the mountain summit into the developing CBL can thus be definitely excluded as explanation.

4.6 Convective injection of surface layer air into levels above the ABL

The highly unstable conditions within the surface layer in the morning hours of 05 September 2005 suggested additional consideration of convective processes as a reason for the development of the O_3 poor layer within the ABL. With a positive sensible heat flux (see Fig. 8a), a shallow but forced convection was established shortly after sunrise (06:00h), initiating the development of a CBL. Increasing sensible heat flux and a simultaneously occurring secondary minimum of u$_*$ led to a dominance of buoyancy created turbulence over shear created turbulence (see Eq. (1)), − a state of free convection. Somewhere, upwind of the mountain, a warm air mass, already heated up for several hours, became sufficiently buoyant and rose in a pulse-like motion up to its equilibrium height. As the air close to the ground was still poor of O_3 but enriched in CO_2, H_2O and NO, a small layer with lower O_3 and higher CO_2, H_2O and NO values (compared to the surrounding air) developed. Together with the surrounding air mass (which was still statically stable), it was horizontally advected towards the mountain. Recalling Fig. 5b, the wind speed at mountain summit remained at very low values for some hours. This explains, why the event duration at 05 September was quite long with a very slow recovery of the O_3 values afterwards.

Two independent confirmations for such a process can be found in the dataset.

(1) The drop of air temperature (Fig. 8b), (not shown: simultaneous drop of H_2O and O_3 and increase of CO_2) at the BASE shortly before the onset of the O_3 decrease at the TOP station (see Fig. 4e). Again, the temporal concurrency of these observations with the TOP station observations suggests a common process. The air mass, being lifted by free convection in the surrounding of the BASE, had to be replaced by another air mass. This replacement air originated most probably from the trunk space of the nearby forest (see Fig. 10), encompassing the BASE from east to southwest. Despite strong irradiance, the air in the trunk space was still relatively cold (air temperature drop), less affected by photochemistry than the air in the open surrounding of the BASE, and due to little vertical transport through the forest canopy still enriched in CO_2, a remainder from the night time respiration of soil and plants. Other possible reasons for the temperature drop, like burning off of fog or mist can be excluded. Although earlier in the morning, the relative humidity ranged close to 100 %, it dropped down from saturation at least half an hour before the onset of the event. Patches of fog can be excluded by comparing the radiation temperature, derived from downwelling longwave radiation, with the air temperature. In case of fog, both temperatures should be very close, as fog temperature and air temperature would be the same (the location where radiative energy transfer occurs would be the upper surface of the fog layer). For 05 September, we observed a downwelling longwave radiation temperature being about 20 K lower than the air temperature. This indicates clear skies. Furthermore, no fog was observed at BASE during the morning hours of 05 September.

(2) A simple backward trajectory estimate confirmed that the source region of the convectively lifted air mass should have been at the southern part of the village Hohenpeissenberg, approx. 500 m northwest of the BASE (Fig. 10). For this estimate, some assumptions had to be made. First, the wind field was assumed to be horizontally homogeneous in all heights. This is a rough estimation, especially at low wind speeds, but for our purpose this approximation can be justified. With that, the wind vector at every time of the calculation was taken from the respective height of the SODAR wind profiles. Second, the convective vertical transport was assumed to be constant at approx. 1.5 m s^{-1} during the ascent from the surface to 288 m a.g.l. This is in accordance with textbook values for the convective velocity scale around 09:00 h in the morning (Stull, 1988). A direct calculation of the convective velocity scale from available data seemed
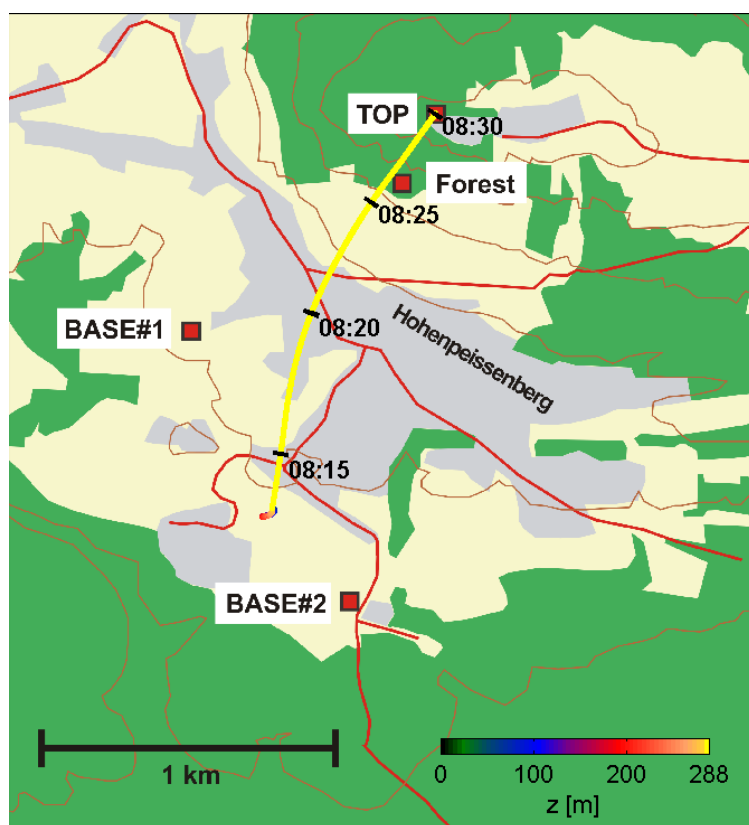
Fig. 10. Map of the village Hohenpeissenberg and the horizontal projection of a backward trajectory, computed for an impact at TOP station at 05 September 2005 08:30 h. The computed height a.g.l. of the air parcel is indicated by the colour of the trajectory. The convective ascent speed of the air mass was presumed to be in the order of 1.5 m s^{-1} from 0 to 288 m a.g.l. (with respect to BASE#2). The wind field was based on SODAR measurements with the assumption of horizontal homogeneity. Note: the ascent needed only 3.2 minutes and is thus barely visible in the figure.

to be inappropriate, as the described process must have been considerably stronger than the convective velocity within the still relatively shallow CBL.

According to (1) and (2), the phenomenon of O_3 drop events at the mountain summit is thus a combination of a free convective pulse in the morning and a subsequent advection process transporting this air parcel towards the TOP station. The trigger of the free convective pulse can either be the wind speed minimum or just a sufficient energy input by solar radiation under low wind conditions. Whether the wind speed drops due to the onset of Alpine Pumping or is just ceasing due to the synoptical situation will not affect the development of an unstable condition and thus the release of a convective pulse. Furthermore, the observation of a wind speed minimum leading to a free convective pulse is subject to some luck, as convective cells are known to have a very limited horizontal dimension (Shen and Leclerc, 1997). On 05 September 2005 we had

measured by chance within or close by such a cell. Nevertheless, convective cells can certainly develop without us being able to observe them in our ground based measurements. This explains, why some of the events listed in Tab. 2 are apparently not associated with a distinct wind speed minimum. The discrimination of O_3 drop events at TOP site, as a result of a pulse of free convection, from other causes is thus the main challenge of evaluating a long time series of O_3 measurements at the TOP station for the occurrence of O_3 drop events with a similar causation as the events described in this paper.

4.7   Long dataset

Starting with one day (05 September 2005), where all observations were made just at the right place and time, and expanding the findings to a more than 5 years period, requires a critical limitation of possible statements. One of these limitations is a clear assignment of observed events to certain processes. The diurnal distribution of O_3 drop event frequencies (Fig. 9) shows a clear difference between days with high global radiation and low global radiation. In the latter case, O_3 drop events were distributed as a diurnal cycle over day times, with a weak maximum between 09:00 h and 10:00 h (Fig. 9, black bars). In contrast, for days with high global radiation, O_3 drop event frequencies sharply peaked between 07:00 h and 09:00 h (Fig. 9, grey bars) and events were restricted to the morning hours. This gives evidence of a process, being restricted to high energy input and being primarily present in the early morning hours. However, it is possible that more than one of such processes exist, which can lead to the same phenomenon in the O_3 time series. As described in Sect. 4.1, the independent phenomenon of Alpine Pumping is also bound to high global radiation days. It is able to provide a (secondary) wind speed minimum in the morning hours. From that we can make two statements: (a) due to Alpine Pumping, conditions favourable for free convection occur frequently in early morning hours of fair weather days, and (b) on fair weather days we observed the maximum frequency of O_3 drop events at the TOP station. Together, this clearly points towards a convective pulse, as it was discussed in the previous section. Almost half of the events with high energy input (84 events) occurred at days when the mesoscale circulation Alpine Pumping occurred. We found Alpine Pumping to occur at 46 % of all days during which total global radiation exceeded 20 MJ m^{-2}. This is in excellent agreement with Lugauer and Winkler (2005), who found 42 %. The onset of the circulation, with its associated change of wind direction, must cause a short minimum of horizontal wind speed. Again, this points to a

convective process, as low wind speeds are known to increase already present thermal instability. The other half of the events with high energy input (85 events) was not connected to Alpine Pumping. At least, characteristics of Alpine Pumping were not observable at the TOP station at these days. But horizontal wind speed is generally not very high during fair weather days, and can furthermore drop to low values for various reasons – leading to the same destabilisation of moist and heated air masses.

Daily total global radiation of more than $20\,MJ\,m^{-2}$ at midlatitudes is restricted to a period approximately from April to September. During this period, the TOP site was in 18 % of the days affected by an O_3 drop event, coupled to high energy input, being most probably the result of a convective pulse. Half of those events are even more likely to originate from a free convective pulse, as they occurred at days with Alpine Pumping, where a short wind speed drop in the morning hours occurs. Furthermore, these numbers have to be taken as a minimum estimation, as the convectively lifted air masses do not necessarily have to be advected towards the TOP site, and they do not have to be trapped at just the right altitude to be intercepted by the TOP station.

Evidence for such free convection phenomena were recently found also for other locations (Eigenmann et al., 2008), although it was often not identified as active free convection (e.g. Hiller et al., 2008).

5   Conclusions

The observed O_3 drop events result from free convection in the morning hours with the strength to rise far above the height of the growing CBL. The trigger of the convection can be manifold and are not necessarily limited to a mesoscale circulation system as it was the case in half of the days in this study. The described processes provide a powerful vertical transport mechanism in the early morning hours, which has a strong impact on atmospheric chemistry (trace gases) and meteorology (air temperature) close to ground as well as in higher altitudes.

The O_3 drop events were not only observed during the field experiment but were present throughout the entire period from October 2000 to December 2005. On 18 % of the days between April and September, the O_3 decreases are most likely the result of a free convective pulse in the early morning.

It can be expected that similar processes are active in many other regions, where appropriate triggers like local or mesoscale circulation systems lead to a convective release of surface layer air masses into the residual layer. Whether or not such transport

events are sufficiently captured by common flux measurement techniques should be carefully investigated. This becomes particular true, when observed trace gas concentrations are to be assigned to possible source regions, only based on the wind direction.

Acknowledgements

Edited by: A. Pszenny

The publication of this article is financed by the Max Planck Society.

References

Aneja, V. P., Arya, S. P., Li, Y., Murray, G. C., JR., and Manuszak, T. L.: Climatology of Diurnal Trends and Vertical Distribution of Ozone in the Atmospheric Boundary Layer in Urban North Carolina, Journal fo the Air & Waste Management Association, 50, 54-64, 2000.

Attmannspacher, W., and Hartmannsgruber, R.: On Extremely High Values of Ozone Near the Ground, Pure Appl. Geophys., 106-108, 1091-1096, 1973.

Beyrich, F., Weisensee, U., Sprung, D., and Güsten, H.: Comparative analysis of sodar and ozone profile measurements in a complex structured boundary layer and implications for mixing height estimation, Boundary-Layer Meteorol., 81, 1-9, 1996.

Beyrich, F.: Mixing Height Estimation from SODAR Data - a Critical Discussion, Atmos. Environ., 31, 3941-3953, 1997.

Cheng, W.-L.: A vertical profile of Ozone concentration in the atmospheric boundary layer over central Taiwan, Meteorol. Atmos. Phys., 75, 251-258, 2000.

Corsmeier, U., Kalthoff, N., Kolle, O., Kotzian, M., and Fiedler, F.: Ozone concentration jump in the stable nocturnal boundary layer during a LLJ-event, Atmos. Environ., 31, 1977-1989, 1997.

Eigenmann, R., Metzger, S., Siebicke, L., Staudt, K., Serafimovich, A., and Foken, T.: Generation of free convection in a valley due to changes of the local circulation system, 18th Symposium on Boundary Layers and Turbulence, Am. Meteorol. Soc., Stockholm, June 09-13, 2008.

Fast, J. D., Doran, J. C., Shaw, W. J., Coulter, R. L., and Martin, T. J.: The evolution of the boundary layer and its effect on air chemistry in the Phoenix area, J. Geophys. Res., 105, 22833-22848, 2000.

Foken, T., Göckede, M., Mauder, M., Mahrt, L., Amiro, B. D., and Munger, J. W.: Post-field data quality control, in: Handbook of Micrometeorology: A Guide for Surface Flux Measurements, edited by: Lee, X., Kluwer, Dordrecht, 81-108, 2004.

Güsten, H., Heinrich, G., and Sprung, D.: Nocturnal depletion of ozone in the Upper Rhine Valley, Atmos. Environ., 32, 1195-1202, 1998.

Hastie, D. R., Narayan, J., Schiller, C., Niki, H., Shepson, P. B., Sills, D. M. L., Taylor, P. A., Moroz, W. J., Drummond, J. W., Reid, N., Taylor, R., Roussel, P. B., and Melo, O. T.: Observational evidence for the impact of the lake breeze circulation on ozone concentrations in Southern Ontario, Atmos. Environ., 33, 323-335, 1999.

Hiller, R., Zeeman, M. J., and Eugster, W.: Eddy-covariance flux measurements in the complex terrain of an Alpine valley in Switzerland, Boundary-Layer Meteorol., 127, 449-467, 2008.

Holzworth, C. G.: Estimates of Mean Maximum Mixing Depths in the Contiguous United States, Mon. Weather Rev., 92, 235-242, 1964.

Holzworth, C. G.: Mixing depths, wind speeds, and air pollution potential for selected locations in the United States, J. Appl. Meteorol., 6, 1039-1044, 1967.

Lee, S.-M., Fernando, H. J. S., Princevac, M., Zajic, D., Sinesi, M., McCulley, J. L., and Anderson, J.: Transport and Diffusion of Ozone in the Nocturnal and Morning Planetary Boundary Layer of the Phoenix Valley, Env. Fluid Mech., V3, 331-362, 2003.

Lin, C.-H., Wu, Y.-L., Lai, C.-H., Lin, P.-H., Lai, H.-C., and Lin, P.-L.: Experimental investigation of ozone accumulation overnight during a wintertime ozone episode in south Taiwan, Atmos. Environ., 38, 4267-4278, 2004.

Lugauer, M., and Winkler, P.: Thermal circulation in South Bavaria - climatology and synoptic aspects, Meteorol. Z., 14, 15-30, 2005.

McKendry, I. G., Steyn, D. G., Lundgren, J., Hoff, R. M., Strapp, W., Anlauf, K., Froude, F., Martin, J. B., Banta, R. M., and Olivier, L. D.: Elevated ozone layers and vertical down-mixing over the Lower Fraser Valley, BC, Atmos. Environ., 31, 2135-2146, 1997.

McKendry, I. G., Steyn, D. G., O'Kane, S., Zawar-Reza, P., and Heuff, D.: Lower Tropospheric Ozone Measurements by Light Aircraft Equipped with Chemiluminescent Sonde, J. Atmos. Ocean. Technol., 15, 136-143, 1998.

Müller, H., and Sladkovic, R.: Case Studies of Frontal Passages in a Mountain Valley with Direct Access to the Bavarian Pre-Alpine Region Results from the German Front Experiment 1987, Meteorol. Atmos. Phys., 43, 77-87, 1990.

Prévôt, A. S. H., Dommen, J., Bäumle, M., and Furger, M.: Diurnal variations of volatile organic compounds and local circulation systems in an Alpine valley, Atmos. Environ., 34, 1413-1423, 2000.

Reitebuch, O., Strassburger, A., Emeis, S., and Kuttler, W.: Nocturnal secondary ozone concentration maxima analysed by sodar observations and surface measurements, Atmos. Environ., 34, 4315-4329, 2000.

Rummel, U.: Turbulent exchange of ozone and nitrogen oxides between an Amazonian rain forest and the atmosphere, University of Bayreuth, Bayreuth, 246 pp., 2005.

Salmond, J. A., and McKendry, I. G.: Secondary ozone maxima in a very stable nocturnal boundary layer: observations from the Lower Fraser Valley, BC, Atmos. Environ., 36, 5771-5782, 2002.

Seibert, P., Beyrich, F., Gryning, S. E., Joffre, S., Rasmussen, A., and Tercier, P.: Mixing layer depth determination for dispersion modeling, in: COST Action 710-Final Report. Harmonisation of the pre-processing of meteorological data for atmospheric dispersion models, edited by: Fisher, B. E. A., Erbrink, J. J., Finardi, S., Jeannet, P., and Thomson, D. J., European Commission, L-2985 Luxembourg, 145-265, 1998.

Shen, S., and Leclerc, M. Y.: Modelling the turbulence structure in the canopy layer, Physical and Biophysical Processes in the Vegetation Environment, 87, 3-25, 1997.

Strong, C., Fuentes, J. D., Davies, R. E., and Bottenheim, J. W.: Thermodynamic attributes of Arctic boundary layer ozone depletion, Atmos. Environ., 36, 2641-2652, 2002.

Stull, R. B.: An introduction to boundary layer meteorology, Kluwer Academic Puplisher, Dordrecht, 666 pp., 1988.

Talbot, R., Mao, H., Troop, D., Moore, B., Johnson, R., and Businger, S.: Smart balloon observations over the North Atlantic: Part I - Mini-O_3 sampling of urban plumes, J. Geophys. Res., in press, 2006.

Vickers, D., and Mahrt, L.: Quality Control and Flux Sampling Problems for Tower and Aircraft Data, J. Atmos. Ocean. Technol., 14, 512-526, 1997.

Wanner, H., Künzle, T., Neu, U., Ihly, B., Baumbach, G., and Steisslinger, B.: On the Dynamics of Photochemical Smog over the Swiss Middleland - Results of the First POLLUMET Field Experiment, Meteorol. Atmos. Phys., 51, 117-138, 1993.

Whiteman, C. D., and Bian, X.: Use of Radar profiler data to investigate large-scale thermally driven flows into the Rocky Mountains., 4th Int. Symp. trop. Profiling, Snowmass, Colorado, 329-331, 1998.

Whiteman, C. D.: Mountain Meteorology, Oxford University Press, 355 pp., 2000.

Yelansky, N. F., and Senik, I. A.: Measurements of surface ozone concentrations at the high-mountain scientific station Kislovodsk: The seasonal and daily variations, Atmos. Ocean. Phys., 31, 235-243, 1995.

Appendix C:

Moving measurement platforms - specific challenges and corrections

J.-C. Mayer[1], K. Hens[1], U. Rummel[2], F.X. Meixner[1,4] and T. Foken[3]

[1] Biogeochemistry Department, Max Planck Institute for Chemistry, Mainz, Germany
[2] Richard Aßmann Observatory Lindenberg, German Meteorological Service, Germany
[3] Department of Micrometeorology, University of Bayreuth, Bayreuth, Germany
[4] Department of Physics, University of Zimbabwe, Harare, Zimbabwe

Abstract

Most sensors do not perfectly reproduce changes of the measured quantity with respect to time and intensity. Delays and damping effects cause the signal to deviate from the true value. These deviations are often caused by combined impacts of the probe itself, the probe's housing, the sensor's inlet system and more. In this work, we will (a) evaluate correction schemes already known from aircraft temperature measurements for their performance on measured vertical temperature profiles, and (b) present an alternative, simpler correction scheme. The temperature profiles were measured with an elevator system at a 99 m mast from 2 m to 98 m a.g.l., parallel to a stationary high quality reference temperature profile. Besides laboratory tests, we will demonstrate and quantify the effect of the corrections applied to the mobile temperature sensor's data in direct comparison with the reference temperature data. This direct comparison (a) exceeds the potential of aircraft measurements, where comparisons with stationary in-situ sensors are hard to realize, and (b) clearly shows the effectiveness and correct magnitude of the corrections. It is demonstrated with temperature measurements, that a mobile sensor can satisfactorily substitute a profile of stationary sensors.

Zusammenfassung

Die meisten Messsysteme können die tatsächliche Änderung der Messgröße bezüglich Zeitpunkt und Intensität nicht exakt abbilden. Es treten Verzögerungs- und

Dämpfungseffekte auf. Diese sind oftmals die Folge eines kombinierten Einflusses von Sensor, Sensorgehäuse, Einlasssystem usw. In dieser Arbeit werden sowohl bereits aus Flugzeugmessungen bekannte, mathematisch aufwändige Korrekturalgorithmen als auch ein mathematisch einfacher Korrekturansatz an realen vertikalen Temperaturprofilen getestet. Die Temperaturprofile wurden mittels eines Aufzuges an einem Mast zwischen 2 m und 99 m parallel zu einem statisch betriebenen Referenzprofil gemessen. Neben Labortests wird der Effekt der Korrekturen im direkten Vergleich mit dem parallel gemessenen Referenzprofil quantifiziert. Diese direkten Vergleiche mit Referenzdaten (a) gehen über die Möglichkeiten von Flugzeugmessungen hinaus, wo parallele, stationäre Messungen kaum zu realisieren sind, und (b) demonstrieren deutlich den Effekt der Korrektur auf die gemessenen Profile sowie die korrekte Intensität der Korrektur. Es wird gezeigt, dass ein mobiler Sensor ein Profil statischer Sensoren zufriedenstellend ersetzen kann.

1 Introduction

When measuring in-situ profiles of meteorological or chemical quantities in the atmospheric boundary layer (ABL), one is usually limited either to stationary tower or mast measurements, or to mobile profiling systems like radiosondes, tethersondes and kite borne systems. Alternatively, elevator systems may be used. Stationary tower and mast systems have the advantage of being operated unattended and providing highly resolved data in the time domain. Data quality of such systems can be maintained at a high level by optimizing sensor housings (radiation shields) or sampling inlets. But at least one disadvantage remains: the achievable vertical spatial resolution is limited due to flow distortion problems and also due to monetary aspects. One faces a different situation when using mobile profiling systems. The vertical spatial resolution is theoretically only limited by the sampling speed, and only one sensor per quantity being measured has to be deployed (limiting measurement errors only to the error of one instrument). Especially in the case of (free) flying systems (e.g. tethersondes and radiosondes, kites), payload is limited. Also the sensor housing and inlet constructions may be limiting. Furthermore, the response time of deployed sensors becomes more important for moving systems as it is for tower and mast systems. In case of moving systems, long response times of the sensors, with respect to the desired resolution, do not only lead to a damped signal, it induces also a dynamical (spatial) error to the measurements (e.g. FOKEN, 2008). Dynamical error means, that the magnitude of the measurement error (i.e. the deviation between measured and true value) depends on the
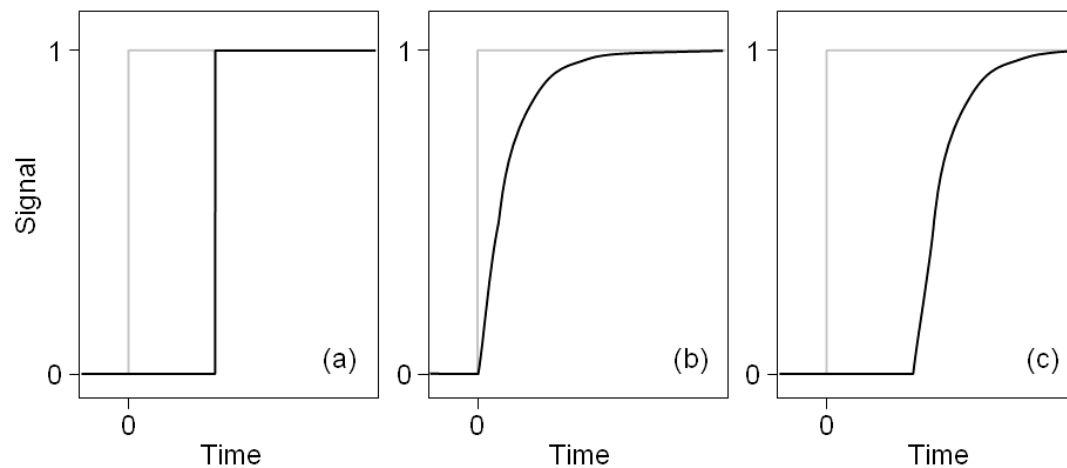
Figure 1: Schematics of a system response (black line) to a prescribed step change at time = 0 (grey line): (a) lag time only, (b) sensor response time only (dynamical error) and (c) lag time and sensor response time.

intensity of changes in the quantity being measured (i.e. on the dynamics). In the case of moving systems, this is also true for spatial changes (e.g. passing through inversion layers) (FOKEN, 2008). Additionally, the dynamical error is often superimposed with lag-times of the sampling system. Lag-times, in contrast to a dynamical error, do not result in change of measured amplitudes, but cause a linear time shift of the signal recorded. Schematics of such system response characteristics for a prescribed step change are shown in Figure 1.

If lag-time effects can be properly separated from dynamical errors, their magnitude can easily be determined by cross correlation and subsequently be corrected by linear shift of the time series.

The most prominent application of fast-response sensors in (micro)meteorological research are turbulence studies as well as aircraft and radiosonde measurements. In the first case, fast temporal changes of the quantity being measured are typical, in the latter case, spatial changes are folded back to fast temporal changes at the sensor, as the aircraft or sonde passes through different air masses. A lot of effort has been done to develop fast and meanwhile stable temperature sensors (e.g. HAMAN, MAKULSKI et al., 1997). Where this was not sufficient, recorded signals were corrected for the influence of response times (RODI and SPYERS-DURAN, 1972; MCCARTHY, 1973; FRIEHE and KHELIF, 1993; MAHESH et al., 1997; INVERARITY, 2000; SAGGIN et al., 2001).

In most applications, the sensing element is not immersed directly into the sample air, but is surrounded by a housing. For temperature measurements, this is for example the radiation shield, or in case of aircraft measurements, a protection against radiation and water droplets (FRIEHE and KHELIF, 1993). The presence of a housing alters the heat

transfer between sensing element and sampled air, because an additional heat transfer between housing and sampled air (and thus the sensing element) occurs (RODI and SPYERS-DURAN, 1972; MCCARTHY, 1973).

Considering aircraft measurements, as reported in most publications dealing with response time corrections, a specific problem appears. Sensor response characteristics are usually determined in laboratory tests. The results of these tests are fed to a correction algorithm (e.g. MCCARTHY, 1973; INVERARITY, 2000) to finally correct the measured signal. But intercomparisons between the corrected signal (from the in-flight measurements) and an independent stationary sensor are virtually impossible. That means that the derived corrections could be validated only in a laboratory environment or by comparison of two independent sensors, where both were still located on the same moving platform (FRIEHE and KHELIF, 1993). For radiosonde temperature measurements, a limited comparison experiment was done by MAHESH et al. (1997), where radiosonde data were compared to quasi co-located measurements done with a tethered kite.

However, having a high quality reference system available (stationary tower and mast measurements) operated in parallel to a moving system (elevator system), two very important questions can be addressed: (a) are the correction algorithms able to correctly reproduce the true values, as determined by the reference system? And (b) how good is the agreement between the moving and the stationary system?

In this paper, we tested (a) two correction algorithms published elsewhere (MCCARTHY, 1973; INVERARITY, 2000) and (b) a simple conceptual model of the interaction between sensing element, housing and sampled air against reference data from tower and mast measurements.

2   Material and Methods

2.1   Site and instrumentation

The LIBRETTO (LIndenBerg REacTive Trace gas prOfiles) campaign took place in late summer 2006, from 01 August 2006 until 31 August 2006 at the Falkenberg Boundary Layer Field Site of the Meteorological Observatory Lindenberg (Richard-Aßmann Observatory) (BEYRICH and ADAM, 2007). The field site is located at 52° 10' 01" N, 14° 07' 27" E 73 m a.s.l.. The topography is a slightly undulating surface with height differences of less than 100 m over distances of about 10 km. The land use in the area is dominated by forest and agricultural field, with some embedded lakes. The

Table 1: Instrumentation details of mast and elevator measurements during the LIBRETTO campaign, used in this work.

	Stationary system		Mobile system
	Tower (99 m)	Mast (10 m)	Elevator (ELM)
Levels (a.g.l.)	10, 20, 40, 60, 80, 98 m	2, 4 m	2 – 99 (1 m resolution)
Temperature sensors	Psychrometer (Frankenberger) with PT100 probes	Psychrometer (Frankenberger) with PT100 probes	Rotronic, MP100H (PT100 probe), aspirated Thermocouples, Ø ca. 1 mm, length ca. 4 mm, Type E (Chromel-Constantan), aspirated

field site comprises a 99 m and a 10 m high profile mast. They will be further on referred to as tower (99 m) and mast (10 m). Two identical setups for the measurement of the net radiation flux, two energy balance stations, a soil monitoring field, and a SODAR-RASS system complete the setup of the Falkenberg site. However, in this paper, we confine our analyses on stationary tower and mast measurements of vertical profiles of temperature, obtained from the mast for the lower part, and from the tower for the upper part of the profile. Details about the instrumentation relevant for this work are summarized in Table 1.

The tower is equipped with an elevator, usually used for service and maintenance. On this elevator, additional sensors for air temperature (T) and some trace gases have been installed. This scanning measurement system will be referred to as the "elevator measurement system" (ELM). However, we limit our evaluations of field data to the air temperature data from the thermocouple probe (TC), because (a) the Rotronic probe of the ELM suffered from frequent electrical disturbances, and (b) the tower was not equipped with trace gas sensors. Nevertheless, results from laboratory test will be shown for both temperature probes. The housing for the temperature sensors at the elevator is shown in Figure 2. The elevator was automatically run up and down once every 10 minutes, interrupted only for data retrieving and service. At bottom and top position, the elevator had approx. 6.5 minutes idle time for intercomparison and equilibration, thus one profile needed approx. 3.5 minutes to be measured.
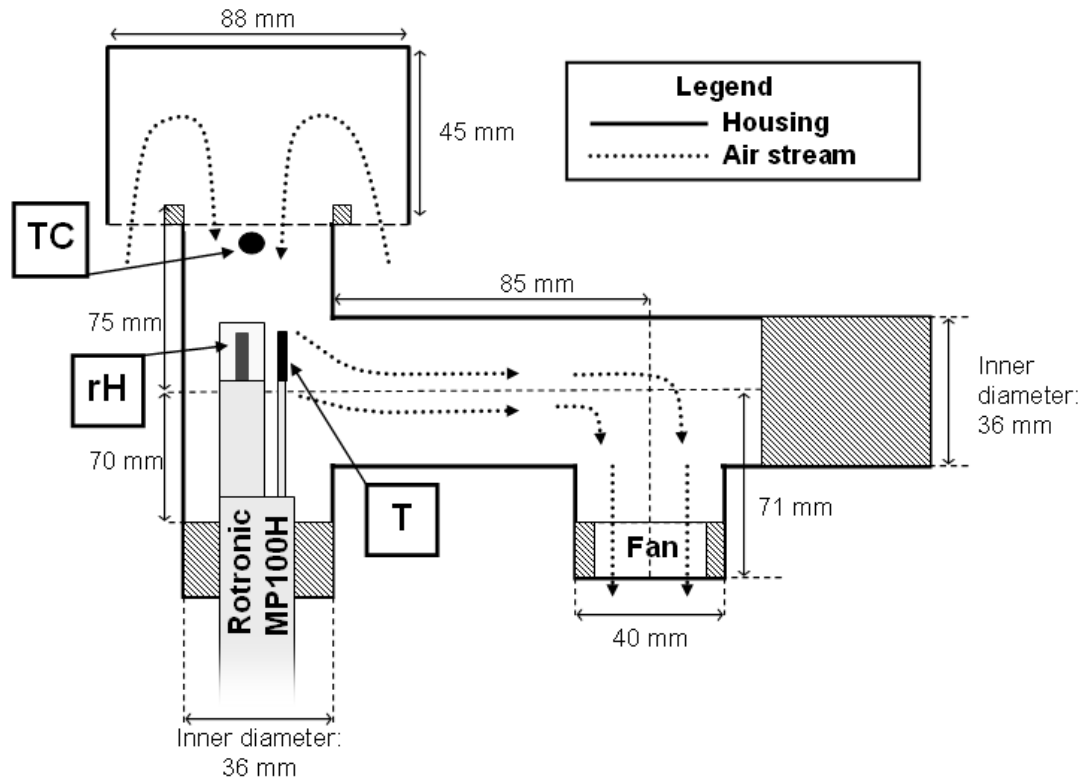
Figure 2: Schematics of the self-made protection housing of the Rotronic probe MP100H (with its temperature (T) and relative humidity (rH) probe) and the thermocouple probe (TC) as it was deployed at the ELM. The housing is made of white painted PVC tubes.

2.1.1   Data processing – tower and mast systems

Data from both stationary systems (tower and mast) were flagged with quality indicators according to BEYRICH and ADAM (2007). The quality flags included indicators set for (a) the representativeness of the value for the field site, (b) checks of differences between neighbour levels, (c) manual correction of visually erroneous data, (d) exceedance of certain threshold values (e.g. relative humidity > 100 %), (e) flow distortion by the mast if the wind blew from the back side of the mast and (f) disturbed measurements due to maintenance activities in the proximity. Only data without any critical flag set were passed on to further analyses.

As the mast data were originally recorded as 10 minutes averages, no further pre-processing steps were applied to them, to maintain their high quality level as basis for later intercomparisons.

2.1.2   Data processing – mobile system (ELM)

Data of the ELM were prepared for further analyses following the scheme shown in Figure 3. Some steps of the data processing need additional explanations: (a) During the quality control, data influenced by service work on or in the proximity of the tower
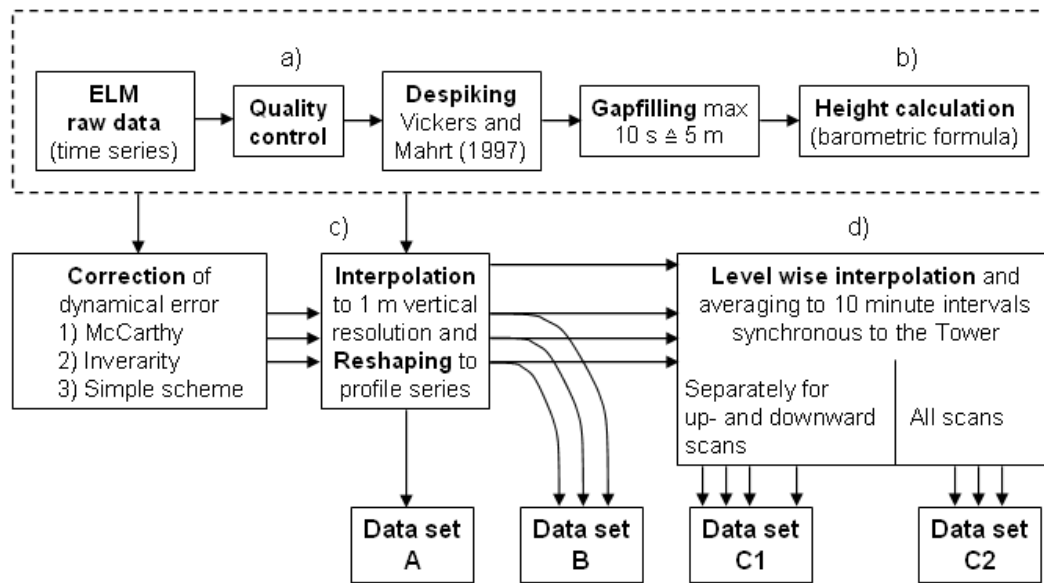
Figure 3: Schematics of the data processing steps of the mobile elevator system. The resulting data set A contains uncorrected profile data; data set B contains the corresponding corrected measurements (separately for all three algorithms). Data set C1 contains corrected and uncorrected profile data, but is synchronized to the tower and mast times (separately for up- and downward scans). Data set C2 contains synchronized corrected profile data without discrimination between up- and downward scans.

were replaced by wild cards. (b) The calculation of the height above ground level (a.g.l.) yielded relative height errors of $\leq 0.04\,\%$. A consideration of these errors was thus negligible. Furthermore, to constrain uncertainties of the height calculation with the barometric formula, a deviation of the computed height at the end of each profile was distributed linearly over the corresponding profile. (c) The vertical resolution was fixed to 1 m by applying a spatial interpolation (AKIMA, 1970). (d) For intended comparisons between ELM and tower data, ELM data were converted into 10 minute averages, synchronous to the tower and mast data by the following procedure: (1) at every level of tower and mast temperature measurements, the measured time series (1 data point per elevator scan) was interpolated to a temporal resolution of 10 seconds by applying an non-linear interpolation algorithm (AKIMA, 1970), (2) from this interpolated time series, 10 minute averages, synchronous to the reference mast measurements were computed. This interpolation with subsequent averaging was introduced to avoid systematic deviations between the two systems due to the different types of data sampling (averages from tower and mast, instantaneous data from the ELM). The data set being used for the individual investigations is indicated in the respective sections. Its selection depended on the type of comparison (elevator only or relative to tower and mast data).

2.2   Low sensor response: correction procedures

To avoid confusion in the following sections, we will use the term "probe" when referring to the measuring device itself (e.g. the thermocouple or a temperature sensitive semi conductor), and the term "sensor" when referring to the combination of probe and housing.

2.2.1   *Normalized response curve (laboratory)*

Fast temperature measurements of the ELM were performed with an aspirated thermocouple. To avoid frequent probe failures due to shock and vibrations of the running elevator, the probe had to be robust (about 1 mm diameter, see Table 1), which led to long response times. Extensive laboratory tests have been performed to develop a suitable scheme to correct the measured data for the dynamical error due to long response times. The sensor was put into a cooled, temperature controlled chamber (about 6 °C). After it had cooled down and equilibrated with the surrounding air, it was put back into room air (about 20 °C). The sensor response to this temperature step change was recorded by a data logger (Campbell Sci, Model 23X, 0.5 Hz sampling frequency). From a total of 23 step change measurements, each comprising 152 data points, a mean, normalized response curve was established. The normalization was done by subtracting the minimum temperature from the response curve and dividing through the temperature difference defined by the applied step change.

Two least-squares fits to the normalized response curve were done with the fit function

$$Fit\_1(t) = 1 - e^{-\frac{t}{\tau_A}} \tag{1}$$

and

$$Fit\_2(t) = A \cdot \left(1 - e^{-\frac{t}{\tau_A}} \right) + B \cdot \left(1 - e^{-\frac{t}{\tau_B}} \right). \tag{2}$$

Eq. (1) is valid in case of probes with an exponential response characteristic (e.g. thermocouples without housing), while Eq. (2) holds for more complex sensors, whose response characteristic can be explained by a superposition of probe response (*A*) and housing response (B). For a normalized response curve, the weighting coefficients *A* and *B* in Eq. (2) must sum up to 1, and the response times are given by τ_A and τ_B.

From the least-squares fits to the measured response curve, A, B, τ_A and τ_B were determined. The results were used to correct the measured signal of the thermocouple sensor by applying the steps described in the following.

2.2.2 Existing correction schemes

Two already existing correction schemes were used in addition to a more simple correction scheme (see below). One approach is that of MCCARTHY (1973), the other one that of INVERARITY (2000). A prerequisite of these approaches is the determined response characteristic of the sensor with a separation into the individual contributions, as described in Section 2.2.1. The starting point of both approaches is to express the relation between measured temperature and the true air temperature in form of a convolution integral

$$T_M(t) = \int_{-\infty}^{t} T_A(t - t') \cdot g(t') dt' \tag{3}$$

where T_A denotes the true air temperature and T_M stands for the measured temperature. The so-called transfer function g is related to the step response function (Eq.(2)) according to

$$Fit\_2(t) = \int_{0}^{t} g(t') dt' \quad . \tag{4}$$

From that we obtain

$$g(t) = k_1 A e^{-k_1 t} + k_2 B e^{-k_2 t} , \tag{5}$$

with A and B being the same weighting factors as in Eq. (2) and in section 2.2.3, and $k_1 = 1/\tau_1$, $k_2 = 1/\tau_2$.

The approach of MCCARTHY (1973) applies a forward difference approximation and uses finite difference approximations for first and second order temporal derivative of the measured time series, although the actual computing of the derivatives is not

described. The finite difference approach is assumed to induce some error in this solution (INVERARITY, 2000). The actual correction after MCCARTHY (1973) is done by solving the following equations, derived from the convolution problem of Eq. (3):

$$T_A(t_{n+1}) = T_A(t_n) + \frac{1}{2}\Delta t\left\{ F\left[T_A(t_n),t_n\right] + F\left[T_A(t_{n+1}),t_{n+1}\right] \right\} \quad , \tag{6}$$

With T_A being a function of time and temperature, defined as:

$$F(T_A,t) = \left(Ak_1 + Bk_2\right)^{-1} \times \left[\frac{d^2T_M}{dt^2} + \left(k_1 + k_2\right)\frac{dT_M}{dt} + k_1k_2\left(T_M - T_A\right)\right] \tag{7}$$

for equally spaced data with time steps $\Delta t = t_{n+1} - t_n = const.$

INVERARITY (2000) proposed a more exact scheme. In the special case of working in the Celsius scale and using 0 °C as an initial value for the ambient temperature T_A each step can be computed by application of

$$T_A(t_n) = \frac{1}{2}\alpha^{-1}\Delta t^{-1}\left[T_M(t_{n+1}) - T_M(t_{n-1})\right] + \beta T_M(t_n) + \gamma\left(1 - \beta\right)I_n \tag{8}$$

with the constants α, β and γ defined as:

$$\alpha = k_1 A + k_2 B \tag{9}$$
$$\beta = \left(k_1 + k_2\right)\alpha^{-1} - k_1k_2\alpha^{-2} \tag{10}$$

$$\gamma = k_1k_2\alpha^{-1}. \tag{11}$$

The function I_n in Eq. (8) has to be determined by using the following recurrence:

$$I_0 = 0, \tag{12}$$

$$I_n = e^{-\gamma(t_n - t_{n-1})}I_{n-1} + 2^{-1}(t_n - t_{n-1}) \times \left[e^{-\gamma(t_n - t_{n-1})}T_M(t_{n-1}) + T_M(t_n)\right] \quad , \quad \forall\, n > 0. \tag{13}$$

2.2.3   Simple correction scheme

A simple correction scheme was developed to correct our measured time series for the influence of the probe housing and the slow response of the probe itself. The advantage of this simple correction scheme compared to the more sophisticated approaches described above is, that it is also applicable to measurements, which are influenced by those sensor housings, whose influence can not be described by an exponential function. According to FOKEN (2008), a stepwise correction of a recorded signal T_M (here in °C) for any dynamic system of the first order (probe only), characterized by the response time τ, is described as follows:

$$T_A(t) = T_M(t) + \tau \cdot \frac{\Delta T_M}{\Delta t} \ . \tag{14}$$

Here, T_A denotes the real air temperature, t stands for time and τ is the time constant of the probe.

The correction of our sensor signal (probe and housing) required a slightly different approach, which comprises the following steps: (1) Given the bulk τ of the sensor (i.e. τ determined directly from the sensor response curve), the first approximation of T_A was computed according to Eq. (14), (2) from this first guess time series of T_A, an artificially damped time series was computed for the temperature of the probe's housing ($T_{Housing}$) with its individual response time (τ_B), (3) the measured signal T_M is assumed to be a superposition of the temperature of both components at a certain time (i.e. T_{Probe} and $T_{Housing}$), weighted by their weighting coefficients A and B:

$$T_M = A \cdot T_{Probe} + B \cdot T_{Housing} \ . \tag{15}$$

(4) to eliminate the influence of the housing from the sensor signal, Eq. (15) is solved for the temperature of the probe (T_{Probe}):

$$T_{Probe} = \frac{T_M - \left(B \cdot T_{Housing} \right)}{A} \ . \tag{16}$$

(5) T_{Probe} is the response of the probe to the true change of air temperature, with an attenuation caused by its individual response time, (6) thus, as a last step, Eq. (14) was

applied to T_{Probe} (T_{Probe} in Eq. (16) is equivalent to T_M in Eq. (14)), to correct for the response time of the probe, giving the true air temperature as result.

2.3   Comparison of ELM and stationary system

All comparisons between the ELM and the stationary system (tower and mast) were limited to night times (i.e. global radiation = 0 Wm^{-2}), to avoid any influence of shortwave radiation on the temperature measurements.

To compare ELM data with the stationary data from the tower and mast, differences in data sampling of both systems had to be taken into account. While the tower and mast data consisted of 10 min averages at a certain level, ELM data were point measurements in spatial and temporal dimensions. Therefore, for the intended comparison, ELM data were converted into 10 minute averages, synchronous to the tower and mast data as described in Section 2.1.2. For all comparisons between the tower and mast measurements and the ELM, data sets C1 or C2 were used together with the corresponding tower and mast data.

3   Results and Discussion

3.1   Normalized response times (laboratory)

The first step towards the correction of the measured temperature signal was a laboratory test of the system response. A step change of ambient temperature was applied to the sensor, and the system response was recorded. The mean response curve of this experiment for our thermocouple probe (TC) and the Rotronic temperature probe is shown in Figure 4. Simple probes, like a bare thermocouple (without housing), typically exhibit an exponentially shaped response curve (following Eq. (1)) when exerting a step change of the measured parameter. However, the fit following Eq. (1) showed strong deviations from the measured sensor response (Figure 4a and 4b). Although the initial, rapid adjustment of the signal to the exerted step change was described reasonably well by Eq. (1), the time actually needed for full equilibration of the sensor was much longer than predicted by Eq. (1). This suggested that the shape of the measured response curve might have been composed as a superposition of two exponential functions (see Eq. (2)). The superposition of two exponential functions however means that beside the probe itself also the probe housing can have considerable influence on the response characteristic of the sensor. The results of the corresponding fits for the TC and the Rotronic probe according to Eq. (2) (see section 2.2.1) are
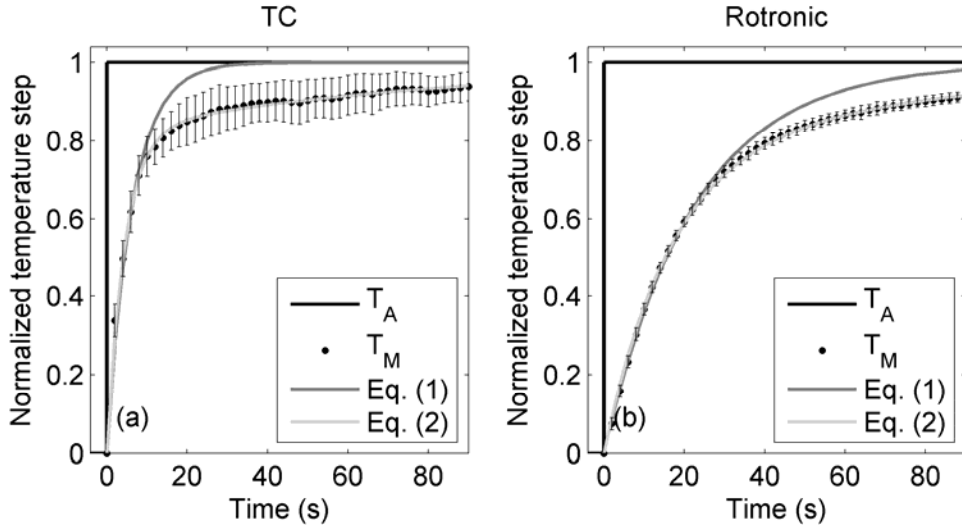
Figure 4: Observed sensor response T_M with thermocouple TC (left panel, black circles) and Rotronic probe (right panel, black circles) to a step change of ambient temperature T_A (black line) at time $t = 0$ s. The dark grey line shows the fit for a first order system (Eq. (1), the light grey line shows the fit for the superposition of two first order systems (Eq. (2)).

summarized in Table 2. The corresponding fit curves (fit with Eq. (1) and (2)) are shown in Figure 4a for TC and Figure 4b for the Rotronic probe.

The fit routine performed well for both temperature probes, with RSS ≤ 0.053 K for 152 data points. The response times τ_A and τ_B exhibited important differences between the two sensors. Especially τ_A, which stands for the response time of the probe, demonstrated the strong difference of thermal mass between TC and the Rotronic temperature probe, where the latter has a considerably larger thermal mass. Both probes were directly immersed into the aspirated air flow (see Figure 2). The second noteworthy pattern is the almost identical time scale of τ_B from the sensors, which stands for the housing. As both probes were located within the same housing (but at slightly different locations (see Figure 2)), the comparable magnitude of τ_B was to be expected.

Table 2: Measured parameters of the temperature sensors used in this study. Coefficients A and B must sum up to 1. N=152.

Sensor	TC	$T_{Rotronic}$
RSS (K)	0.053	0.051
R^2	0.999	0.999
τ_A (s)	4.4	16.4
τ_B (s)	81.1	82.5
A	0.82	0.76
B	0.18	0.24

3.2   Application of the corrections

Before applying the correction schemes to our measured data, the schemes had to prove their ability of correctly reconstruct the original time series from the damped recorded signal. We will address this in the first subsection. Afterwards, the performance of the ELM will be compared to reference tower and mast data.

3.2.1   Artificial time series - reconstruction accuracy

To ascertain the proper performance of the correction schemes (MCCARTHY (1973), INVERARITY (2000) and our simple correction scheme), they were applied to an artificially damped time series. This artificial, damped time series was generated in the following way: (a) A time series consisting of sine waves with constant frequency and amplitude 1 was generated, and (b) this time series was damped with the coefficients of the TC probe (Table 2), as if it was measured with the TC probe. The correction schemes were applied to this time series, and the reconstructed signal was compared to the original time series. To determine a potential frequency dependency of the peak deviations (amplitude and phase) between the reconstructed and the original, artificial time series, this procedure was done with different frequencies of the original artificial sine wave, ranging from 10 Hz to 0.01 Hz, corresponding to period lengths from 0.1 s to 100 s. An example of the original artificial time series, the damped time series and the reconstructed time series is shown in Figure 5a. Note, that the amplitude of the damped signal was only about 5 % of the original amplitude. This means, that the amplitude had to be increased by the algorithms by about 20 times to yield to original values. In this respect, all three corrections performed very well. A slight overcorrection became visible for the correction schemes of INVERARITY (2000) and MCCARTHY (1973), while our simple scheme ended up in a slight undercorrection (-14 % at 0.5 Hz, see Figure 5b). Nevertheless, this was a very good result when considering the simplicity of mathematics behind our scheme and taking into account, that a sine input can be considered as an extreme case.

The result of the frequency dependency test is presented in Figure 5c. While the correction schemes of INVERARITY (2000) and MCCARTHY (1973) lead to similar results, with a quasi constant but small peak reconstruction error over all frequencies, our simple correction scheme exhibits a peak underestimation of about 15 % at period length less than 10 s. For longer waves, the error decreased and eventually reached zero at period durations of about 40 s.
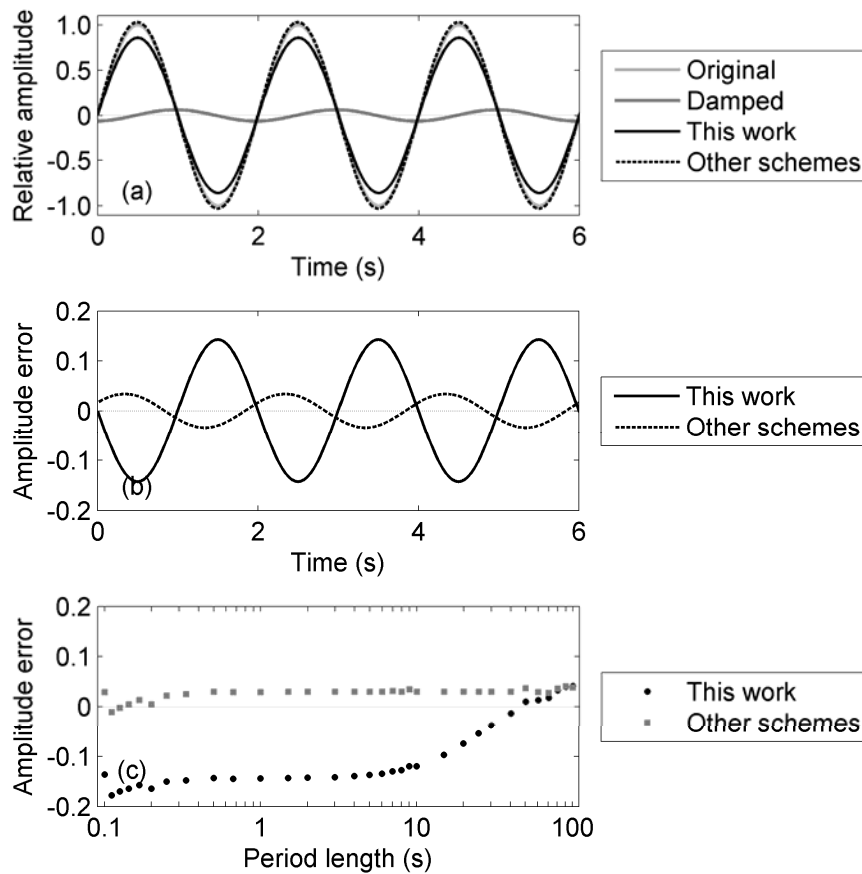
Figure 5: (a) Reconstruction of sine signal (black lines) at 0.5 Hz by correction schemes described in sections 2.2.2 (McCarthy, 1973 and Inverarity, 2000: other schemes)) and 2.2.3 (simple scheme: this work). Note the strongly damped time series (dark grey line), which was corrected to match the original time series (light grey line). (b) Amplitude error of reconstructed signal (reconstructed time series – original time series). (c) Dependence of amplitude error on the period length of the original time series (sine waves). The amplitude of the damped signal was less than 5 % of the original amplitude for period lengths of less than 1 s.

The frequency of the input signal was reconstructed well for every tested frequency. Even at short periods, being much shorter than the response times used for the corrections (i.e. the response times of the sensor), no frequency shifts in the reconstructed time series occurred.

3.2.2   Measured profiles – effect of corrections

With the determined sensor response times ($\tau_A = 4.4$ s, $\tau_B = 81.1$ s, see Table 2), the measured profiles of air temperature were corrected. The correction had to adjust two aspects: firstly, the small scale temporal fluctuations (with durations of some seconds) had to be intensified, because the low sensor response had damped their amplitude in the records. Secondly, the mean shape of the (uncorrected) profiles should have been altered if (strong) vertical gradients have been present, because the delay effect of

warming and cooling of the housing should have been eliminated from the records (after applying the correction).

In order to demonstrate the power of the correction schemes, we selected from the entire experimental period that sub-set of data where the largest dynamical errors of the moving sensor have to be expected ("worst case scenario"). Corresponding profiles of air temperature (19 August, 2006; 21:30 h local), for upward and downward movement of the elevator, are shown in Figure 6. A very strong surface inversion is visible in the lowest 40 m, with a temperature increase of more than 6 K. Above the inversion, the temperature profile shows neutral conditions with respect to static stability. Besides this mean profile shape, the ELM profiles show small scale fluctuations in the order of meters, embedded in the mean profile. The strongest can be seen in the upward scanned profile at 25 m. It shows a neutral layer of approx. 3 m thickness within the stably stratified surrounding. Especially noteworthy is the discrepancy between the upward and the downward scanned profile of the ELM in Figure 6a (data set A). At 99 m, both profiles yield the same value, but at lower levels they differ significantly. This is the result of a hysteresis, introduced by the slow part of the sensor, i.e. the housing. In the presence of a gradient, such as the temperature inversion shown here, the low sensor response leads to a memory of the sensor about temperatures encountered in the seconds before. If it was colder, the actual measured value will be too cold compared to the true value (upward scan under inversion conditions), and vice versa.

Applied to measured data, all three correction schemes (MCCARTHY (1973), INVERARITY (2000) and our more simple scheme) performed well and yielded virtually the same result. After the application of the correction scheme (Figure 6b, data set B), important changes compared to Figure 6a (data set A) can be observed. The mean shape of the ELM profiles (up and down) now coincides well with the reference profile from tower and mast, and the hysteresis between upward and downward scanned profile has vanished. This indicates that the influence of the slow probe housing on the sensor signal has been correctly eliminated from the dataset. When we focus on the small scale fluctuations, we find the prominent one mentioned above also in Figure 6b at approximately 25 m. Compared to the uncorrected profile in Figure 6a, it is much more pronounced, now showing a small layer of even unstable conditions embedded in the surrounding stable stratification, and not only neutral as it was before the correction. This enhancement of the small scale fluctuations is the result of the correction of the response time of the probe itself, eliminating the damping effect.
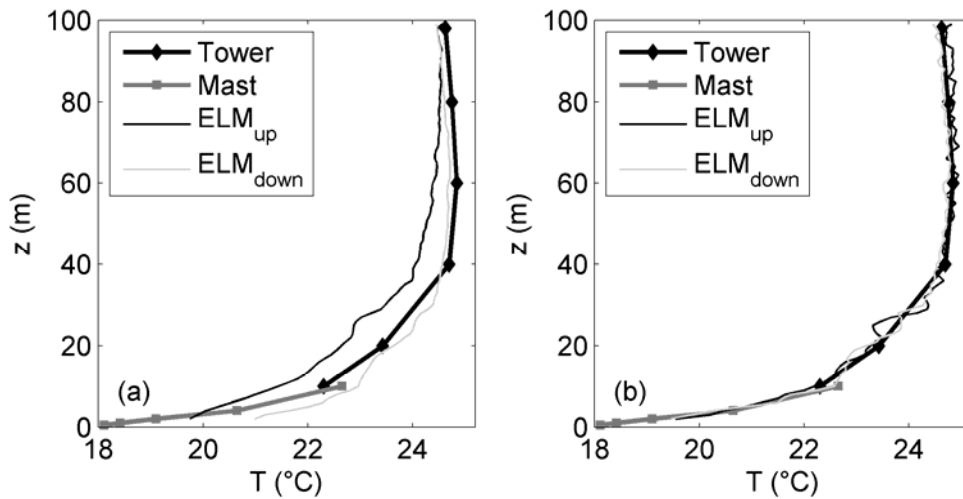
Figure 6: Vertical profiles of air temperature around 21:30 h (19 August, 2006). Between 2 m and 40 m, there is a very strong surface inversion (>6 K). The deviation of the profiles measured by the elevator (thin lines) from the reference tower and mast profile (thick lines) vanishes after application of the corrections, while the intensity of small scale fluctuations increases visually.

A small, but systematic undercorrection by the simple scheme, as it has been observed when being applied to the artificial sine wave time series (section 3.2.1) was never identified when applying it to measured data. The good agreement between the corrected ELM profiles and the reference profiles from tower and mast clearly demonstrates the ability of all three correction schemes to eliminate even the influence of slow parts of the sensor with time constants in the order of minutes.

The unbeatable advantage of the LIBRETTO setup was the coexistence of (a) high quality reference data, provided by the stationary measurements at the tower and mast, and (b) the high-resolution experimental data, provided by the ELM. This allowed us to directly quantify the effect of the applied corrections relative to parallel measured reference data.

As it was shown in Figure 6, the dynamical error led to a hysteresis at a certain level, if the sensor was moved. This hysteresis was most pronounced where gradients were strongest, because it depended on the temporal gradient of the quantity being measured and on the sensor's response time (FOKEN, 2008). During night time, temperature gradients typically increase towards the ground (see Figure 6 as an example) due to radiative cooling of the ground. Because the change to the dataset (when applying the correction schemes) must be strongest where the hysteresis due to dynamical error is strongest, we selected the 10 m level for the quantification of the correction effect. Because of the nature of the dynamical error, the deviation between ELM and reference data (tower and mast) should strongly depend on the magnitude of the actual gradient.
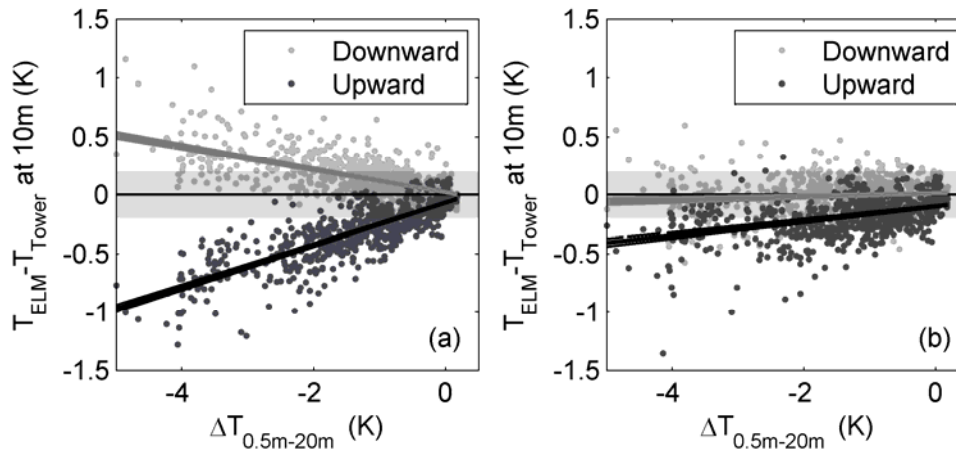
Figure 7: Dependence of deviation between mast/tower readings and ELM readings at z = 10 m on the temperature difference (mast/tower) between 0.5 and 20 m ("base difference"). Left hand panel (a): before application of response time correction, right hand panel (b): after response time correction. The grey shaded horizontal band indicates the combined sensor uncertainty (mast and elevator sensors) of ± 0.2 K. N = 739.

But after correcting for the dynamical error, this dependency should vanish. To demonstrate this effect, we investigated the dependency of the deviation between ELM and the reference data at 10 m on the temperature difference between 0.5 m and 20 m (mast/tower). The latter is further on referred to as the "base difference". Encouraged by the performance of the correction schemes for the worst case scenario (very strong surface inversion), we extended further investigations to all night time data.

In order to avoid an unintended attenuation of the hysteresis, the 10 min averages from the ELM (corrected and uncorrected data) used in the following were computed separately for upward and downward scanned data (data set C1), as described in Section 2.1.2.

The magnitude of deviation between ELM and mast/tower readings for the uncorrected system (Figure 7a) depended clearly on the magnitude of the "base difference". The different signs for the deviations of upward and downward scans were a result of the hysteresis, where the sensor remained too cold relative to the true air temperature when coming out of the cool near-surface air, while it remained too warm when immersing back into the cooler air.

The magnitude of the slope for the uncorrected ELM data (Figure 7a) indicated a substantial difference between upward and downward scanned data (0.180 ± 0.005 and -0.098 ± 0.004, respectively). The stronger slope associated with the upward scans was a result of the shape of the actual temperature profile. As the air was cooled by the radiative cooling at ground, the strongest temperature gradient was found in the lowest
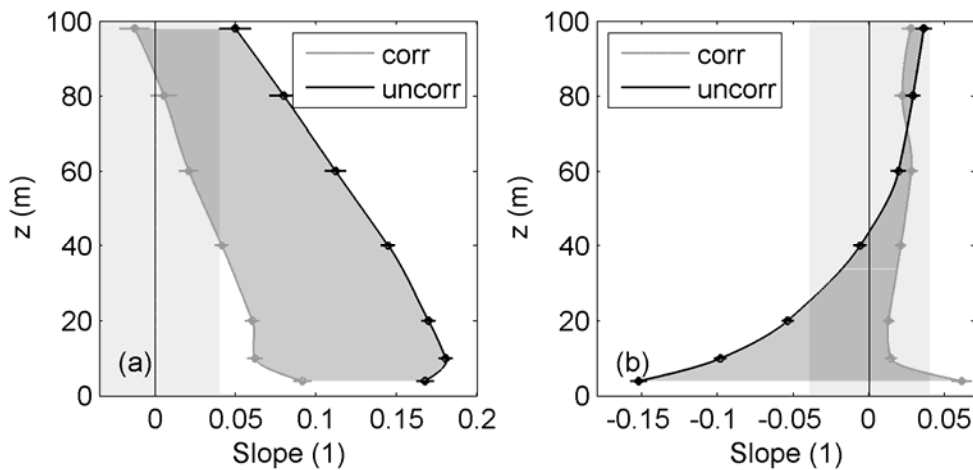
Figure 8: Vertical profiles of the slope of the linear regressions between the deviation "ELM readings − mast/tower readings" (at all 7 reference levels) and the "base difference" (temperature difference of the reference data between 0.5 m and 20 m) for uncorrected data and corrected data. Left hand panel (a): upward scanned profile, right hand panel (b): downward scanned profile. The strongest effect (i.e. horizontal width of the dark shaded area) of the corrections is found in the lowest part of the profile. Slope data within the light grey shaded "dead band" are considered to be insignificant (details see text).

part of the profile. During upward scans, the sensor was thus exposed to faster temperature changes before passing the 10 m level compared to downward scans. This led for the observed deviation between mast and elevator during upward scans to a stronger dependence on the "base difference" than during the downward scans.

After the application of the response time correction, a dependence of the deviation between the ELM and the tower and mast data on the "base difference" vanished for downward scanned data (slope 0.014 ± 0.004) and was reduced 3-fold for upward scanned data (slope 0.062 ± 0.005) (Figure 7b).

For the remaining levels of the stationary profile (4, 20, 40, 60, 80 and 98 m), each slope of the corresponding linear regression between each deviation (ELM readings minus mast/tower reading) and the "base difference" was also determined. This was done for the uncorrected and the corrected system, separately for up- and downward movements of the elevator. The magnitude of each slope is a measure, how strongly the measurements at each level are influenced by the presence of a surface inversion. The results are summarized in Figure 8, where vertical profiles of these slopes are shown. Slopes were considered to be insignificant, if they remain within the sensor uncertainty (grey shaded dead band in Figure 7). For maximum observed "base differences" of -5 K, this corresponds to a slope of ± 0.04. The insignificant slope band is indicated in Figure 8 as the light grey shaded "dead band". The dark grey shaded areas in Figure 8 represent the difference between the slopes, when using corrected and uncorrected data,

respectively. At each reference level, the horizontal width of the dark grey shaded area indicates the intensity of the corresponding correction. For upward scanned ELM data (Figure 8a), the strongest effect of the correction was found at 10 m; above that level, the correction's magnitude is almost linearly decreasing with increasing height. While the dependence of the observed deviation between the uncorrected ELM and the reference data on the "base difference" remained significant at all levels, it became insignificant for the corrected ELM data at levels above 40 m. Below the 40 m level, only a weak dependence remained even after the correction. A different situation was observed for downward scanned ELM data (Figure 8b). In the uncorrected case, only ELM data below 25 m depended significantly on the "base difference", while after the applied correction, only the 4 m level showed a weak dependence on the "base difference". This followed the expectation, because the ELM system coming down from upper levels had to immerse very deep into the surface inversion before showing any dependency on the "base difference".

The remaining weak dependency of the deviation between mast/tower and elevator data on the "base difference" for the corrected ELM data in Figure 8a may be attributed to different flow regimes around the probe's housing during upward and downward scans, which may have affected the probe housing's response time to a minor extent and thus the dynamical error of the sensor, correspondingly.

After the effectiveness of the applied correction has been demonstrated, we will now present direct comparisons between tower and the ELM. We will address the question, whether the scanning ELM, after applying the correction scheme, is able to adequately reproduce the reference data from the stationary tower measurements.

3.3   Measured profiles – consistency of ELM with tower data

For each reference level at the tower (10, 20, 40, 60, 80 and 98 m), 739 pairs of data were used for the direct comparison of reference air temperature with the corresponding ELM air temperature (after the application of the correction schemes, data set C2). Linear regression between ELM data sets and the reference temperature has been used for the comparison and mean absolute residuals have been calculated. Results are listed in Table 3. At each level and for every correction algorithm applied, the coefficient of determination (R^2) was greater than 0.992, indicating an excellent agreement between tower and corrected ELM data. Up to 60 m, the slopes of the linear regression between tower and ELM data range between 0.993 and 1.006 and increase slightly for higher

Table 3: Slope, mean absolute residual and coefficient of determination (R^2) of linear regressions between air temperature reference data (stationary tower measurements) and corrected ELM data. N = 739 at each reference level.

Level , m	Slope [1]	Abs. residual (mean), K	R^2
98	1.018 ±0.002	0.173	0.992
80	1.013 ±0.002	0.155	0.993
60	1.006 ±0.002	0.137	0.995
40	1.000 ±0.001	0.112	0.997
20	0.993 ±0.002	0.121	0.996
10	0.999 ±0.002	0.139	0.994

reference levels. A similar behaviour was observed for the mean absolute residual (Table 3).

We like to recall, that the reference data (stationary tower measurements) are 10 minute averages, while the corresponding ELM data are based on instantaneous samples. Although the latter were converted to 10 minute averages (synchronous to the tower data), small scale temporal fluctuations, being not observable with the tower sensors, might have influenced the comparison between the ELM and the tower data.

4   Conclusions

Laboratory tests with respect to response characteristics of the applied sensors (probe and housing) were of great importance for the final quality of data being measured with a moving system. In this context it should be emphasized, that it is necessary to consider not only the response time of the probe itself – the entire system (with all components) must be carefully examined in order to correct data from a moving system properly for its overall error.

For the correction of the dynamical error of a moving sensor (ELM), established mathematically demanding correction schemes as well as a simple correction scheme have been applied. Both schemes proved to work well with artificially generated time series (sine waves) as well as with respect to temperature reference data (measured on a stationary tower in parallel to the moving sensor). Given the more random nature of the measured data, differences in the performance of the different correction schemes became negligible.

Data of the ELM were compared to reference data (stationary mast and tower measurements). For that, we selected from the entire experimental period a sub-set of data obtained during night time, where surface inversions could lead to large dynamical

errors of the moving sensor. It has clearly been demonstrated, that the deviation between the shapes of the scanned profiles and the reference profiles vanished after the application of the correction schemes. Furthermore, small scale spatial fluctuations in the order of some meters were enhanced by the same correction procedure (i.e. by accounting for damping effects of the moving sensor). This was particularly demonstrated using data from artificial time series, but also with data from measured temperature profiles.

The presented comparison clearly proved the capability of the ELM to produce data of a reliability which is comparable to the stationary tower and mast measurements, but with the benefit of a high vertical spatial resolution. Furthermore, if there is a particular interest in vertical gradients, the ELM does not suffer from systematic deviations between different sensors at different levels.

5   Acknowledgements

6   References

AKIMA, H., 1970: A new method of interpolation and smooth curve fitting based on local procedures. --J. Assoc. Comput. Mach. **17**, 589-602.

BEYRICH, F., W. K. ADAM, 2007: Site and Data Report for the Lindenberg Reference Site in CEOP – Phase I. Berichte des Deutschen Wetterdienstes **230**, 55 pp.

FOKEN, T., 2008: Micrometeorology. --Springer, Heidelberg, New York, 306 pp.

FRIEHE, C. A., D. KHELIF, 1993: Fast-Response Aircraft Temperature Sensors. J. Atmos. Ocean. Techn. **9**, 784-795.

HAMAN, K. E., A. MAKULSKI, S. P. MALINOWSKI, R. BUSEN, 1997: A New Ultrafast Thermometer for Airborne Measurements in Clouds. --J. Atmos. Ocean. Techn. **14**, 217-227.

INVERARITY, G. W., 2000: Correcting Airborne Temperature Data for Lags Introduced by Instruments with Two-Time-Constant Responses. --J. Atmos. Ocean. Techn. **17**, 176-184.

MAHESH, A., V. P. WALDEN, S. G. WARREN, 1997: Radiosonde Temperature Measurements in Strong Inversions: Correction for Thermal Lag Based on an Experiment at the South Pole. --J. Atmos. Ocean. Techn. **14**, 45-53.

MCCARTHY, J., 1973: A Method for Correcting Airborne Temperature Data for Sensor Response Time. --J. Appl. Meteorol. **12**, 211-214.

RODI, A. R., P. A. SPYERS-DURAN, 1972: Analysis of Time Response of Airborne Temperature Sensors. --J. Appl. Meteorol. **11**, 554-556.

SAGGIN, B., S. DEBEI, M. ZACCARIOTTO, 2001: Dynamic error correction of a thermometer for atmospheric measurements. Measurement **30**, 223-230.

VICKERS, D., L. MAHRT, 1997: Quality Control and Flux Sampling Problems for Tower and Aircraft Data. --J. Atmos. Ocean. Techn. **14**, 512-526.

Appendix D:

Distributed Modified Bowen Ratio Method for Surface Layer Fluxes of reactive and non-reactive Trace Gases

J.-C. Mayer[1], A. Bargsten[1], U. Rummel[2], F.X. Meixner[1,4] and T. Foken[3]

[1] Biogeochemistry Department, Max Planck Institute for Chemistry, Mainz, Germany
[2] Richard Aßmann Observatory Lindenberg, German Meteorological Service, Germany
[3] Department of Micrometeorology, University of Bayreuth, Bayreuth, Germany
[4] Department of Physics, University of Zimbabwe, Harare, Zimbabwe

Abstract

Modified Bowen ratio technique was used in a horizontally distributed form to determine turbulent fluxes of CO_2, H_2O, O_3, NO and NO_2 over a semi-natural grassland site in Northern Germany. Turbulent NO fluxes were compared to laboratory measurements of biogenic NO emission from soil samples, which have been taken at the field site. Good agreement (within a factor of two) was observed. Under favourable night time conditions, we performed a detailed comparison of turbulent fluxes of CO_2 and O_3 with those CO_2 and O_3 fluxes which derived by the boundary layer budget technique. While there was agreement between these fluxes in a general sense, specific deviations were observed. They could be attributed to different footprint sizes of both methods and to in-situ chemistry within the nocturnal boundary layer.

1   Introduction

Temporal and spatial variations of trace gas fluxes from and to the surface are crucial for understanding exchange processes between the atmosphere and terrestrial surfaces. A lot of effort in this respect has been done for the species carbon dioxide (CO_2), mostly using eddy covariance (EC) techniques (see e.g. Baldocchi et al., 1988; Aubinet et al., 2000; Baldocchi et al., 2001; Suni et al., 2003). Turbulent fluxes of reactive trace gases, e.g. those of ozone (O_3), nitrogen oxide (NO) and nitrogen dioxide (NO_2), are currently measured more on campaign than on a continuous basis (see e.g. Wesely et al., 1982; Rummel et al., 2002; Keronen et al., 2003). If fast enough sensors for EC measurements

for these trace gases are available at all, they often need permanent maintenance, making them less suitable for permanent measuring networks.

An alternative technique to measure turbulent fluxes of trace gases is the so-called Modified Bowen Ratio (MBR) method as proposed by Businger (1986) and Müller et al. (1993). Originally, fluxes of trace gases have been derived from the sensible heat flux (H) and differences of air temperature (ΔT) and concentration (Δc) of the corresponding, where H has been typically determined by the Bowen Ratio method (Bowen, 1926; Lewis, 1995). With the development of sonic anemometers, a direct measurement of H became feasible, reducing the instrumental effort because radiation and soil heat flux measurements were no longer needed (Liu and Foken, 2001).

The traditional setup of a MBR station includes EC measurements of H and the determination of ΔT and Δc at the same location. Furthermore, ΔT and Δc have to be measured at the same heights. However, if several trace gases have to be measured and analyzer or inlet constructions are somewhat bulky, measurement errors due to flow distortion could be substantial. But this error source can be tackled (if a sufficiently large, homogeneous site is available) by using distributed locations for the individual measurements of Δc, ΔT and H. Moreover, for intercomparison studies, this reduces potential deviations between different measuring systems to the trace gas part of the measurements, as all flux calculations will relate on the same data set of H and ΔT. This approach will be presented in this paper and will be referred to as the Distributed Modified Bowen Ratio (DMBR) method.

The methods for measuring the fluxes of reactive trace gases are in principle the same as for non-reactive trace gases. The concept, whether the reactivity of a trace gas has to be taken into account was firstly described by Damköhler (1940). Therefore, the ratio of the characteristic time scale for chemical reactions to the time scale of turbulence is referred to as the Damköhler number (DA). As long as DA is much smaller than one, the reactivity can be neglected. Otherwise, chemical alteration during the transport must be considered. A determination of the fluxes of reactive trace gases independent from the risk of chemical alteration would be a great advantage. In the case of NO, laboratory measurements would be a suitable approach because of the absence of reaction partners for NO. But such laboratory measurements do provide only a sound parameterization of soil NO fluxes under varying humidity and temperature conditions. They are not actual field measurements, being made under very variable ambient conditions, with respect to

the chemical composition of air. Therefore, a laboratory determination of soil NO fluxes is compared to field observations in order to quantify their degree of agreement.

A similar statement holds, if methods to derive fluxes differ in the characteristic time of measurements being used to compute the fluxes. For example, if the concentration difference of a trace gas is to be measured, the characteristic time of the measurements doubles if the vertical spacing between the two levels is doubled. In the same way, the influence of chemical alterations increases. This has to be taken into account, when comparing methods with large spatial extend to methods with only small spatial spread.

If vertical profile data of a quantity, whose flux has to be determined, are available up to the equilibrium height (i.e. where no temporal concentration changes are observable anymore), the so-called boundary layer budget method can be used (Pattey et al., 2002). This method integrates vertical profiles of the desired quantity and assigns its temporal change to a vertical flux into the corresponding volume (Denmead et al., 1996; Levy et al., 1999). If horizontal advection can be excluded, and the top end of the profile is capped by a "lid", the temporal change should equal the vertical flux at the bottom end of the profile, i.e. the flux determined by the DMBR or EC method. The "lid" can either be a strong inversion, or the presence of strong wind shear due to a low-level jet (Mathieu et al., 2005). As a case study, H and the fluxes of CO_2 and O_3 obtained from the DMBR method will be compared to the respective fluxes obtained from the boundary layer budget method. This comparison should show (a) the similarity of both methods for conservative quantities and (b) the increasing influence of chemical reactions for the method with the larger spatial extend (the boundary layer budget method).

2   Material and Methods

2.1   Site and Setup

The LIBRETTO (LIndenBerg REacTive Trace gas prOfiles) campaign took place in late summer 2006, from 01 August 2006 until 31 August 2006 at the Falkenberg Boundary Layer Field Site of the Meteorological Observatory Lindenberg (Richard-Aßmann Observatory) (Beyrich and Adam, 2007). The field site is located at 52° 10' 01" N, 14° 07' 27" E, 73 m a.s.l. The topography is a slightly undulating surface with height differences of less than 100 m over distances of about 10 km. The land use in the area is dominated by forest and agricultural field, with some embedded lakes. The
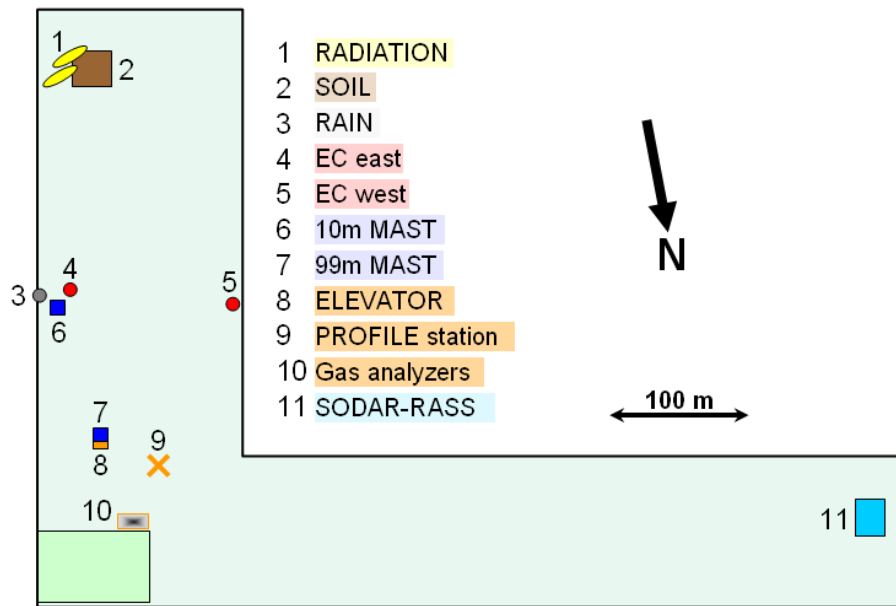
Fig. 1. Spatial arrangement of the different stations at the Falkenberg Boundary Layer Field Site. Additional instrumentation during the LIBRETTO campaign is indicated by orange color.

setup of the field site comprises one 99 m and one 10 m high profile masts (air temperature (T), relative humidity (rH), wind speed (U) and wind direction), two identical setups for the measurement of the net radiation flux, two stations for the measurement of turbulent fluxes of momentum, sensible and latent heat (further on referred to as the EC stations), and a sub-site to monitor physical soil quantities (soil temperatures, soil heat flux and soil moisture). A SODAR-RASS system completes the permanent setup of the Falkenberg site. Details about the instrumentation relevant for this work are summarized in Table 1, the spatial situation is shown in Figure 1. All heights given in this paper are heights above ground level, unless otherwise stated.

The 99 m profile mast is equipped with an elevator, usually used for service and maintenance. On this elevator, additional sensors for T and rH as well as for ozone (O_3), carbon dioxide (CO_2) and water vapor (H_2O) have been installed (see Table 1). However, we limit our evaluation from this system to T, CO_2 and O_3, because the H_2O channel of the deployed instrument has unfortunately not worked properly. The elevator was automatically run up and down once every 10 minutes, interrupted only for data retrieving and service. At bottom and top position, the elevator had approx. 6.5 minutes idle time for intercomparison and equilibration, thus one profile needed approx. 3.5 minutes to be measured. A detailed description of the algorithms which have been applied to correct the dynamical error of the elevator based measurements are given by Mayer et al. (2008).

Table 1. Setup of the field site during the LIBRETTO campaign. Only instruments being relevant for this work are listed.

Parameter	Symbol	Unit	Temporal resolution (min)	Sampling height (m) a.g.l.	Instrument (Model)
Permanent setup					
Sensible Heat Flux	H	W m^{-2}	10	2.4	METEK USA1
Air temperature, EC station	T	°C	10	0.5, 2.8	Pt-100
Friction velocity	u$_*$	m s^{-1}	10	2.4	METEK USA1
Global radiation	Rg	W m^{-2}	10	2.4	Kipp&Zonen CM22
Air temperature, 10m profile	T	°C	10	0.5, 4	Pt-100
Wind speed	U	m s^{-1}	10	0.5, 4	Thies
Rain		mm	10	1	NSA 181/K
Additional LIBRETTO setup					
Ground based					
Air temperature	T	°C	10	0.25, 0.5, 1.0, 2.0	Aspirated Thermocouple
Carbon dioxide	CO$_2$	ppm	10	0.15, 2.0	LiCor LI 7000
Water vapor	H$_2$O	‰	10	0.15, 2.0	LiCor LI 7000
Nitrogen monoxide	NO	ppb	10	0.15, 2.0	EcoPhysics CLD 780
Nitrogen dioxide	NO$_2$	ppb	10	0.15, 2.0	EcoPhysics CLD 780
Ozone	O$_3$	ppb	10	0.15, 2.0	Thermo Electron 49C
Additional LIBRETTO setup					
Elevator					
Air temperature	T	°C	10	2 - 99	Thermocouple
Carbon dioxide	CO$_2$	ppm	10	2 - 99	LiCor LI 840
Water vapor	H$_2$O	‰	10	2 - 99	LiCor LI 840
Air pressure	P	hPa	10	2 - 99	Vaisala PTB 101B
Ozone	O$_3$	ppb	10	2 - 99	GFAS OS-G-2

For the LIBRETTO campaign, an additional set of profile instruments was installed comprising the measurement of the trace gases CO_2, H_2O, O_3, NO and NO_2 at three levels and air temperature at 4 levels (0.25, 0.5, 1.0, 2.0 m). The trace gas inlets were located at 0.15 m, 1.0 m and 2.0 m. A fourth sampling tube collected air from the base position of the elevator (at 2.0 m) for continuous adjustment of the ground based measurements and the elevator profiles. Air samples were pumped from the corresponding intake devices (downward directed funnel and particle filter) via heated Teflon tubes to a switching valve manifold (see Fig. 2), located next to the trace gas analyzers in an air conditioned container, approx. 50 m NE from the "PROFILE station" (s. Fig. 1). After completion of set-up and test of the instrumentation, the measuring period of the LIBRETTO campaign consisted of 20 days, from 11 to 30 August, 2006.
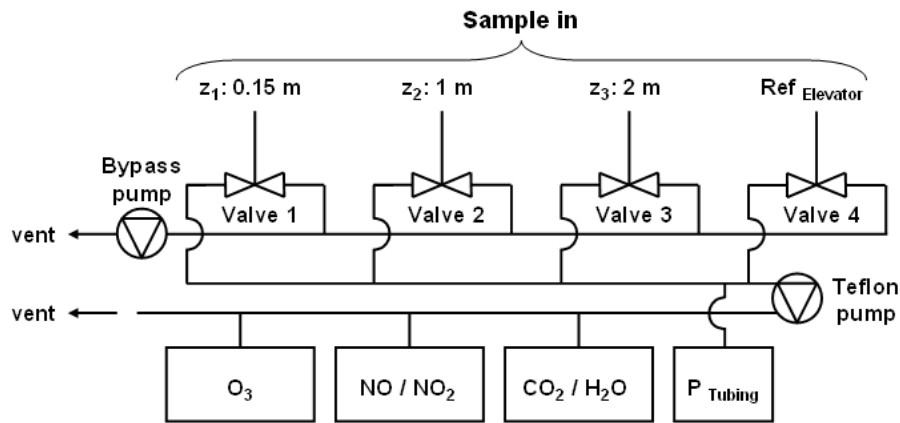
Fig. 2. Scheme of the gas flow of the switched trace gas profile. A computer system with a customized control software was used for switching the valves 1 – 4 as well as for data acquisition and for controlling the NO / NO_2 analyzer to be in phase with valve switching. While only one sample line per time was connected with the sampling Teflon pump, the three other sampling lines were flushed with a bypass pump to avoid stagnant air and increased lag times.

2.2   Quality Control and gap filling

2.2.1   Reference data

Routinely measured data from the permanent setup of the Lindenberg site are called "reference data" in the following, in order to contrast the experimental data from those instruments which have been added to the site during LIBRETTO (s. Tab. 1).

Reference data (from EC and radiation flux stations, data of soil physical quantities) were flagged with quality indicators according to Beyrich and Adam (2007). Because the EC stations were located at the western and eastern side of the south-lag of the field site (see Fig. 1), at least one EC dataset (being representative for the field site) was available under every "fetch" (upwind) conditions. A so-called "limited fetch condition" occurred for the western EC station at wind directions from 180°-360° and for the eastern EC station from 30°-150°. These data are flagged correspondingly. Only data without any critical flag set were passed on to further analyses.

Friction velocity (u_*) and H are key parameters in most of our calculations. Therefore, special attention was paid to gap-filling procedures for these parameters. If EC data were not available (critical flag), u_* and H were computed according to Arya (2001) from ΔT and Δu, measured at $z = 0.5$ m and $z = 4.0$ m at the 10 m profile mast. We made use of the following equations:

a) geometrical mean height z_m of the layer (z_1;z_2):

$$z_m = \sqrt{z_1 \cdot z_2} \ . \tag{1}$$

b) Richardson number Ri (a measure of dynamic stability of the layer $(z_1;z_2)$) as function of ΔT and ΔU:

$$Ri = \frac{g}{T_1} \cdot \frac{\Delta \Theta \cdot z_m}{\left(\Delta U \right)^2} \ln \frac{z_2}{z_1} \ , \tag{2}$$

where g stands for the acceleration due to gravity, T_1 is the absolute temperature at level z_1 and Θ denotes the potential temperature. The following relation exists between Ri and the Monin-Obukhov stability parameter ζ :

$$\varsigma = Ri \qquad\qquad \text{if } Ri < 0 \text{ (unstable)}$$

$$\varsigma = \frac{Ri}{\left(1 - 5 \cdot Ri \right)} \qquad \text{if } 0 \le Ri < 0.2 \text{ (stable)} \tag{3}$$

c) friction velocity u_*, dynamic temperature T_* and H:

$$u_* = \frac{\kappa \cdot \Delta U}{\left(\varphi_m \cdot \ln \frac{z_2}{z_1} \right)} \tag{4}$$

$$T_* = \frac{\kappa \cdot \Delta T}{\left(\varphi_h \cdot \ln \frac{z_2}{z_1} \right)} \ . \tag{5}$$

$$H = -T_* \cdot u_* \cdot \rho_{air} \cdot c_p \ , \tag{6}$$

where c_p is the heat capacity of air at constant pressure, ρ_{air} denotes the density of air and κ is the von-Kármán constant ($\kappa=0.4$). For the universal functions for momentum and heat (φ_m and φ_h, respectively) we make use of those given by Businger et al (1971) with the modifications by Högström (1988).

Before and after each gap, the deviation of the profile-derived values of u_* and H were calibrated against the EC values. If a trend was present, it was distributed linearly over the gap.

Remaining gaps, and gaps of other quantities, limited to a maximum length of 30 minutes, were filled by using a non-linear interpolation algorithm (Akima, 1970). Finally, from these data, 30 minute averages were computed for further evaluation.

2.2.2   Profile station data

Two primary data sets were recorded at the profile station: (a) air temperature data and (b) trace gas data. Data recorded during servicing the profile station or during farming activities within the fetch were deleted and replaced by a wildcard. The same was done with data measured during rainfall periods. Subsequently, calibration factors were applied and a despiking scheme based on Vickers and Mahrt (1997) was used to identify spikes. All groups of spikes being smaller than 3 consecutive spikes were replaced by wild cards. Next, a gap filling procedure based on non-linear interpolation (Akima, 1970) was applied, but limited to a maximum gap size of 30 minutes. As a last step, all data were averaged to 30 minutes for further evaluation.

2.3   Distributed Modified Bowen Ratio (DMBR)

The MBR as well as the DMBR method requires (a) simultaneous measurements of ΔT and Δc at identical levels and (b) that the measured H is representative for the same source area (i.e. that area which is influencing the flux measurements). Due to technical reasons, the lower level (z_1) for trace gas measurements was 0.15 m, while it was 0.25 m for the temperature measurements. The upper level (z_2) was 2.0 m in both cases. Therefore, a ΔT_c corresponding to a height interval from 0.15 m to 2.0 m had to be computed from the measured ΔT_m between 0.25 m and 2.0 m. This was done by using the Monin-Obukhov similarity theory. For that, the state of atmospheric stability can be expressed by the Obukhov length L:

$$L = -\frac{u_*^3}{\kappa \frac{g}{T} \frac{H}{c_p \cdot \rho_{air}}} \cdot \tag{7}$$

The calculation of L was performed using H and u_* from the EC measurements. Within the surface layer, fluxes are assumed to be constant with height, thus L is also independent of z. Then, ΔT_c can be computed from ΔT_m by:

$$\Delta T_c = \Delta T_m \cdot \frac{\left[\ln\frac{z_{2,c}}{z_{1,c}} - \Psi_h\left(\frac{z_{2,c}}{L}\right) + \Psi_h\left(\frac{z_{1,c}}{L}\right) \right]}{\left[\ln\frac{z_{2,m}}{z_{1,m}} - \Psi_h\left(\frac{z_{2,m}}{L}\right) + \Psi_h\left(\frac{z_{1,m}}{L}\right) \right]} \cdot \tag{8}$$

The index m refers to the measured values and index c refers to computed values. Ψ_h denotes the integrated universal stability function for H (Businger et al., 1971) with the

modifications according to Högström (1988). For unstable stratification, this integration in general form was firstly done by Paulson (1970).

The calculation of ΔT_c (at "PROFILE station") requires the sensible heat flux (H), which has been measured at both EC stations (s. 2.2.1), which were located about 150 m SSW and 165 m SSE of the "PROFILE station" (s. Fig. 1). This spatial separation of measurements of H and ΔT (and Δc) is characteristic of the DMBR method, and it is obvious, that the successful application of the DMBR demands horizontal homogeneity of the measurement site. A first-order check of this condition could be provided. Simultaneously to the EC measurements of H, measurements of air temperature were performed at $z = 0.5$ m and $z = 2.8$ m. By applying Eq. 8 to this measured temperature difference, it was recalculated to match the levels of T measurements at the "PROFILE station" (0.5 m and 2.0 m). By the comparison of ΔT measured at the "PROFILE station" and ΔT computed at the EC station, a good agreement would indicated the fulfillment of horizontal homogeneity at the site.

Finally, assuming identical eddy diffusivities for the scalars sensible heat and trace gases, fluxes ($F_{TraceGas}$) of the trace gases CO_2, H_2O, O_3, NO and NO_2 were computed from observed H, Δc and ΔT_c according to Foken (2008):

$$F_{TraceGas} = \frac{\Delta c}{\Delta T_c} \cdot H \; . \tag{9}$$

2.4 Laboratory measurements

The net release and uptake of nitric oxide (NO) was determined by using an automated laboratory system described by van Dijk and Meixner (2001) and modified by Feig et al (2008). In short, pressurized ambient air passed a purification system (traps consisting of glass wool, activated charcoal, silica gel and molecular sieve) to provide dry and NO-free air. This NO-free air is supplied to five soil chambers (one reference and 4 incubation chambers; each of approx. 1 liter volume). A continuous flow rate of 2.5 L min^{-1} through each chamber is provided by 5 mass flow controllers (MFC, range: $0 - 5000$ sccm, MKS instruments, United States). The outlet of each chamber is connected to a switching valve system, which in turn connects each sampling line consecutively to a chemiluminescence analyzer (detection limit (3σ): 250 ppt; Model 42i Trace Level, Thermo Electron Corporation, U.S.A.) and a CO_2-/H_2O-analyzer (LICOR 840, Licor, U.S.A.). The NO-analyzer was calibrated using a gas phase titration unit (GPT, Thermo Electron Corporation, U.S.A.). For that we used NO-free

air from the purification system and a NO gas standard (5.05 ppm NO, Air Liquid, Germany). For fumigation of the incubated soil samples with known NO mixing ratios, a standard gas (200 ppm NO, Air Liquid, Germany) was diluted into the air flow from the purification system via a MFC (range: $0 - 10$ sccm, Bronkhorst, Germany). The loss of water vapor was related to the gravimetric soil moisture content at the start and the end of the laboratory analyses. The gravimetric soil moisture content was converted into water filled pore space (WFPS) using the field bulk density (1.245 g cm^{-3}). That is useful as the WFPS is not only a term for water available to microorganisms in the soil. It also represents the air-water ratio in the soil, which is important for the gas diffusion in or out the soil (Ormeci et al., 1999). All connections and tubes consist out of inert material. A custom built control unit (V25) was controlling the system and was also used for the data acquisition. More details concerning the laboratory setup is given by Van Dijk and Meixner (2001).

Mixed soil samples were taken in May 2008 on the Lindenberg site, air-dried, sieved (< 2 mm) and stored at 4° C. All samples were measured within 4 weeks after sampling. The NO measurements were conducted at three different temperatures (10, 20 and 30° C), two different NO mixing ratios (0 and 50 ppb NO) and over a full range of soil moisture ($0 - 100$ % WFPS). Twelve hours before starting the laboratory measurement the soil samples were preincubated: the soil samples were moisturized with deionised water to WFPS of nearly 100 % and put into a thermo-controlled cabinet at the temperature we used for measuring. Afterwards the cuvettes were flushed with dry, NO-free air to determine the NO release or with a known concentration of NO (50 ppb NO), to determine the NO uptake. Every two minutes switched the active cuvette so that all five cuvettes were measured within 10 minutes.

NO release (J) was calculated from the mixing ratio difference between the reference cuvette (NO$_{ref}$) and the incubation cuvettes (NO$_{out}$):

$$J = \left(\frac{Q}{M_{soil}} \right) \times \left([NO_{ref}] - [NO_{out}] \right) \times \left(\frac{M_N}{V_m} \right) \tag{10}$$

where Q is the flow through the cuvette (L min^{-1}), M$_{soil}$ is the sample weight (kg), M$_N$ is the molecular weight (14.0076 kg kmol^{-1}) and V$_m$ is the molar volume (m^3 kmol^{-1}) dependent on the actual temperature and pressure (1013.25 hPa).

The flux calculation is described in detail elsewhere (Feig et al., 2008a; Feig et al., 2008b). The NO emissions determined in the laboratory were fitted as a function of

temperature and soil moisture (in terms of WFPS) according to the method of Meixner and Yang (2006).

2.5   Boundary layer budget method

The boundary layer budget (BLB) method is based on calculating the budget of any quantity within the boundary layer (Denmead et al., 1996; Eugster and Siegrist, 2000). A surface flux of trace gases into (emission) or out of (deposition) the boundary layer changes the amount of the considered trace gas within the boundary layer. Vertical integration of the concentration yields the total concentration being present at a certain time. The upper boundary of integration must be at least the height, where no temporal changes of concentration due to surface fluxes occur. The concentration change between two subsequent integrations thus should equal the surface flux during this period. This approach however is only valid in the absence of advection. The upper integration limit is usually set to the top of the NBL at night or the top of the CBL at day.

2.6   Characteristic time scales

The characteristic time scales denote the time needed for certain processes to occur. In case of the turbulent time scale τ_{turb}, it is a measure of the intensity of turbulent transport. For near neutral conditions, τ_{turb} can be expressed as (Vilà-Guerau de Arellano and Duynkerke, 1992)

$$\tau_{turb} = \frac{\kappa \cdot (z + z_0)}{A \cdot u_*} \ ,$$
(11)

with the roughness length z_0 and the height above ground z. A is the ratio of the vertical velocity variance and the friction velocity squared. However, this formulation can not be used for diurnal cycles, because the method is only valid for near neutral conditions (Wyngaard, 1982). Furthermore under neutral conditions, A is constant. As an alternative, τ_{turb} can be computed from the coefficient of turbulent diffusion K_m and the thickness Δz of the layer being considered by defining the mean transfer velocity v_t as

$$v_t = \frac{K_m}{\Delta z} \ .$$
(12)

τ_{turb} can then be computed as

$$\tau_{turb} = \frac{\Delta z}{v_t}$$
(13)

which finally yields

$$\tau_{turb} = \frac{\Delta z^2}{K_m} \ .$$

(14)

K_m can be derived from measured u_* and determined stability according to

$$K_m = \frac{\kappa \cdot z_m \cdot u_*}{\varphi_m(\varsigma)} \ .$$

(15)

Thus, τ_{turb} for the transfer of momentum is expressed as

$$\tau_{turb} = \frac{\Delta z^2 \cdot \varphi_m(\varsigma)}{\kappa \cdot z_m \cdot u_*} \ .$$

(16)

If turbulent transport of matter is considered, the turbulent Schmidt Number (Sc_t, approx. 0.8) must be included. It is defined as

$$Sc_t = \frac{K_m}{K_e} \ ,$$

(17)

where K_e is the coefficient of turbulent diffusion of water vapor, which is assumed to be valid also for other trace gases. Also the universal function for momentum must be replaced by that for heat, being valid also for trace gases. The final expression for the time scales of turbulent trace gas transport thus reads:

$$\tau_{turb} = \frac{\Delta z^2 \cdot \varphi_H(\varsigma) \cdot Sc_t}{\kappa \cdot z_m \cdot u_*} \ .$$

(18)

For the chemical time scales τ_{chem}, we consider only the triad of NO-NO$_2$-O$_3$ including the (photo-) chemical reactions

$$O_3 + NO \xrightarrow{k_1} NO_2 + O_2 \quad k_1 = 1.40 \cdot 10^{-12} \exp\left(\frac{-1310}{T}\right)$$

(R1)

and

$$NO_2 + O_2 \xrightarrow{h\nu} NO + O_3 \quad h\nu < 420 \ nm.$$

(R2)
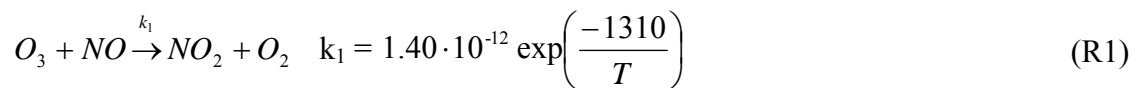
Confined to this triad, the individual time scale of NO$_2$ (τ_{NO2}) depends only on the present radiation flux for the photolysis of NO$_2$, giving jNO$_2$. According to Bahe et al. (1980), a linear relationship between global radiation (R_g, units: Wm^{-2}) and jNO$_2$ (units: s^{-1}) exists:

$$jNO_2 = a + b \cdot R_g$$

(19)

with a = $1.33 \cdot 10^{-4}$ s^{-1} and b = $8.86 \cdot 10^{-6}$ m^2 J^{-1}.

When only the triad NO-NO$_2$-O$_3$ is considered, the photolysis frequency of NO$_2$ controls the destruction of NO$_2$ and thus reformation of NO and O$_3$. Under night time

conditions, NO_2 is assumed to have a constant time scale of about 2 days. This is for calculation purposes only, to avoid an infinite time scale due to absence of radiation. The individual time scale of O_3 and NO depends on the reaction rate k_1 for (R1) and the number density N (molecules cm^{-3}) of NO in case of τ_{O3} and the number density of O_3 in the case of τ_{NO}:

$$\tau_{O_3} = \frac{1}{k_1 \cdot N_{NO}} \tag{20}$$

$$\tau_{NO} = \frac{1}{k_1 \cdot N_{O_3}} \tag{21}$$

$$\tau_{NO2} = \frac{1}{jNO_2} \quad . \tag{22}$$

The combined τ_{chem} for the NO-NO_2-O_3 triad is given by Lenschow (1982). It provides a measure about the intensity of the chemical conversions within the triad in order to compare it with τ_{turb}.

$$\tau_{chem} = \frac{2}{\sqrt{j_{NO_2} + k_1^2 \cdot \left(N_{O_3} - N_{NO}\right)^2 + 2 \cdot k_1 j_{NO_2}\left(N_{O_3} + N_{NO} + 2 \cdot N_{NO_2}\right)}} \tag{23}$$

With τ_{turb} and τ of the individual species or the combined τ_{chem}, the Damköhler number (DA) can be computed:

$$DA = \frac{\tau_{turb}}{\tau_x} \quad . \tag{24}$$

τ_x denotes either the τ of the individual species or the combined τ_{chem}. DA indicates, whether turbulent transport is faster than the chemical reaction, allowing the reactive species to be treated as quasi passive or if chemistry has to be taken into account. An overview about typical magnitudes for τ_{turb} and τ_{chem} are given by Foken et al. (1995).

3   Results and Discussion

The results chapter is divided into 5 parts. They cover (a) the aspect of horizontal homogeneity, (b) the characteristic time scales, (c) an overview about the atmospheric conditions for turbulent exchange, (d) median diurnal courses of trace gas mixing ratios, and (e) trace gas fluxes computed with the DMBR method. The last part comprises additionally a comparison between field measurements and laboratory parameterization of NO fluxes and a comparison of night time fluxes (H, CO_2, O_3) derived from DMBR method and from the nocturnal boundary layer budget method for the first 100 m of the atmosphere.
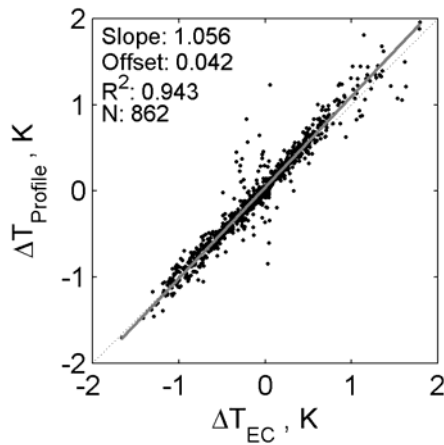
Fig. 3. Comparison of measured temperature differences at the profile station with the computed temperature differences at the EC station. The dashed lines give the 1:1 ratio, the solid grey lines indicate the linear regression.

3.1   Horizontal homogeneity

Temperature differences at the EC station, measured between 0.5 m and 2.8 m were recalculated to match the measuring heights of the profile station (0.5 m and 2.0 m) by utilizing the MO theory (see Eq. (8)). Figure 3 shows the comparison between the computed ΔT at the EC station and the actually measured ΔT at the profile station. The comparison of the temperature differences showed a close correlation. It indicated the fulfillment of the precondition of horizontal homogeneity at the site.

3.2   Characteristic time scales

As soon as reactive trace gases are investigated in transport processes, their characteristic chemical time scales (τ_{chem}) must be considered and compared to the characteristic turbulent time scale (τ_{turb}), which is a measure for the transport time. If τ_{turb} is considerably smaller than τ_{chem}, i.e. transport is much faster than chemical reactions during the transport, the trace gases can be treated like non-reactive trace gases. In case of τ_{chem} is close to τ_{turb}, chemical reaction during the transport must be considered. For the entire LIBRETTO campaign, τ_{turb} and τ_{chem} for the NO-NO$_2$-O$_3$ triad is shown in Figure 4. During daytime, turbulence was always faster than chemical conversion between O$_3$, NO and NO$_2$ (Figure 4a). Both showed lowest values in the early afternoon. These low values of both time scales coincided with maximum turbulence intensity and fastest photochemistry (NO$_2$ photolysis). Because photolysis is the only destruction mechanism for NO$_2$ in this null-cycle, it fully determines τ_{NO2} (Figure 4b). During night time, without photolysis, the life time of NO$_2$ is infinite, if
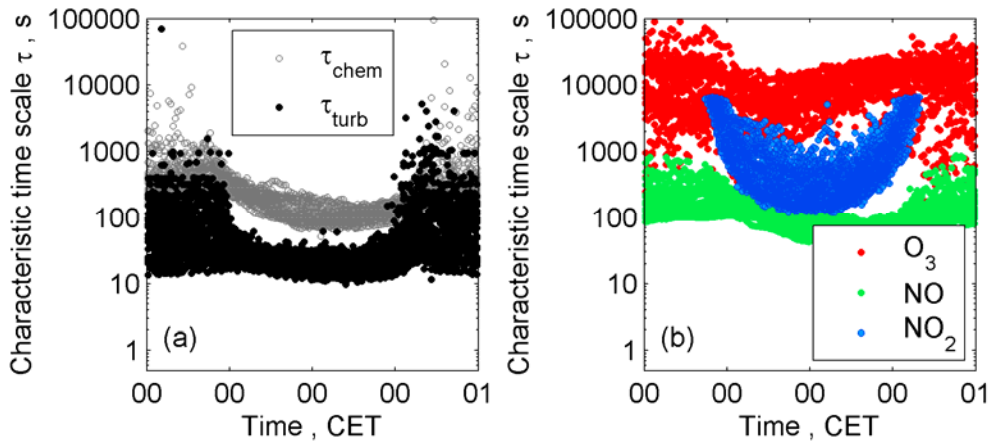
Fig. 4. Characteristic time scales of (a) turbulence (τ_{turb}) and chemistry ($\tau_{chem.}$) and (b) of the individual species of the O_3-NO-NO_2 triad. Time scales were computed for a layer from 0.15 m to 2.0 m a.g.l.

only the NO-NO_2-O_3 triad is considered. In the early afternoon, τ_{NO2} decreased to about 3 minutes. The diurnal cycle of τ_{turb} was much more pronounced than of τ_{chem}, resulting in comparable time scales during the night. Nevertheless, the actual ratio of τ_{chem} to τ_{turb}, defining DA, must be considered. The median diurnal courses of DA are shown in Figure 5. For O_3 and NO_2 (Figure 5, a and c) DA indicates a quasi passive behavior. Because O_3 had much higher mixing ratios than NO, it was expected to be only weakly
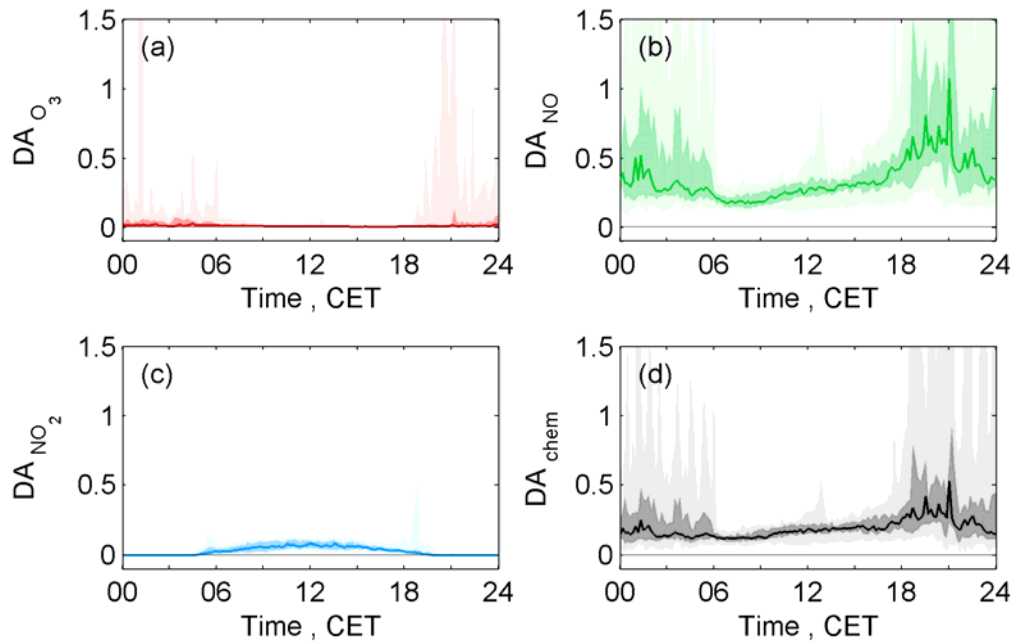
Fig. 5. Median diurnal cycle of the dimensionless Damköhler numbers (DA) for the period of 11 August 2006 – 30 August 2006. The individual Damköhler numbers for (a) O_3, (b) NO and (c) NO_2 are shown together with (d) the Damköhler number for the entire triad. The solid line indicates the median, the dark shaded areas cover the interquartile range, and the light shaded areas comprise the range from the 5 % percentile to the 95 % percentile.

affected by chemistry. In contrast, NO was expected to be strongly affected by reaction with O_3. This was confirmed by DA_{NO} (Figure 5b), indicating time scales comparable to τ_{turb} at night. Nevertheless, during daytime, chemical reaction seemed to remain sufficiently slow to treat NO as quasi passive. The overall DA_{chem} (Figure 5d) confirmed that the triad $NO-NO_2-O_3$ could be treated as quasi passive during daytime, while night time data would need a correction. Thus, for the calculation of NO fluxes, we limited the evaluation of NO data to values of $DA_{NO} < 0.25$ in order to minimize the influence of chemical reactions.

3.3   Dynamical exchange conditions

Because trace gases interact with the underlying surface, their mixing ratios within the surface layer are strongly dependent on exchange conditions and thus atmospheric stability. Figure 6a shows the median diurnal course of u_*, Figure 6b shows the median diurnal course of the stability parameter ζ, determined at $z = 2.4$ (i.e. the height of the EC measurements). During night (18:00 h – 06:00 h), low values of u_* around 0.1 m s^{-1} indicated only low turbulence, allowing a possible accumulation of soil emitted trace gases or a depletion of those trace gases having a net sink at the surface. This is also supported by ζ with its positive values during night indicating stable stratification. Around 06:00 h stability changed to unstable conditions. Coincidentally, u_* increased and reached values around 0.3 m s^{-1} at noon. Strongest unstable conditions however were already observed around 09:00 h. When the atmosphere became stable again around 18:00 h, u_* decreased rapidly to its low nocturnal values.
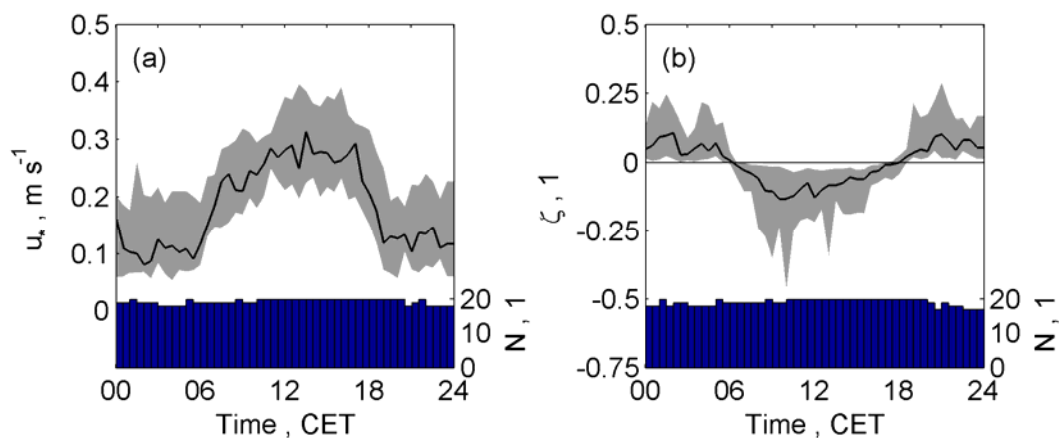
Fig. 6. Median (lines) diurnal course of (a) friction velocity u* and (b) atmospheric stability ζ from 11 August 2006 to 30 August 2006. Shaded areas comprise the respective inter quartile ranges. The bars at the bottom of each graph show the number of values available for the corresponding median and quartiles.

3.4   Trace gases - mixing ratios

The median diurnal courses of all measured scalars (CO_2, H_2O, O_3, NO, NO_2, T) from 11 August 2006 to 30 August 2006 are shown in Figure 7 (left panels) together with the respective difference (Δc) between 0.15 m and 2.0 m (right panels). The temporal resolution was 30 minutes. CO_2 mixing ratios (Figure 7, a and b) reached its highest values of about 420 ppm in the second part of the night. At this time, ΔCO_2 was about -40 ppm, indicating strong accumulation processes close to the ground, with the soil and plants being the source of CO_2. After sunrise, CO_2 gradually decreased until it reached its minimum mixing ratios of 365 ppm around 12:00 h. ΔCO_2 changed its sign to positive values at 07:00 h, indicating a net sink at the ground. Its magnitude remained very small during the day, being often lower than 1 ppm. In the afternoon, CO_2 mixing ratios started to increase again, and also ΔCO_2 became negative again and larger. The water vapor (Figure 7, c and d) mixing ratio exhibited a period of slight increase from 14 ppth to 15 ppth between 06:00 h and 09:00 h followed by a slight decrease until 12:30 h. During the afternoon, H_2O remained around 14 ppth until it changed around 18:00 h to about 15 ppth. During the night, the H_2O mixing ratio gradually decreased to about 14 ppth at the end of the night. The H_2O mixing ratio difference between the 2 levels showed a much clearer diurnal cycle. At 06:00 h, it became negative, indicating evapotranspiration. Between 08:00 h and 15:00 h, ΔH_2O remained around -1.5 ppth. After that, it slowly increased and became positive at the end of the night. The median diurnal course of O_3 (Figure 7, e and f) showed minimum mixing ratios of about 12 ppb in the hours before sunrise. After sunrise, O_3 mixing ratios increased to about 40 ppb at 12:00 h. With sunset around 18:00 h, O_3 mixing ratios started to decrease monotonically. Around 01:30 h the low night time values were reached again. ΔO_3 showed little variation over the day, remaining all the time at about 3 ppb. Only in the hours between 18:00 h and 01:30 h slightly higher ΔO_3 values were observed. The higher ΔO_3 values coincided with the period of decreasing O_3 mixing ratios. While the intensity of the turbulent transport decreased in the evening, the intensity of the O_3 sink at the ground must have remained high during the early evening hours, leading to an increase of ΔO_3. Because turbulent transport is stronger during day time than during night time, the relatively constant ΔO_3 points to a variable intensity of the O_3 sink at the surface. This could be stomatal uptake of O_3 by plants. The diurnal course of NO mixing ratio (Figure 7g) exhibited a sharp peak around 08:30 h, reaching values of about 1.8 ppb. During the night hours, mixing ratios were typically below 0.5 ppb.
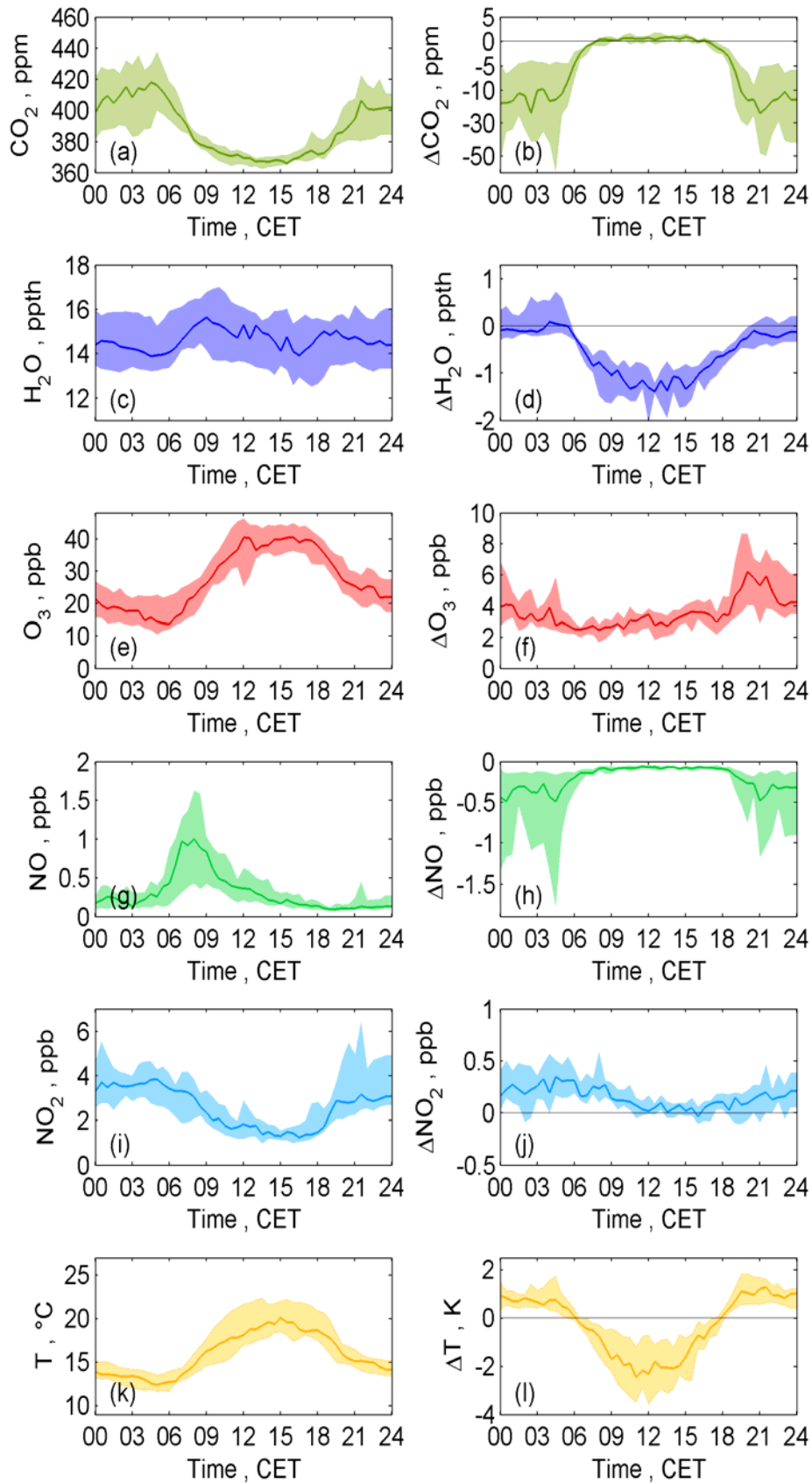
Fig. 7. Median (lines) diurnal course of (a, b) CO_2, (c, d) H_2O, (e, f) O_3, (g, h) NO, (I, j) NO_2 and (k, l) T from 11 August 2006 to 30 August 2006. Colored areas comprise the respective inter quartile ranges. The left panels show the diurnal courses of the values measured at $z = 2$ m, the right panels show the difference between the measurements in $z = 2$ m and $z = 0.15$ m.

However, no noticeable simultaneous excursion was observed in ΔNO (Figure 7h). The reason for the NO peak was advection, which affected both measuring heights with the same magnitude. We will address the advection topic in more detail below. The diurnal course of ΔNO showed strong fluctuation during night times, while during the day, ΔNO was small but always negative. NO is known to originate from microbial processes within the soil. At low background NO mixing ratios, NO is thus released from the soil. This is in accordance with the negative ΔNO. NO_2 mixing ratios (Figure 5, i) exhibited a diurnal course similar to that of CO_2: highest values (4 ppb) during the second part of the night, a decrease to 1.8 ppb between 06:00 h and 12:00 h, quasi constant until 18:00 h and then increasing again. But the diurnal course of ΔNO_2 was different from that of ΔCO_2. From night until the late morning, ΔNO_2 was positive. In the afternoon hours, small but negative ΔNO_2 values were observed. During the evening, ΔNO_2 remained close to 0 ppb and eventually increased around midnight. In contrast to NO, NO_2 did not exhibit a peak around 08:30 h, but a slight increase of ΔNO_2. For T, the diurnal courses (Figure 7, k and l) both followed the expected shape. T started to increase directly after sunrise and reached its highest values in the afternoon. Directly after sunset, T dropped rapidly, followed by a more gradual decrease during the night time, caused by radiative energy loss. Positive ΔT at night indicated thermally stable conditions, while negative ΔT during the day confirmed thermally unstable conditions, enhancing the turbulent transport.

3.4.1 Advection

The median diurnal course of NO mixing ratios showed an unexpected maximum around 08:30 h (see Section 3.3). Because both measuring heights were affected at the same magnitude, advection of NO from traffic emissions was suspected. All days of the LIBRETTO campaign were analyzed for the occurrence of the NO peak. Out of 20 days, the peak was clearly identified on 7 days. On 6 days, definitely no peak was observed. The remaining days were either influenced by local farming activities and thus excluded from the analyses, or instationarities from the preceding night obscured a clear identification. All peaks occurred between 07:00 h and 09:00 h.

Three evidences for the advection of traffic emissions have been found: (a) all 3 Sundays covered by the LIBRETTO campaign did not have a NO peak. (b) Air flow at days with NO peak approached the site from a different sector than it did at days without an NO peak (Figure 7) and (c) trucks from a beverage marked, located in
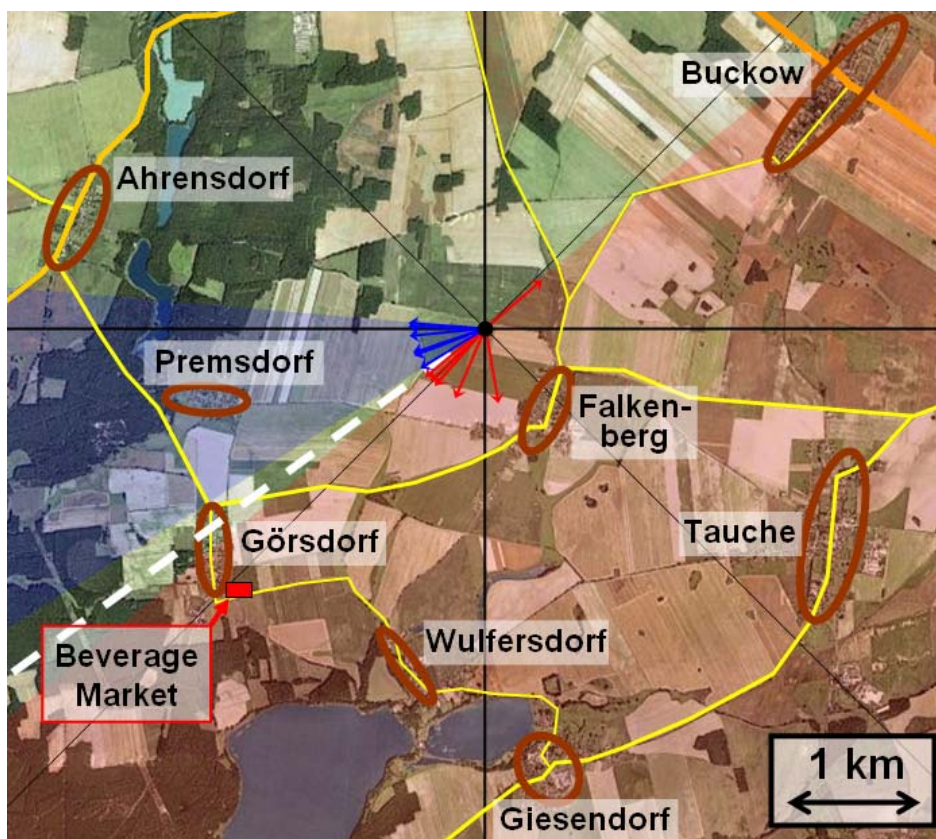
Fig. 8. Aerial view of the surrounding of the field site with sectors of the approaching flow during NO peaks (red arrows and sector) and at days without NO peak (blue arrows and sector).

Görsdorf (see Figure 8), left the market typically around 08:00 h, providing a strong NO source. The red sector, from where the wind came during the NO peaks, is characterized by a relatively close rural road (1.5 km or closer). In contrast, the blue sector, corresponding to the absence of NO peaks, provides a much longer distance to the next traffic related sources of NO.

3.4.2   Trace gases – fluxes

The trace gas fluxes, derived with the DMBR method, are shown in Figure 9. We used the convention, that downward (i.e. towards the surface) directed fluxes get a negative sign, upward fluxes are taken as positive ones. The DMBR method yielded significant results for all measured trace gas fluxes with clear diurnal cycles being visible. CO_2 (Figure 9a) showed peak respiration fluxes of about 5 μmol m^{-2} s^{-1} due to soil and plant respiration in the first part of the night, while it gradually decreased in the second part. Shortly after sunrise, the CO_2 flux changed its sign, indicating the onset of photosynthesis. Maximum downward fluxes were reached at 12:00 h with -6 μmol m^{-2} s^{-1}. The median flux of H_2O (Figure 9b) was always positive, although very small towards the end of the night. Short periods of negative H_2O fluxes, i.e. dew fall,
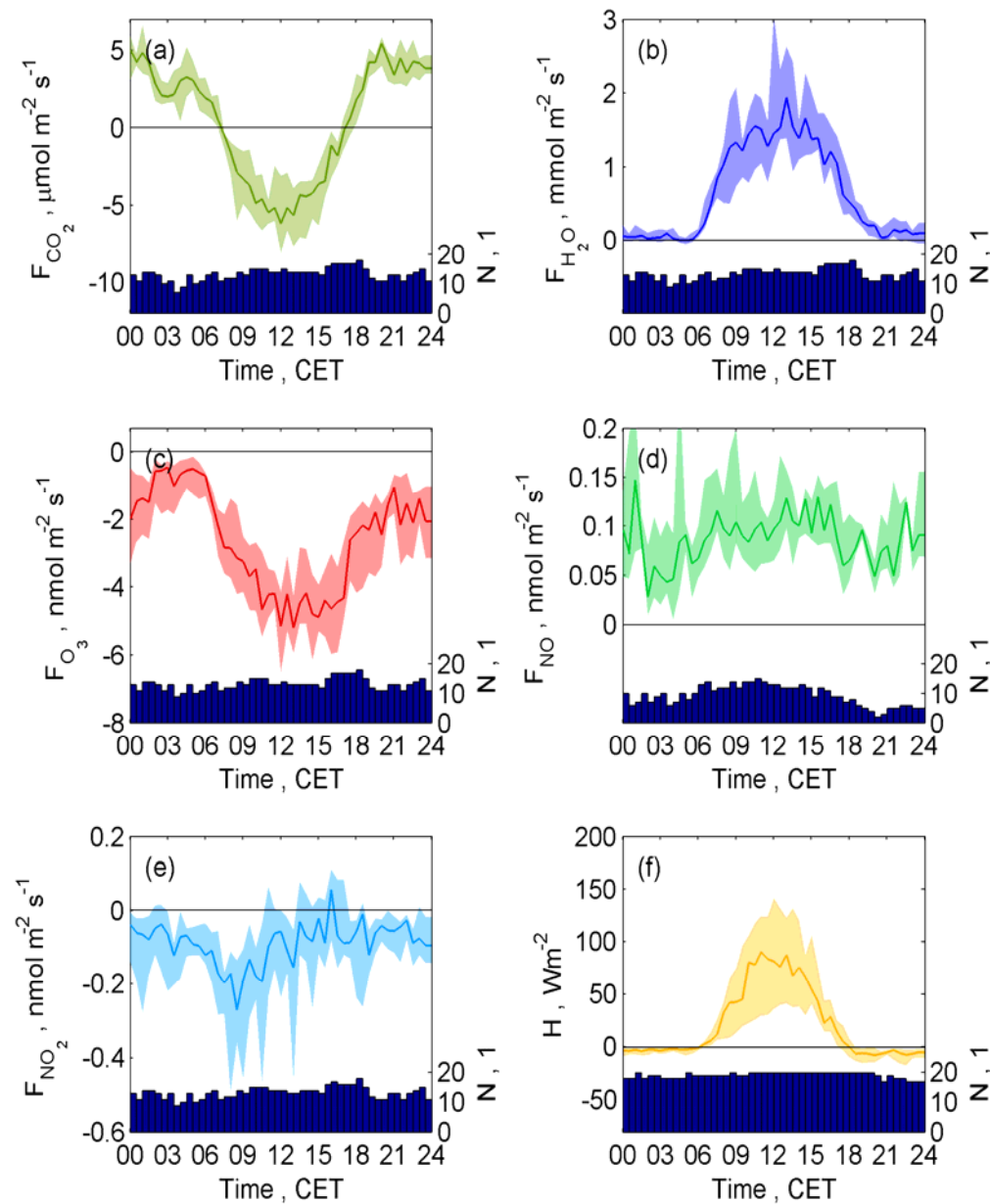
Fig. 9: Median (lines) diurnal course of the fluxes of (a) CO_2, (b) H_2O, (c) O_3, (d) NO, (e) NO_2 and (f) sensible heat from 11 August 2006 to 30 August 2006. Colored areas comprise the respective inter quartile ranges. The bars at the bottom of each graph show the number of values available for the corresponding median and quartiles.

were possible then. With sunrise, the H_2O flux increased rapidly, reaching about 1.8 mmol $m^{-2} s^{-1}$ around noon. This strong upward flux of H_2O was the result of evaporation from surfaces and transpiration of plants. With sinking sun, the H_2O flux decreased and eventually reached its low night time values of less than 0.1 mmol $m^{-2} s^{-1}$ at 20:00 h. The flux of O_3 was found to be always directed towards the surface (Figure 9c). This was expected, as no source of O_3 is known at the surface, while O_3 is destroyed by dry deposition onto surfaces (soil, plants) and during daytime additionally

by stomatal uptake. An additional O_3 sink at the surface results from NO emission from the soil. The effect of the additional sink of O_3 during daytime is clearly visible in the median diurnal flux of O_3, showing strongest downward fluxes in the early afternoon, with peak values of about -5.5 nmol $m^{-2} s^{-1}$. The higher fluxes start with sunrise around 06:00 h and end with sunset around 18:00 h. During the first part of the night, the O_3 flux remained around -2 nmol $m^{-2} s^{-1}$ and decreased after midnight to about -0.5 nmol $m^{-2} s^{-1}$. In contrast to O_3, NO has a source at the ground. It is produced by microorganisms in the soil, leading to a net production and thus a positive flux (Figure 9d). Because microbial NO production is, besides soil moisture, primarily dependent on soil temperature, highest production rates and thus fluxes were expected around noon. While positive fluxes were observed throughout the day, a diurnal cycle was not clearly visible. A more or less constant flux of about 0.1 nmol $m^{-2} s^{-1}$ was observed instead. Nevertheless, a small decrease of the NO flux down to 0.05 nmol $m^{-2} s^{-1}$ was observed shortly before sunset. During the night, the NO flux slowly increased back to 0.1 nmol $m^{-2} s^{-1}$. The median NO_2 flux remained most of the time negative (Figure 9e), indicating a net deposition. A maximum deposition flux reaching -0.25 nmol $m^{-2} s^{-1}$ was observed at 08:30 h, the time with advective influence. If days with advection were excluded in the analysis, the NO_2 flux remained also at this time around -0.1 nmol $m^{-2} s^{-1}$ (not shown). In the afternoon, positive but small NO_2 fluxes were observed. During the night, the NO_2 flux remained around -0.1 nmol $m^{-2} s^{-1}$. For the sake of completeness, the sensible heat flux H is also shown (Figure 9f). It exhibited very small, negative values during night time (not more than -5 W m^{-2}). With sunrise, H increased rapidly, reaching median values of 70 W m^{-2} around noon. In the afternoon, H decreased again and dropped below zero around 18:00 h, indicating the onset of surface cooling.

3.4.3   *Comparison field vs. laboratory*

The dependency of soil NO emission on soil temperature and water content was investigated in the laboratory with soil samples taken from the field site. The laboratory results were parameterized with the measured soil moisture and soil surface temperature during the LIBRETTO campaign. The resulting range of computed NO fluxes data is shown in Figure 10. Considering the very different types of measurements, the agreement between the two curves was quite good. The median NO flux observed with
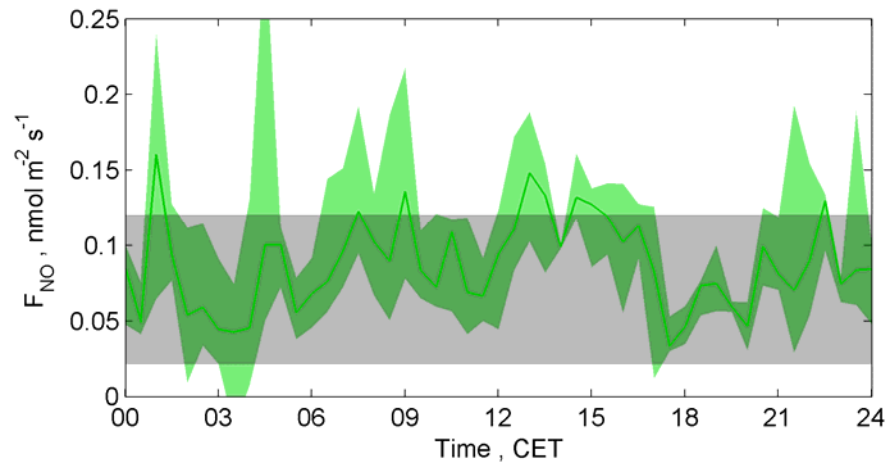
Fig. 10. Median diurnal course of NO flux from field measurements (green) and range of data obtained with laboratory parameterization (grey area) for the period of 11 August 2006 – 30 August 2006. The laboratory data were parameterized with the field data of soil moisture and soil surface temperature.

the DMBR method remained during most times of the day within the range of the laboratory derived results.

3.4.4   Comparison DMBR – NBL budget method (NBLB)

The coexistence of surface layer flux measurements of CO_2, O_3 (DMBR method) and H (EC method) and highly resolved vertical profiles of CO_2, O_3 and T up to 100 m provided the option to compare the surface layer fluxes with fluxes derived from the NBLB.

One night provided sufficient stability and stationarity for this comparison. Time-height cross sections of potential temperature (θ), CO_2 and O_3 are shown in Figure 11. After the transition of the sensible heat flux to negative values (indicating cooling) (left vertical dashed line, Figure 11), the entire air column started to cool down from about 23 °C to approximately 16 °C within 3 hours, while the strongest cooling was at the beginning of this period. Later during the night, the air was cooled by the surface, which in turn was cooled by outgoing longwave radiation. Shortly before 06:00 h in the morning, the sensible heat flux changed to positive values, indicating surface heating. This became immediately visible in the profiles of θ, showing unstable thermal stratification near the ground. The situation for CO_2 was somewhat different. After the atmosphere became stable, CO_2 enrichment started from close to the ground (Figure 11b). The mixing ratio of CO_2 close to the ground increased with time, while the layer with increased CO_2 mixing ratios compared to the afternoon values, deepened, and eventually exceeded the range covered by the mast data. Highest mixing ratios occurred
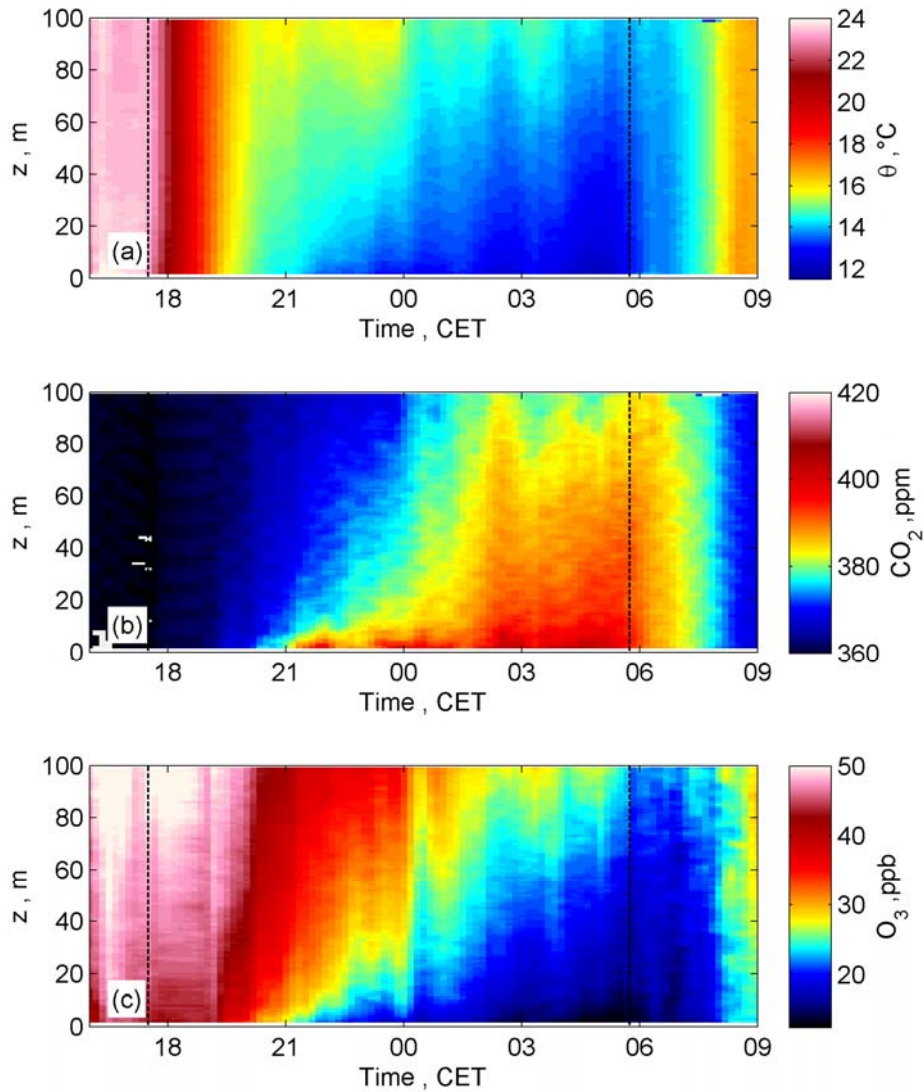
Fig. 11. Time-height cross section of (a) potential temperature, (b) CO_2 mixing ratio and (c) O_3 mixing ratio for 20 August 2006 16:00 h to 21 August 2006 09:00 h. The dashed vertical lines denote the zero crossing of the sensible heat flux, measured at $z = 2.4$ m, being negative during night times.

on the second half of the night, exceeding 410 ppm at 2 m. With sensible heat flux changing back to positive values shortly before 06:00 h in the morning, CO_2 mixing ratio began to drop back to lower values simultaneously in the entire observable column. This was the result of the zero crossing of the CO_2 flux (from upward to downward, Figure 12a) and the simultaneous growing of the mixing layer. The time-height cross section of O_3 (Figure 11c) shows small positive vertical gradients of O_3 mixing ratios during daytime with only small temporal changes of the mixing ratios. After 19:30 h, mixing ratios decreased fast at all heights, while the vertical gradients increased. This was primarily the effect of reduced turbulence, with only slow transport velocities. It led to a loss of O_3 in the entire observable column, while being strongest

close to the ground. Low O_3 mixing ratios prevailed in the observable column until approximately two hours after sunrise. During these two hours, only O_3 depleted air from the former NBL was entrained into the newly developing boundary layer. At 08:00 h, O_3 mixing ratios started to increase, an indication that now air from the residual layer (not affected by nocturnal O_3 depletion) was entrained.

A direct comparison of the surface layer fluxes (DMBR and EC method) with the fluxes derived with the NBLB method revealed further nocturnal dynamics (Figure 12). The time series of the fluxes (Figure 12 a, c, e) exhibited a close correlation between the two methods. The magnitude of the fluxes as well as the time of their zero crossing agreed well. Only H showed major differences before 20:00 h. Nevertheless, fluxes derived with the NBLB method had a larger temporal variability. A different way of comparing the temporal evolution of the fluxes, is a plot of the cumulative flux of heat or matter into or out of the NBL. For the cumulative heat flux (Figure 12b), two nocturnal episodes can be discerned: an initial stabilization phase, and a subsequent cooling phase for the remaining night. During the first part until 20:30 h, H measured with the EC method yielded only -12.8 J m^{-2} h^{-1} while H from the NBLB yielded -104.6 J m^{-2} h^{-1}. Such a discrepancy was already suggested by Figure 11a, where an initial rapid cooling throughout the entire observable air column was visible. It could be explained by the adjustment of the air temperature to the altered radiation regime after sunset. Consequently, because this temperature decrease occurred "in situ", the H from EC measurements did not reflect the magnitude of heat change. In the second part from 20:30 h until sunrise, both methods yielded similar values of H (-6.1 J m^{-2} h^{-1} from EC and -7.7 J m^{-2} h^{-1} from NBLB). The division of the nocturnal dynamics into a first part before 20:30 h and a second part after 20:30 h until sunrise was also observable in trace gas data. The cumulative flux of CO_2 was similar from both methods in the second part (DMBR: 13.5 mmol m^{-2} h^{-1}, NBLB: 11.9 mmol m^{-2} h^{-1}). It indicated, that the temporal change of CO_2 mixing ratios within the NBL was only controlled by the surface. All CO_2 accumulating in the NBL had thus to pass the DMBR measuring level. In the first part, a slight deviation between the two methods was observed. The NBLB method yielded slightly higher CO_2 fluxes (25.1 mmol m^{-2} h^{-1}) than the DMBR method (12.9 mmol m^{-2} h^{-1}). A very different situation was found for O_3. In the second part of the night, the cumulative fluxes of O_3 showed great difference between the NBLB (-8.3 µmol m^{-2} h^{-1}) and the DMBR O_3 fluxes (-2.5 µmol m^{-2} h^{-1}). The important difference of O_3 compared to CO_2 and sensible heat is the fact that it is a reactive trace
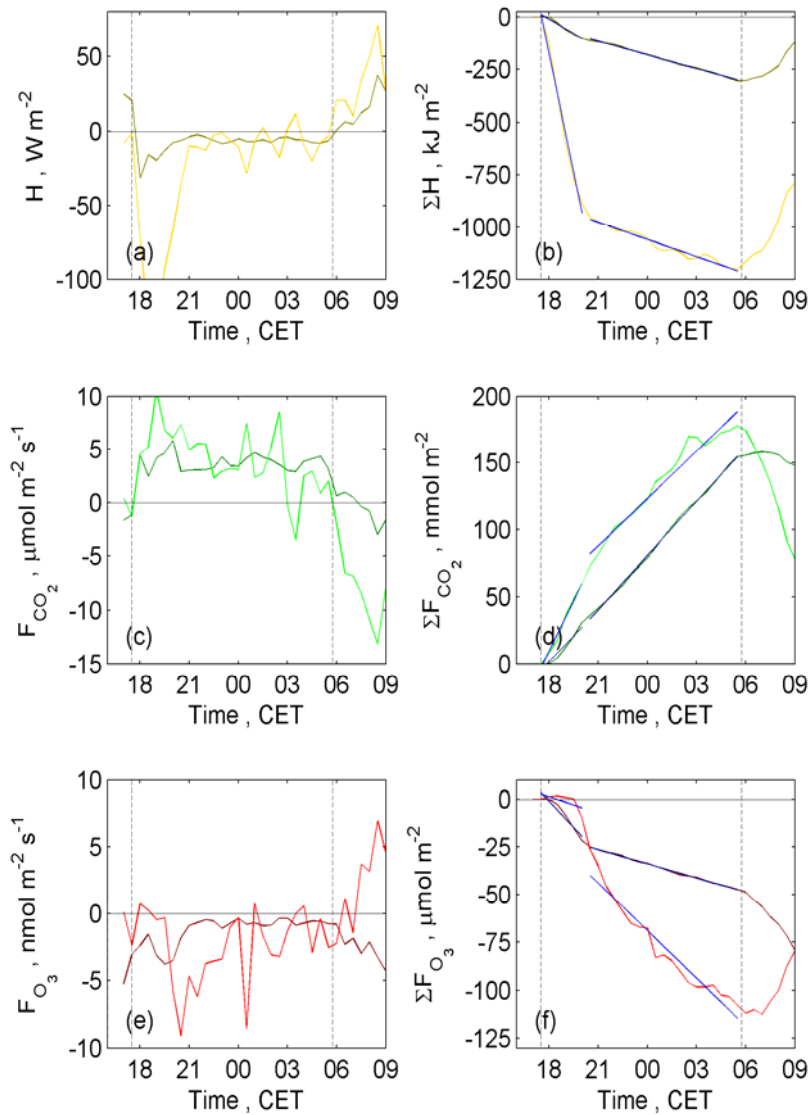
Fig. 12. Comparison of fluxes of sensible heat (H), CO_2 (F_{CO2}) and O_3 (F_{O3}) measured with the DMBR or EC method (dark colors) and derived with the NBLB (light colors). Panels (a), (c) and (e) show the 30 minute values of the respective fluxes, while panels (b), (d) and (f) show the cumulative flux since onset of surface cooling (indicated by the left dashed line) The right dashed line marks the onset of heating after sunrise.

gas. Because vertical exchange was suppressed during night time, even relatively slow chemical reactions led to a depletion of O_3. This does not only occur at the surface, but happened also within the NBL. Because of the absence of short wave radiation, photolytical reformation of O_3 from NO_2 (R2) did not occur. Furthermore, additional O_3 was destroyed by reaction with NO_2, forming NO_3. The DMBR method captured only the O_3 towards the surface. In contrast, the NBLB was affected additionally by the in-situ destruction of O_3 within the NBL, leading to a temporal change and thus an apparent flux. While the NBLB did obviously not provide correct flux data in case of

reactive trace gases, a comparison between the two methods can give an estimate about the magnitude of in-situ chemical O_3 loss within the NBL.

It has to be noted, that the fluxes derived by the NBLB did not only represent the field site, as it did the surface layer fluxes. Due to the large fetch, different types of land use upwind of the mast affected the profiles and thus the actual temporal change (Beyrich et al., 2002). Nevertheless, the general patterns described in this section display the temporal evolution of the fluxes and of the corresponding scalars at and above the field site.

4   Conclusions

As long as the terrain is homogeneous with respect to roughness and soil/vegetation properties, the MBR method can be used in its distributed version (DMBR), where sensible heat flux and corresponding temperature gradient are measured a few tens of meters apart from the trace gas gradient measurements. This provides the option of using one EC station for several, distributed trace gas flux measurements at one site. Nevertheless, horizontal homogeneity remains critical, as already variations of soil parameters can lead to different heat transfers into the soil and thus different sensible heat fluxes. This would invalidate the representativeness of the sensible heat flux obtained at the EC station for the respective location.

If the DMBR method is applicable, it provides a quick way to reliably compute the vertical surface layer fluxes of trace gases, as it was demonstrated for the passive trace gases CO_2 and H_2O and for the reactive trace gases O_3, NO and NO_2. It has to be noted, that such a flux is neither necessarily the flux at the very surface, nor the flux as it is derived from the integration of trace gas profiles up to their equilibrium level. Under stable conditions, with strong surface inversions, trace gases are trapped already close to the ground, leading there to very high concentrations. The surface layer flux observed, as a mean flux within the layer covered by the gradient measurements, is only the outflow from (or inflow into) this pool of trapped trace gas. But still it represents the lower flux boundary condition for the trace gas profile above.

The comparison of the fluxes derived with the DMBR method and from integration of the respective trace gas profiles up to 100 m (NBL budget) revealed very clearly the different spatial domains of both approaches. While the DMBR method provided the local vertical turbulent flux in the surface layer, precisely spoken: between the two levels of the concentration measurements, the NBL budget method covers a large footprint, i.e. a large horizontal area from which the fluxes originate. The principal

differences between the fluxes of the conservative quantities CO_2 and heat points out, that transport dynamics of temperature and trace gases may differ significantly. Furthermore, with increasing height an increasing lateral heterogeneity of the surface is included into the profiles. This leads to variations, not representative for the surface directly underlying the profile.

Acknowledgements

References

Akima, H.: A new method of interpolation and smooth curve fitting based on local procedures, J. Assoc. Comp. Mach., 17, 589-602, 1970.

Arya, S. P. S.: Introduction to Micrometeorology, Intern. Geophys. Ser., Academic Press, San Diego, CA., 420 pp., 2001.

Aubinet, M., Grelle, A., Ibrom, A., Rannik, Ü., Moncrieff, J., Foken, T., Kowalski, A. S., Martin, P. H., Berbigier, P., Bernhofer, C., Clement, R., Elbers, J., Granier, A., Grunwald, T., Morgenstern, K., Pilegaard, K., Rebmann, C., Snijders, W., Valentini, R., and Vesala, T.: Estimates of the annual net carbon and water exchange of forests: The EUROFLUX methodology, in: Advances in Ecological Research, Vol 30, Advances in Ecological Research, ACADEMIC PRESS INC, San Diego, 113-175, 2000.

Bahe, F. C., Schurath, U., and Becker, K. H.: The frequency of NO2 photolysis at ground level, as recorded by a continuous actinometer, Atmos. Environ., 14, 711-718, 1980.

Baldocchi, D., Falge, E., Gu, L. H., Olson, R., Hollinger, D., Running, S., Anthoni, P., Bernhofer, C., Davis, K., Evans, R., Fuentes, J., Goldstein, A., Katul, G., Law, B., Lee, X. H., Malhi, Y., Meyers, T., Munger, W., Oechel, W., U, K. T. P., Pilegaard, K., Schmid, H. P., Valentini, R., Verma, S., Vesala, T., Wilson, K., and Wofsy, S.: FLUXNET: A new tool to study the temporal and spatial variability of ecosystem-

scale carbon dioxide, water vapor, and energy flux densities, Bull. Amer. Meteorol. Soc., 82, 2415-2434, 2001.

Baldocchi, D. D., Hicks, B. B., and Meyers, T. P.: Measuring Biosphere-Atmosphere Exchanges of Biologically Related Gases with Micrometeorological Methods, Ecology, 69, 1331-1340, 1988.

Beyrich, F., Richter, S. H., Weisensee, U., Kohsiek, W., Lohse, H., de Bruin, H. A. R., Foken, T., Gockede, M., Berger, F., Vogt, R., and Batchvarova, E.: Experimental determination of turbulent fluxes over the heterogeneous LITFASS area: Selected results from the LITFASS-98 experiment, Theoretical and Applied Climatology, 73, 19-34, 2002.

Beyrich, F., and Adam, W. K.: Site and Data Report for the Lindenberg Reference Site in CEOP – Phase I, Deutscher Wetterdienst, Offenbach, 230, 55 pp., 2007.

Bowen, I. S.: The Ratio of Heat Losses by Conduction and by Evaporation from any Water Surface, Phys. Rev., 27, 779-787, 1926.

Businger, J. A., Wyngaard, J. C., Izumi, Y., and Bradley, E. F.: Flux-profile relationships in the atmospheric surface layer., Journal of Atmospheric Sciences, 28, 181-189, 1971.

Businger, J. A.: Evaluation of the Accuracy with Which Dry Deposition Can Be Measured with Current Micrometeorological Techniques, J. Clim. Appl. Meteorol., 25, 1100-1124, 1986.

Damköhler, G.: Der Einfluss der Turbulenz auf die Flammengeschwindigkeit in Gasgemischen, Z. f. Elektroch., 46, 601-652, 1940.

Denmead, O. T., Raupach, M. R., Dunin, F. X., Cleugh, H. A., and Leuning, R.: Boundary layer budgets for regional estimates of scalar fluxes, Global Change Biology, 2, 255-264, 1996.

Eugster, W., and Siegrist, F.: The influence of nocturnal CO_2 advection on CO_2 flux measurements, Bas. Appl. Ecol., 1, 177-188, 2000.

Feig, G. T., Mamtimin, B., and Meixner, F. X.: Use of laboratory and remote sensing techniques to estimate vegetation patch scale emissions of nitric oxide from an arid Kalahari savanna, Biogeosciences Discuss., in press, 2008a.

Feig, G. T., Mamtimin, B., and Meixner, F. X.: Soil biogenic emissions of nitric oxide from a semi-arid savanna in South Africa, Biogeosciences Discuss., 5, 2795-2837, 2008b.

Foken, T., Dlugi, R., and Kramm, G.: On the determination of dry deposition and emission of gaseous compounds at the biosphere-atmosphere interface, Meteorol. Z., 4, 91-118, 1995.

Foken, T.: Micrometeorology, Springer, Heidelberg, New York, 310 pp., 2008.

Högström, U.: Non-dimensional wind and temperature profiles in the atmospheric surface layer: A re-evaluation., Boundary-Layer Meteorol., 42, 55-78, 1988.

Keronen, P., Reissell, A., Rannik, Ü., Pohja, T., Siivola, E., Hiltunen, V., Hari, P., Kulmala, M., and Vesala, T.: Ozone flux measurements over a scots pine forest using eddy covariance method: performance evaluation and comparison with flux-profile method, Boreal Env. Res., 8, 425-443, 2003.

Lenschow, D. H.: Reactive trace species in the boundary layer from a micrometeorological perspective, J. Meteorol. Soc. Jpn., 60, 472-480, 1982.

Levy, P. E., Grelle, A., Lindroth, A., Mölder, M., Jarvis, P. G., Kruijt, B., and Moncrieff, J. B.: Regional-scale CO2 fluxes over central Sweden by a boundary layer budget method, Agric. For. Meteorol., 98-99, 169-180, 1999.

Lewis, J. M.: The Story behind the Bowen Ratio, Bull. Amer. Meteorol. Soc., 76, 2433-2443, 1995.

Liu, H., and Foken, T.: A modified Bowen ratio method to determine sensible and latent heat fluxes, Meteorol. Z., 10, 71-80, 2001.

Mathieu, N., Strachan, I. B., Leclerc, M. Y., Karipot, A., and Pattey, E.: Role of low-level jets and boundary-layer properties on the NBL budget technique, Agric. For. Meteorol., 135, 35-43, 2005.

Mayer, J.-C., Hens, K., Rummel, U., Meixner, F. X., and Foken, T.: Moving measurement platforms - specific challenges and corrections, Meteorol. Z., resubmitted, 2008.

Meixner, F. X., and Yang, W. X.: Biogenic emissions of nitric oxide and nitrous oxide from arid and semi-arid land, in: Dryland Ecohydrology, edited by: D'Odorio, P., and Porporat, A., Springer, Dordrecht, 233-255, 2006.

Müller, H., Kramm, G., Meixner, F., Dollard, G. J., Fowler, D., and Possanzini, M.: Determination of HNO3 Dry Deposition by Modified Bowen-Ratio and Aerodynamic Profile Techniques, Tellus Series B, 45, 346-367, 1993.

Ormeci, B., S.L., S., and Peirde, J. J.: Laboratory study of NO flux from agricultural soil: Effects of soil moisture, pH, and temperature, J. Geophys. Res., 104, 1621-1629, 1999.

Pattey, E., Strachan, I. B., Desjardins, R. L., and Massheder, J.: Measuring nighttime CO2 flux over terrestrial ecosystems using eddy covariance and nocturnal boundary layer methods, Agric. For. Meteorol., 113, 145-158, 2002.

Paulson, C. A.: The Mathematical Representation of Wind Speed and Temperature Profiles in the Unstable Atmospheric Surface Layer, J. Appl. Meteorol., 9, 857-861, 1970.

Rummel, U., Ammann, C., Gut, A., Meixner, F. X., and Andreae, M. O.: Eddy covariance measurements of nitric oxide flux within an Amazonian rain forest, J. Geophys. Res., 107, 8050, doi:10.1029/2001JD000520, 2002.

Suni, T., Rinne, J., Reissell, A., Altimir, N., Keronen, P., Rannik, Ü., Dal Maso, M., Kulmala, M., and Vesala, T.: Long-term measurements of surface fluxes above a Scots pine forest in Hyytiala, southern Finland, 1996-2001, Boreal Env. Res., 8, 287-301, 2003.

van Dijk, S. M., and Meixner, F. X.: Production and Consumption of NO in Forest and Pasture Soils from the Amazon Basin, Water, Air, & Soil Pollution: Focus, 1, 119-130, 2001.

Vickers, D., and Mahrt, L.: Quality Control and Flux Sampling Problems for Tower and Aircraft Data, J. Atmos. Ocean. Technol., 14, 512-526, 1997.

Vilà-Guerau de Arellano, J., and Duynkerke, P. G.: Influence of chemistry on the flux-gradient relationships for the NO-O3-NO2 system, Boundary-Layer Meteorol., 61, 375-387, 1992.

Wesely, M. L., Eastman, J. A., Stedman, D. H., and Yalvac, E. D.: An eddy-correlation measurement of NO2 flux to vegetation and comparison to O3 flux, Atmos. Environ., 16, 815-820, 1982.

Wyngaard, J. C.: Boundary-Layer Modelling, in: Atmospheric Turbulence and Air Pollution Modelling, edited by: Nieuwstadt, F. T. M., and van Dop, H., Reidel, Dordrecht, The Netherlands, 69-106, 1982.

Erklärung

Hiermit erkläre ich, dass ich die Arbeit selbständig verfasst habe und keine anderen als die angegebenen Quellen und Hilfsmittel verwendet habe.

Ferner erkläre ich, dass ich nicht anderweitig mit oder ohne Erfolg versucht habe, eine Dissertation einzureichen oder mich einer Doktorprüfung zu unterziehen.

Mainz, den

_____

Jens-Christopher Mayer